Master's thesis

NTNU
Norwegian University of Science and Technology
Faculty of Natural Sciences
Department of Chemical Engineering

Blanca Yuritzi Cervantes Gameros

Simulation of gas dehydration process with MEG using Aspen Plus

Master's thesis in Chemical Engineering

June 2019

NTNU
Kunnskap for en bedre verden

Blanca Yuritzi Cervantes Gameros

Simulation of gas dehydration process with MEG using Aspen Plus

Master's thesis in Chemical Engineering
June 2019

Norwegian University of Science and Technology
Faculty of Natural Sciences
Department of Chemical Engineering

NTNU
Kunnskap for en bedre verden

NTNU – Trondheim
Norwegian University of
Science and Technology

Simulation of gas dehydration process with MEG using Aspen Plus

Blanca Yuritzi Cervantes Gameros

Submission date: June 2019
Responsible professor: Hanna Knuutila
Supervisor: Eirini Skylogianni

Norwegian University of Science and Technology
Department of Chemical Engineering

Abstract

Gas dehydration offshore is crucial for achieving the required gas specifications, complying with regulations and ensuring safe flow in export pipelines. The gas dehydration process in offshore operations usually takes place at the wellhead using methanol or monoethylene glycol, MEG, but also on a platform after the gas has undergone a sweetening treatment. Then it is usually performed through the absorption of water using triethylene glycol, TEG, which is regenerated afterwards.

In this master thesis gas dehydration process using MEG is simulated, and the different MEG regeneration methods are compared through simulation in Aspen Plus, a commercial process simulator. The model validation was the first step of this work, since it defines whether the model predicts acceptable results or not.

MEG regeneration is unusual compared to other glycol regeneration processes offshore, such as stripping gas usage and the DRIZO process which are designed for TEG. The traditional regeneration methods limit the achievable MEG purity due to limitations in the temperature at which MEG degrades, effectively restraining the achievable dry gas quality. The traditional choice is the use of vacuum to keep the process temperature below MEG degradation, MEG losses and equipment fouling.

The different regeneration schemes were implemented in Aspen Plus for application to MEG, using the ELECNRTL thermodynamic model to simulate vapor-liquid equilibrium. Results were outstanding for vacuum and the DRIZO processes. Subsequently, these two regeneration methods were modified by implementing a MEG recovery loop. In addition, a heat recovery design was implemented.

The methods were compared and the optimal set of parameters found. Based mainly on the amount of water removed from the gas, the total amount of MEG losses and energy consumption we can conclude that the DRIZO process can be applied to MEG regeneration, as this was the method with the best performance.

Preface

This thesis was written as the final work of the master program in Chemical Engineering at the Norwegian University of Science and Technology.

I would like to thank my supervisor Hanna Knuutila for allowing me to be part of the Environmental engineering and reactor technology group and letting me work on this project. I would like to thank my co-supervisor Eirini Skylogianni for her time, patience, and feedback.

I will always be grateful to my caring, loving and supporting parents, Ruben Cervantes and Patricia Gameros for their co-operation, trust and constant encouragement which were the sustaining factors in completing this goal.

I would like to give special thanks to my dear friends Andres Carranza, Zawadi Mdoe, Dumitrita Spinu, Adriana Reyes and Ernesto Casalegno that supported me in this journey and listened to me on the hard days. I am also extremely grateful to Nicolai Stubbrud, who motivated and encouraged me to accomplish this master's degree.

Declaration of Compliance:

I declare that this is an independent work according to the exam regulations of the Norwegian University of Science and Technology (NTNU).

Trondheim, Norway;
10^{th} of June, 2019

Blanca Yuritzi
Cervantes Gameros

Contents

List of Figures xi

List of Tables xv

List of Symbols xxi

List of Acronyms xxiii

1 Introduction 1
- 1.1 Motivation . . . 1
- 1.2 Objective . . . 2
- 1.3 Thesis Structure . . . 2

2 Background 5
- 2.1 Offshore production processes . . . 5
- 2.2 Flow assurance . . . 6
  - 2.2.1 Corrosion and scale formation . . . 7
  - 2.2.2 Hydrate formation . . . 7
  - 2.2.3 Hydrate prevention . . . 9
- 2.3 Gas dehydration methods . . . 12
- 2.4 MEG as an absorbent . . . 13

3 VLE simulation in Aspen Plus 15
- 3.1 Aspen Plus thermodynamic methods . . . 15
  - 3.1.1 Phases equilibrium calculation . . . 16
- 3.2 Property selection method . . . 18

4 Vapor-liquid equilibrium validation 21
- 4.1 Validation methodology . . . 21
- 4.2 Literature review - VLE data . . . 24
- 4.3 H_2O pressure validation . . . 24
- 4.4 Solubility of H_2O in MEG . . . 25
- 4.5 Solubility of CH_4 in MEG . . . 27

4.6 Solubility of CH_4 in H_2O . . . 29
4.7 Solubility of CO_2 in MEG . . . 31
4.8 Solubility of CO_2 in H_2O . . . 32

5 Basis for process simulation **35**
5.1 Problem statement . . . 35
5.2 Gas composition and assumptions . . . 36
5.3 Water content specification in export gas . . . 38

6 Process simulation **39**
6.1 Gas dehydration process description . . . 39
6.1.1 Gas dehydration simulation. . . . 42
6.2 Regeneration methods . . . 43
6.2.1 Regeneration under vacuum . . . 43
6.2.2 Regeneration with stripping gas . . . 46
6.2.3 DRIZO process . . . 48
6.3 Results and regeneration methods comparison . . . 53

7 Process modification for MEG recovery **55**
7.1 Regeneration with vacuum and MEG recovery . . . 55
7.2 DRIZO process with MEG recovery . . . 60
7.3 Results comparison and discussion . . . 65

8 Concluding remarks **69**
8.1 Conclusions . . . 69
8.1.1 Further work . . . 70

References **71**

Appendices

A Appendix **77**
A.1 VLE validation deviations . . . 77

B Appendix **107**
B.1 Basis for process simulation . . . 107
B.1.1 Glycols Properties . . . 107
B.1.2 Gas composition and assumptions. . . . 108
B.1.3 Calculation method for water specification. . . . 109

C Appendix **113**
C.1 Process simulation diagrams . . . 113
C.1.1 Gas dehydration with vacuum regeneration . . . 114
C.1.2 Gas dehydration with vacuum regeneration and stripping gas 115

C.1.3 Gas dehydration with DRIZO regeneration 116
C.1.4 Gas dehydration with vacuum regeneration and MEG recovery 117
C.1.5 Gas dehydration with DRIZO regeneration and MEG recovery 118

List of Figures

2.1 Offshore production chain. Picture taken from TEP4185 – Natural Gas Technology[4] 6
2.2 Hydrate plug offshore. Picture taken from SPE presentation[66]. 8
2.3 Methane hydrate stability chart. Chart modified after NOOA[55] 9
2.4 Hydrate inhibition by using MEG.[27]. 10
2.5 Dielectrical heating in the left side and bundles and pipe-in-pipe in the right side.[41]. 11
2.6 MEG plants worldwide in 2009. Picture taken from SPE international: "MEG Regeneration Technical Meeting 18 June 2009, Port Campbell". . 13

4.1 Flowsheet used for validations. 22
4.2 Vapor pressure of water in the temperature range of $30-120°C$. Triangles represent the models, squares represent literature data and circles represent experimental data from previous work. 25
4.3 Total pressure on a log scale as a function of liquid H_2O mole fraction in MEG, in the temperature range of $50-80°C$. The dotted lines represent the models and the circles represent the experimental data. 26
4.4 Total pressure on a log scale as a function of liquid CH_4 mole fraction in MEG, in the temperature range of $125-150°C$. The dotted lines represent the models and the circles represent the experimental data. 27
4.5 Total pressure on a log scale as a function of liquid CH_4 mole fraction in MEG, in the temperature range of $30-100°C$. The dotted lines represent the models and the circles represent the experimental data. 28
4.6 Total pressure on a log scale as a function of liquid CH_4 mole fraction in H_2O, in the temperature range of $25-50°C$. The dotted lines represent the models and the circles represent the experimental data. 30
4.7 Total pressure on a log scale as a function of liquid CO_2 mole fraction in MEG, in the temperature range of $25-50°C$. The dotted lines represent the models and the circles represent the experimental data. 31
4.8 Total pressure on a log scale as a function of liquid CO_2 mole fraction in MEG, in the temperature range of $100-150°C$. The dotted lines represent the models and the circles represent the experimental data. 32

4.9 Total pressure on a log scale as a function of liquid CO_2 mole fraction in H_2O, in the temperature range of $25 - 120°C$. The dotted lines represent the models and the circles represent the experimental data. 33

5.1 Typical offshore gas process from extraction to onshore treatment. . . . 36

6.1 Typical simplyfied gas dehydration process[57]. 40
6.2 MEG regeneration and reclamation offshore system (Picture taken from Schlumberger "PUREMEG" brochure). 41
6.3 Effect of number of stages in absorber on dry gas water content (ppm). 42
6.4 Simulation in Aspen Plus of the regeneration process under vacuum. . . 43
6.5 Stages effect on regeneration with vacuum. 45
6.6 Simulation in Aspen Plus of the regeneration process with stripping gas. 46
6.7 Stages effect on regeneration with stripping gas and vacuum. 47
6.8 DRIZO process diagram[57] 49
6.9 Simulation in Aspen Plus of the regeneration process with DRIZO. . . . 50
6.10 Stages effect on CONCENT1 with DRIZO process. 52
6.11 Stages effect on CONCENT2 with DRIZO process. 52

7.1 Modified vacuum regeneration with MEG recovery. 56
7.2 CONCENT2 stages effect on the modified vacuum regeneration with MEG recovery, with CONCENT1 set to 5 stages. 57
7.3 CONCENT1 stages effect on the modified vacuum regeneration with MEG recovery and CONCENT2 set to 5 stages. 58
7.4 Modified DRIZO with MEG recovery. 61
7.5 DRIZO regeneration with MEG recovery - Stages effect on CONCENT3 column with CONCENT1 and CONCENT2 fixed to 5 stages. 62
7.6 DRIZO regeneration with MEG recovery - Stages effect on CONCENT1 with CONCENT2 fixed to 5 stages. 63
7.7 DRIZO regeneration with MEG recovery - Stages effect comparison on CONCENT1 with CONCENT2 fixed to 5 stages against CONCENT2 with CONCENT1 fixed to 5 stages. 63
7.8 Comparison of the vacuum and the DRIZO modified regeneration processes. 65

B.1 Water content of sweet natural gas at standard conditions at different pressures and water dewpoints.[8]. 110

C.1 Diagram of gas dehydration with vacuum regeneration showing pressure and temperature results. 114
C.2 Diagram of gas dehydration with vacuum and stripping gas regeneration showing pressure and temperature results. 115
C.3 Diagram of gas dehydration with DRIZO regeneration showing pressure and temperature results. 116

C.4 Diagram of gas dehydration with vacuum regeneration and MEG recovery showing pressure and temperature results. 117
C.5 Diagram of gas dehydration with DRIZO regeneration and MEG recovery showing pressure and temperature results. 118

List of Tables

4.1 Available experimental VLE data for the relevant systems. 24

5.1 Base case gas composition used in this work. 37
5.2 Base case operating conditions 37

6.1 Specifications used in Aspen Plus for the absorption column. 42
6.2 Specifications used in Aspen Plus for the FLASH tank and the CONCENTR column in the regeneration process under vacuum. 44
6.3 Energy requirements for MEG regeneration under vacuum. 45
6.4 Specifications used in Aspen Plus for the flash tank and the stripping column in the regeneration process under vacuum. 47
6.5 Energy requirements for MEG regeneration with stripping gas and vacuum. 48
6.6 Specifications used in Aspen Plus for the flash tank and the different stripping columns used in the DRIZO regeneration process. 51
6.7 Energy requirements for MEG regeneration with DRIZO process. 53
6.8 Results overview for the different regeneration schemes simulated. . . . 54

7.1 Composition of distillate stream coming from the top of the CONCENT1 column under vacuum. 55
7.2 Specifications used in Aspen Plus for the MEG recovery option in the vacuum regeneration process. 57
7.3 Energy requirements for MEG recovery with the modified vacuum regeneration. 59
7.4 Composition of water stream from the 3-phase separator in the DRIZO process. 60
7.5 Specifications used in Aspen Plus for the MEG recovery option in the modified DRIZO regeneration process. 61
7.6 Energy requirements for MEG recovery with the modified DRIZO regeneration. 64
7.7 Results overview for the modified regeneration schemes simulated. . . . 66

A.1 Aspen Plus pressures obtained by interpolation at 50° C for the system H_2O-MEG and their respective calculated deviations from literature . . 77
A.2 Aspen Plus water mole fractions obtained by interpolation at 50° C for the system H_2O-MEG and their respective calculated deviations from literature 78
A.3 Aspen Plus pressures obtained by interpolation at 60° C for the system H_2O-MEG and their respective calculated deviations from literature . . 79
A.4 Aspen Plus water mole fractions obtained by interpolation at 60° C for the system H_2O-MEG and their respective calculated deviations from literature 80
A.5 Aspen Plus pressures obtained by interpolation at 60° C for the system H_2O-MEG and their respective calculated deviations from literature . . 81
A.6 Aspen Plus water mole fraction obtained by interpolation at 60° C for the system H_2O-MEG and their respective calculated deviations from literature 82
A.7 Aspen Plus pressures obtained by interpolation at 80° C for the system H_2O-MEG and their respective calculated deviations from literature . . 83
A.8 Aspen Plus water mole fraction obtained by interpolation at 80° C for the system H_2O-MEG and their respective calculated deviations from literature 84
A.9 Aspen Plus pressures obtained by interpolation at 30° C for the system CH_4-MEG and their respective calculated deviations from literature . . 85
A.10 Aspen Plus methane mole fraction obtained by interpolation at 30° C for the system CH_4-MEG and their respective calculated deviations from literature 85
A.11 Aspen Plus pressures obtained by interpolation at 50° C for the system CH_4-MEG and their respective calculated deviations from literature . . 85
A.12 Aspen Plus methane mole fraction obtained by interpolation at 50° C for the system CH_4-MEG and their respective calculated deviations from literature 86
A.13 Aspen Plus pressures obtained by interpolation at 100° C for the system CH_4-MEG and their respective calculated deviations from literature . . 86
A.14 Aspen Plus methane mole fraction obtained by interpolation at 100° C for the system CH_4-MEG and their respective calculated deviations from literature 86
A.15 Aspen Plus pressures obtained by interpolation at 125° C for the system CH_4-MEG and their respective calculated deviations from literature . . 87
A.16 Aspen Plus methane mole fraction obtained by interpolation at 125° C for the system CH_4-MEG and their respective calculated deviations from literature 87

A.17 Aspen Plus pressures obtained by interpolation at 150° C for the system CH_4-MEG and their respective calculated deviations from literature . . 87
A.18 Aspen Plus methane mole fraction obtained by interpolation at 150° C for the system CH_4-MEG and their respective calculated deviations from literature 88
A.19 Aspen Plus pressures obtained by interpolation at 50° C for the system CH_4-MEG and their respective calculated deviations from literature . . 88
A.20 Aspen Plus methane mole fractions obtained by interpolation at 50° C for the system CH_4-MEG and their respective calculated deviations from literature 88
A.21 Aspen Plus pressures obtained by interpolation at 100° C for the system CH_4-MEG and their respective calculated deviations from literature . . 89
A.22 Aspen Plus methane mole fractions obtained by interpolation at 100° C for the system CH_4-MEG and their respective calculated deviations from literature 89
A.23 Aspen Plus pressures obtained by interpolation at 125° C for the system CH_4-MEG and their respective calculated deviations from literature . . 89
A.24 Aspen Plus methane mole fractions obtained by interpolation at 125° C for the system CH_4-MEG and their respective calculated deviations from literature 90
A.25 Aspen Plus pressures obtained by interpolation at 50° C for the system CH_4-MEG and their respective calculated deviations from literature . . 90
A.26 Aspen Plus methane mole fraction obtained by interpolation at 50° C for the system CH_4-MEG and their respective calculated deviations from literature 90
A.27 Aspen Plus pressures obtained by interpolation at 100° C for the system CH_4-MEG and their respective calculated deviations from literature . . 91
A.28 Aspen Plus methane mole fractions obtained by interpolation at 100° C for the system CH_4-MEG and their respective calculated deviations from literature 91
A.29 Aspen Plus pressures obtained by interpolation at 125° C for the system CH_4-MEG and their respective calculated deviations from literature . . 91
A.30 Aspen Plus CH_4 mole fraction obtained by interpolation at 125° C for the system CH_4-MEG and their respective calculated deviations from literature 92
A.31 Aspen Plus pressures obtained by interpolation at 25° C for the system CH_4-H_2O and their respective calculated deviations from literature . . . 92
A.32 Aspen Plus CH_4 mole fraction obtained by interpolation at 25° C for the system CH_4-H_2O and their respective calculated deviations from literature 92
A.33 Aspen Plus pressures obtained by interpolation at 40° C for the system CH_4-H_2O and their respective calculated deviations from literature . . . 93

A.34 Aspen Plus CH_4 mole fraction obtained by interpolation at 40° C for the system CH_4-H_2O and their respective calculated deviations from literature 93
A.35 Aspen Plus pressures obtained by interpolation at 50° C for the system CH_4-H_2O and their respective calculated deviations from literature . . . 93
A.36 Aspen Plus CH_4 mole fraction obtained by interpolation at 50° C for the system CH_4-H_2O and their respective calculated deviations from literature 94
A.37 Aspen Plus pressures obtained by interpolation at 25° C for the system CH_4-H_2O and their respective calculated deviations from literature . . . 94
A.38 Aspen Plus CH_4 mole fraction obtained by interpolation at 25° C for the system CH_4-H_2O and their respective calculated deviations from literature 94
A.39 Aspen Plus pressures obtained by interpolation at 40° C for the system CH_4-H_2O and their respective calculated deviations from literature . . . 95
A.40 Aspen Plus CH_4 mole fraction obtained by interpolation at 40° C for the system CH_4-H_2O and their respective calculated deviations from literature 95
A.41 Aspen Plus pressures obtained by interpolation at 25° C for the system CO_2-MEG and their respective calculated deviations from literature . . 95
A.42 Aspen Plus CO_2 mole fraction obtained by interpolation at 25° C for the system CO_2-MEG and their respective calculated deviations from literature 96
A.43 Aspen Plus pressures obtained by interpolation at 50° C for the system CO_2-MEG and their respective calculated deviations from literature . . 96
A.44 Aspen Plus CO_2 mole fraction obtained by interpolation at 50° C for the system CO_2-MEG and their respective calculated deviations from literature 96
A.45 Aspen Plus pressures obtained by interpolation at 100° C for the system CO_2-MEG and their respective calculated deviations from literature . . 97
A.46 Aspen Plus CO_2 mole fraction obtained by interpolation at 100° C for the system CO_2-MEG and their respective calculated deviations from literature 97
A.47 Aspen Plus pressures obtained by interpolation at 125° C for the system CO_2-MEG and their respective calculated deviations from literature . . 97
A.48 Aspen Plus CO_2 mole fraction obtained by interpolation at 125° C for the system CO_2-MEG and their respective calculated deviations from literature 98
A.49 Aspen Plus pressures obtained by interpolation at 50° C for the system CO_2-MEG and their respective calculated deviations from literature . . 98
A.50 Aspen Plus CO_2 obtained by interpolation at 50° C for the system CO_2-MEG and their respective calculated deviations from literature 99
A.51 Aspen Plus pressures obtained by interpolation at 100° C for the system CO_2-MEG and their respective calculated deviations from literature . . 99

A.52 Aspen Plus CO_2 mole fraction obtained by interpolation at 100° C for the system CO_2-MEG and their respective calculated deviations from literature . . . 99
A.53 Aspen Plus pressures obtained by interpolation at 125° C for the system CO_2-MEG and their respective calculated deviations from literature . . 100
A.54 Aspen Plus CO_2 mole fraction obtained by interpolation at 125° C for the system CO_2-MEG and their respective calculated deviations from literature . . . 100
A.55 Aspen Plus pressures obtained by interpolation at 150° C for the system CO_2-MEG and their respective calculated deviations from literature . . 100
A.56 Aspen Plus CO_2 mole fraction obtained by interpolation at 150° C for the system CO_2-MEG and their respective calculated deviations from literature . . . 101
A.57 Aspen Plus pressures obtained by interpolation at 50° C for the system CO_2-MEG and their respective calculated deviations from literature . . 101
A.58 Aspen Plus CO_2 mole fraction obtained by interpolation at 50° C for the system CO_2-MEG and their respective calculated deviations from literature . . . 101
A.59 Aspen Plus pressures obtained by interpolation at 100° C for the system CO_2-MEG and their respective calculated deviations from literature . . 102
A.60 Aspen Plus CO_2 mole fraction obtained by interpolation at 100° C for the system CO_2-MEG and their respective calculated deviations from literature . . . 102
A.61 Aspen Plus pressures obtained by interpolation at 125° C for the system CO_2-MEG and their respective calculated deviations from literature . . 102
A.62 Aspen Plus CO_2 mole fraction obtained by interpolation at 125° C for the system CO_2-MEG and their respective calculated deviations from literature . . . 103
A.63 Aspen Plus pressure obtained by interpolation at 25° C for the system CO_2-H_2O and their respective calculated deviations from literature . . . 103
A.64 Aspen Plus CO_2 mole fraction obtained by interpolation at 25° C for the system CO_2-H_2O and their respective calculated deviations from literature 104
A.65 Aspen Plus pressure obtained by interpolation at 50° C for the system CO_2-H_2O and their respective calculated deviations from literature . . . 104
A.66 Aspen Plus CO_2 mole fraction obtained by interpolation at 50° C for the system CO_2-H_2O and their respective calculated deviations from literature 105
A.67 Aspen Plus CO_2 mole fraction obtained by interpolation at 40, 80 and 120° C for the system CO_2-H_2O and their respective calculated deviations from literature . . . 105
A.68 Aspen Plus pressure obtained by interpolation at 40, 80 and 120° C for the system CO_2-H_2O and their respective calculated deviations from literature 105

B.1 Properties of glycols. Source: Union Carbide 1971, Worley 1966. 107
B.2 Different gas compositions obtained from literature review. 108
B.3 Typical rich gas transport specifications[20]. 109

List of Symbols

Symbol	Description
A_ϕ	Debye-Huckel parameter
A_x	Ionic strength on a mole fraction basis
D_s	Dielectric constant of the mixed solvent
D_w	Dielectric constant of water
e	Electron charge [C]
f_i^L	Fugacity of compound i in the liquid phase
f_i^V	Fugacity of compound i in the vapor phase
g^{ex^*}	Molar excess Gibbs free energy
$g^{ex^*,LR}$	Molar excess Gibbs free energy contribution from long range forces
$g^{ex^*,local}$	Molar excess Gibbs free energy contribution from local forces
K_i	Equilibrium constant for reaction i
Mm_{water}	Molar mass of water [kg/mol]
M_s	Molecular weight of solvent [kg/kmol]
n	Number of moles
n_{gas}	Number of moles of gas
n_{water}	Number of moles of water
N_o	Avogadro number [mol^{-1}]
P	Pressure [Pa/Atm/Bar]
P_i	Pressure of component i [kPa]
P_i^{sat}	Saturation pressure of component i [kPa]
P_{sim}	Simulated pressure [kPa]
P_{tot}	Total pressure[kPa]
R	Ideal gas constant [L atm/mol K]
r_k	Born radius of specied k
T	Temperature [°C/K]

Symbol	Description
ΔT	Temperature difference [°C]
$V_{m,std}$	Molar volume at standard conditions [L]
wt%	Weight percentage
x_i	Mole fraction of component i in liquid phase
x_k	Mole fraction of component k in liquid phase
y_i	Mole fraction of component i in vapor phase
z_k	Charge on species k
α_i	Loading component i
α_{exp}	Experimental loading
$\%\Delta_i$	Relative deviation
ϕ_i^L	Fugacity coefficient in liquid phase
ϕ_i^V	Fugacity coefficient in vapor phase
γ_i	Activity coefficient

List of Acronyms

AA Anti-agglomerants.

AARD Average Absolute Relative Deviation.

ARD Absolute Relative Deviation.

BOP Blowout preventor.

BTEX Benzene, toluene, ethylbenzene, xylene.

CH_4 Methane.

CO_2 Carbon dioxide.

DEG Diethylene glycol.

DRIZO a proprietary enhanced glycol concentration process.

ELECNRTL Electrolyte non-random two-liquid.

EOS Equations of state.

H_2CO_3 Carbonic acid.

H_2O Water.

H_2SO_4 Sulfuric acid.

KHI Kinetic hydrate inhibitors.

LACM Liquid activity coeffiient methods.

LDHI Low dosage hydrate inhibitors.

LLE Liquid liquid equilibrium.

LLV Liquid liquid vapor.

MEG Ethylene glycol.

nm Nanometer.

NOAA National oceanic and atmospheric administration.

NRTL Non-random two-liquid.

NTNU Norges teknisk-naturvitenskapelige universitet.

pH Potential hydrogen.

ppm Parts per million.

ppmv Parts per million volume.

VLE Vapor liquid equilibrium.

VLLE Vapor liquid liquid equilibrium.

Chapter 1
Introduction

Gas treating offshore refers to the set of processes that are required to achieve certain gas specifications in order to transport the gas from the reservoir to the onshore gas facilities in a safe and environmentally friendly manner. Each reservoir fluid is unique and requires specific treatment depending on its composition and physical conditions. It is of special interest for the oil and gas industry to bring the gas specifications to the optimum with the most efficient and economical process performance.

This work focuses on gas dehydration using glycol offshore by simulating different process options using commercial software Aspen Plus.

1.1 Motivation

The oil industry is divided into three major sectors: upstream, midstream and downstream. The upstream sector, which is also known as the exploration and production sector, consists of searching for underground deposits of hydrocarbons including crude oil and natural gas, and the drilling of exploration, appraisal and production wells to extract these hydrocarbons to the surface.

These underground deposits known as oil and gas reservoirs can be located in remote locations which turn the drilling, production and transportation of oil and gas streams into a very complex and challenging task. One of the biggest challenges offshore is to achieve the required flow assurance for the transport of natural gas in subsea pipelines. Treating natural gas is therefore important to achieve the required gas specifications for transportation, but also to protect equipment as well as for environmental and safety reasons.

Gas dehydration along with e.g. sour gas removal, mercury removal, salts removal and heavy hydrocarbon removal is an important process within natural gas treating,

mainly because water vapor is the most common unwanted impurity in natural gas[38].

Absorption of water by hygroscopic liquids is a very common commercial process and TEG has become the standard for natural gas dehydration on offshore gas processing facilities, especially through the use of a process known as DRIZO[38]. MEG on the other hand is injected directly into the sour gas stream coming from the wellhead as an alternative to methanol, to inhibit hydrates formation, mainly because of its low viscosity at low temperatures[32].

However, the use of MEG for water removal in sweetened natural gas is very interesting since it would eliminate the use of different glycols offshore, and allow the use of one single glycol for both sour and sweetened natural gas dehydration.

1.2 Objective

The overall objective is to simulate in Aspen Plus the application of MEG for water removal from natural gas. This work focuses on the simulation of the different MEG regeneration schemes and their application offshore to reach water content specifications for transportation.

1.3 Thesis Structure

This thesis is divided in 8 chapters.

Chapter 1 gives a brief introduction to the motivation and objectives of the thesis.

Chapter 2 provides an overview of the operations in the oil and gas industry and the challenges involved, especially in the natural gas processing offshore.

Chapter 3 gives an introduction to simulation of vapor-liquid equilibrium in Aspen Plus and the considerations to select the appropriate thermodynamic method, which is the foundation of this work.

Another important step that is imperative for the foundation and validity of the process simulation in Aspen Plus, is the validation of the main binary models used in this work. The validation process is described in chapter 4 together with the results analysis obtained.

Chapter 5 describes the definition of the problem, including the basis of design covering the different assumptions made in detail.

Chapter 6 describes the process of gas dehydration offshore and the different regeneration methods simulated in Aspen Plus, including the process parameters used and a comparison of the results obtained.

In chapter 7, two regeneration methods are selected based on the results obtained in chapter 6, and each process is modified by recovering the glycol that is being lost with the water vapors exiting the top of the regeneration column.

Conclusions are given in Chapter 8.

Chapter 2
Background

In petroleum exploration and production operations several challenges and risks are present during the process of oil and gas extraction from the reservoirs, especially offshore. In this chapter the main issues related to gas production are covered with a special focus on gas hydrates, which are a serious economic and safety concern. Hydrates in general can be both a problem and an opportunity, since they are considered to have a huge potential as an energy resource in the form of methane clathrates on e.g. the seabed, but they also represent a major flow assurance issue for the oil and gas industry[37].

One clear example of the potential risk that hydrates can represent was the challenges faced in the containment of the oil leak following the deepwater oil/gas well blowout of the Macondo well, back in 2010 in the Gulf of Mexico. At the water depths where the oil leak happened, the rapid formation of gas hydrate contributed to the failure of a 100 ton containment structure, leading to a spill of approximately 4.9 million barrels[37].

2.1 Offshore production processes

An offshore processing centre consists of several facilities, which may include oil production ships, condensate storage vessels and/or production platforms. The main elements in a typical production chain are shown in Figure 2.1. Multiphase flow is received on the processing platform, usually from several wells. The different flows often come from tie-back of subsea fields located nearby. Once the fluids are received on the platform the gas is separated from the water and the condensate, to be treated as single phase rich gas and transported to shore where the gas is further processed to sales gas[4].

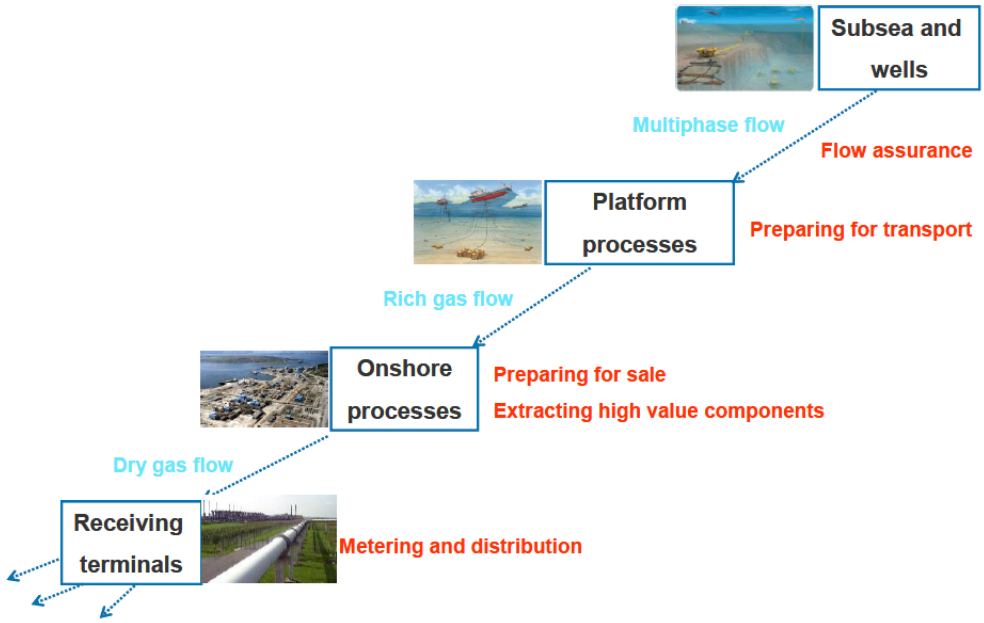

Figure 2.1: Offshore production chain. Picture taken from TEP4185 – Natural Gas Technology[4]

2.2 Flow assurance

Flow assurance is an important topic in the oil and gas industry. The objective is to secure and optimize the transport of oil and gas flow coming from the wellbore to the offshore processing facility and finally sent onshore. However, flow assurance is a major technical challenge in offshore fields development[64].

A minimum gas rate is required to avoid dynamic instabilities in pipelines, ensure that surge waves do not exceed liquid handling capacity, maintain continuous MEG injection and avoid hydrate incidents. From the different challenges mentioned, continuous MEG injection at the wellhead is extremely important to prevent hydrates formation in the pipelines. The used MEG is regenerated and re-injected to suppress hydrate formation[7]. A certain gas velocity is needed to be able to transport the injected MEG together with condensed water If the velocity becomes too low MEG will tend to accumulate in the pipeline and afterwards produced in the form of slugs. Therefore it is important to maintain the required minimum flow rate at which it is still possible to handle the largest liquid slug[47].

2.2.1 Corrosion and scale formation

Among the main flow assurance issues encountered in a gas or condensate system corrosion, scale and wax formation are very common problems.

The use of MEG for hydrate control by lowering the freezing point has an impact that can lead to corrosion, due to temperature drop. Water in the pipeline will at some point condensate and be in contact with H_2S and CO_2 present in the natural gas coming from the reservoir. The H_2S will form sulfuric acid (H_2SO_4) which causes corrosion when coming in contact with iron, however the corrosive effect and its impact increase at high temperatures (above 100°C)[40].

The CO_2 in contact with water will form a weak carbonic acid (H_2CO_3), which will corrode the iron in the pipeline wall producing iron carbonate. Corrosion is controlled by pH stabilization, by injecting an alkaline chemical together with MEG to decrease the solubility of the iron carbonate, and thereby neutralizing the sour condition of the reservoir gas. The iron carbonate will precipitate forming a thin iron carbonate film covering and protecting the pipeline wall surface from carbonic acid and water contact[16].

Solid scale formation happens due to precipitation of salt components from produced water, when the solubility changes with pressure and temperature varies. Precipitation will continue as long as the reservoir produces water, and this will eventually result in a thick layer of scale which at some point will completely restrict the flow through the pipeline. Scale control and removal is often done by adding chemicals to the produced fluid[12].

Wax formation occurs when long chained paraffinic hydrocarbon components precipitate due to a change in solubility resulting from a decrease in temperature, forming solids at temperature around ambient conditions. Wax formation is controlled by keeping the temperature of the fluid above the wax formation temperature or also by adding chemicals to the produced fluid. The removal of wax and cleaning of the pipeline is usually done by launching a scraper pig. Pigging is often required for general maintenance, liquid control or inspection[48].

2.2.2 Hydrate formation

Gas clathrates better known as hydrates, are crystalline solids consisting of water with small gas molecules (<0.9nm), trapped in an ice-like cage structure which is generated by hydrogen bonding of adjacent water molecules. The gas molecules, which typically consist of methane but it can also contain other hydrocarbons, N_2, H_2S and CO_2, creates a repulsion force against the water cage that prevents it from

collapsing. 1 cubic meter of hydrate can contain up to 170 cubic meters of gas[61]. Hydrates are found in nature at the bottom of cold seas and in arctic permafrost regions.

Most gases except hydrogen and helium can form hydrates but also, hydrates may form in completion fluids, which are control fluids used during the completion phase of a well before production starts, these are typically composed of water, MEG and different enhancement additives. Hydrates can also be formed in produced fluids coming from the reservoir, specially when formation water is produced with the natural gas[36].

Gas hydrates represent one of the main challenges for flow assurance. They are a big economical and a serious safety concern since they can not only cause blockages in pipelines and processing facilities, but also block the subsea control systems (riser, wellhead, BOP stack, kill lines and chokes), obstruct the movement of the drill string and lead to serious operational incidents[66]. In comparison to other risks or operational concerns such as the formation of waxes, scales or asphaltenes, hydrate plug formation rates are the highest and occur without any warning in offshore lines leading to days or even months of remediation[64]. Figure 2.2 shows an example of a hydrate plug in an offshore pipeline.

Figure 2.2: Hydrate plug offshore. Picture taken from SPE presentation[66].

Hydrates are typically formed at low temperature and high pressure, as a result of physical combination of water and gas. As shown in Figure 2.3, depending on temperature and pressure the total mixture may consist of a single phase with gas, a two phase with water and gas, a two phase with condensate and gas or a three phase with water, condensate and gas. The line labeled "hydrate-gas phase boundary" is significant, below this line, the free water phase will be converted to a solid hydrate phase and above this line methane hydrate will not form[55].

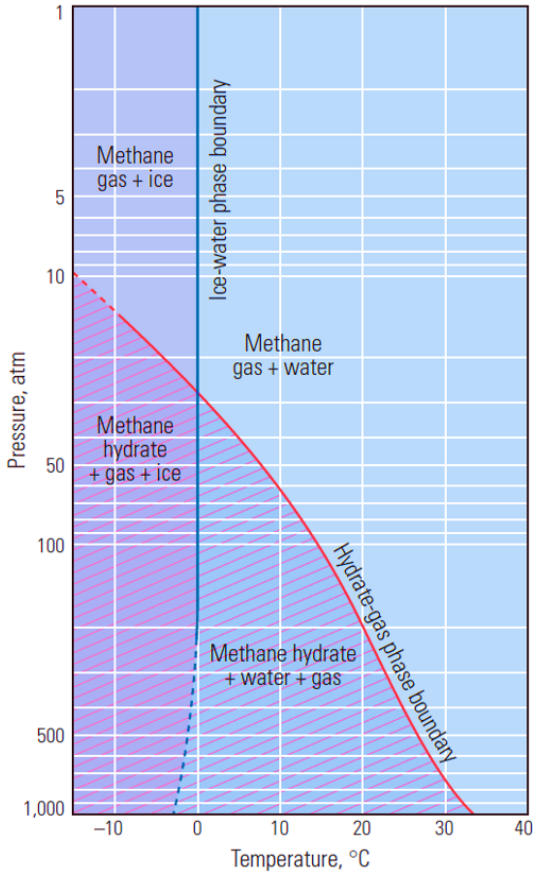

Figure 2.3: Methane hydrate stability chart. Chart modified after NOOA[55]

2.2.3 Hydrate prevention

Thermodynamic hydrate inhibition

Hydrates formation can be prevented by different methods. One inhibition method consists of shifting the hydrate stability zone to colder temperatures and/or higher

pressures. This can be achieved by adding a thermodynamic inhibitor such as methanol or MEG[27]. It can be observed from Figure 2.4 that the addition of MEG shifts the hydrate equilibrium curve to the left region of the original curve towards higher pressures and lower temperatures, such that the operational temperature and pressure of the pipeline system remains outside of the hydrate forming curve.

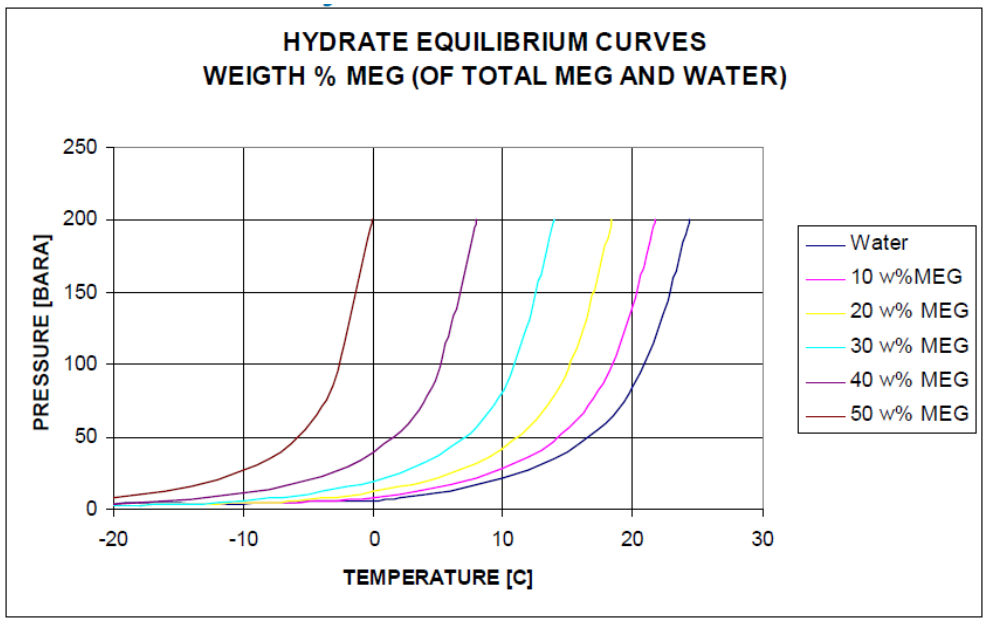

Figure 2.4: Hydrate inhibition by using MEG.[27].

Hydrate inhibition with insulation and heat

Among the different hydrate inhibition methods, one is based on prevention by using insulation or heating. Such as applying direct electrical heating to the pipeline or by using bundles and pipe-in-pipe. A heated bundle is shown in Figure 2.5, this *"consists of a pipe in which production fluids are flowed through the inner pipe and heated fluid is flowed through the outer pipe"*[42].

Electrical heating is shown in Figure 2.5. *"Similar to a heated bundle, electrical heating consists of heating the external surface of the production flowline. However, instead of using a temperature-controlled medium, a thermal blanket which applies constant heat flux is applied to the pipeline. This method has been used for plugs in onshore pipelines in the Arctic"*[42].

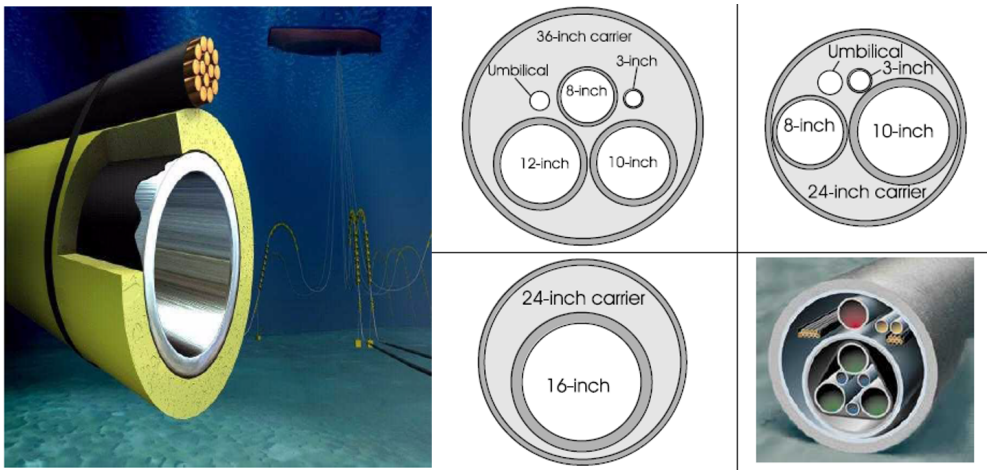

Figure 2.5: Dielectrical heating in the left side and bundles and pipe-in-pipe in the right side.[41].

Kinetic hydrate inhibition

Kinetic hydrate inhibitors (KHI) are normally water soluble polymers which prevent or delay the hydrate nucleation and growth for a certain time. These inhibitors are classified as "low dosage hydrate inhibitors" (LDHI), since the required effective dosages are much lower than those required for thermodynamic inhibitors. It is used for gas-water and gas-oil-water systems and there is no water cut limit. The best KHI's can prevent hydrate formation at subcooling to 12-10° C for 1-2 days and can handle higher subcooling if combined with MEG[22].

Anti-agglomerants hydrate inhibition

Anti-agglomerants (AA) form hydrate-in-oil dispersions that are transportable as slurry particles, they do not inhibit the formation of gas hydrates to the same level as kinetic inhibitors but rather preventing the agglomeration of hydrate crystals. Anti-agglomerants contain head-groups absorbing on hydrate crystal surfaces and oil-soluble tails that drag the hydrate particles into an oil phase which works as the transport medium for hydrate slurries. The overall viscosity is kept low to allow transport along the pipeline. The best AAs can prevent hydrate formation when subcooling to 15-17° C and can handle higher degrees of subcooling if combined with MEG but are limited to a maximum of 40% water cut[1].

2.3 Gas dehydration methods

It is important to keep in mind that the water removal process starts at the wellhead but also that the natural gas will be saturated with water after the sour gas removal process and therefore it is important that sweetened gas is dehydrated after sour gas treating.

Among the different methods for gas dehydration the two most common ones are adsorption with a solid material of crystalline structure and absorption with glycol which is a liquid desiccant.

In an adsorption process, the efficiency will depend on the adsorbent used. There are several types of adsorbents available, but the most efficient adsorbents are molecular sieves. Molecular sieves are aluminosilicates that have been altered to improve the adsorption characteristics, making it possible to achieve water contents below 0.1 ppmv[34].

In dehydration by absorption, it is possible to achieve very low water contents in the natural gas stream, as low as 10 ppmv depending on the purity of the lean glycol used[34]. The water is removed by a glycol solution because this is a liquid with strong affinity for water. The water is removed from the gas in an absorption column and the rich glycol will exit the bottom of the absorption column to be regenerated by distillation before it can be reused. Gas dehydration by glycol absorption will be discussed more thoroughly in chapter 6.

A different method that is not as common as the previous two is refrigeration, which employs cooling to condense the water molecule followed by inhibitor injection to prevent hydrate formation[45]. There is also a fourth method to dehydrate gas, which utilizes membrane processes and is considered a new alternative technology that can be applied to unmanned subsea operations[13]. However, membranes are considered noncompetitive due to disadvantages in the dehydration process such as lower selectivity, easy fouling by gas contaminants and high costs especially for large gas flow rates applications[59].

Finally, gas can also be dehydrated with supersonic processes. These processes consist of a twister supersonic separator that combines physical, aerodynamics, thermodynamics and fluid dynamics to condense and separate water at supersonic velocity[19]. Dehydration by membrane permeation and supersonic processes are seldom used.

2.4 MEG as an absorbent

Glycols are organic compounds with very high affinity to water due to the two hydroxil groups attached to the carbon atoms. Ethylene glycol, also called 1,2-ethanediol or mono ethylene glycol (MEG) is the simplest from the glycols[18]. MEG is the most used thermodynamic inhibitor for hydrate prevention in multiphase flow lines, from medium to long range transport distances[43].

After the multiphase flow stream coming from the well has been separated and stabilized, the gas is sweetened and is ready to dehydrate for exporting. TEG being the most popular glycol used in dehydration units on offshore facilities. TEG is the most popular compared to other glycols, because it is easy to regenerate and presents lower solvent losses[5]. Nonetheless, selecting a different glycol from TEG, such as MEG, may have several benefits. MEG is well known to be a less costly option when selecting a glycol for gas dehydration. It requires less energy for regeneration and since MEG is the least polar among other glycols i.e. TEG and DEG, it absorbs the least amount of BTEX (benzene, toluene, ethylbenzene and xylene) compounds, which will have an added benefit in emission reduction[6]. Other added benefits of choosing MEG over other glycols are relatively low toxicity and low flammability. MEG is quite commonly used in the oil and gas industry globally, an overview from 2009 is shown in Figure 2.6.

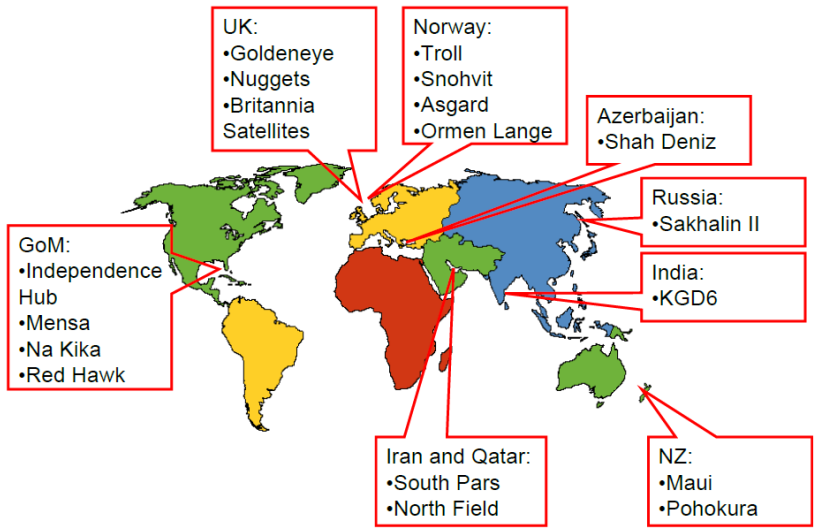

Figure 2.6: MEG plants worldwide in 2009. Picture taken from SPE international: "MEG Regeneration Technical Meeting 18 June 2009, Port Campbell".

However, MEG has the disadvantage that is less stable. It's initial decomposition temperature is 165° C which makes it more challenging to regenerate with the necessary degree of purity[38]. In Appendix Table B.1 the characteristics of the different glycols that are used for gas treating are listed.

Other common issues related to MEG regeneration, is fouling of equipment by iron carbonate, Ca^{+2}/Mg^{+2} salt deposits and contamination of MEG and condensate. Also, corrosion in pipelines due to accumulation of glycol that is lost due to carryover with dehydrated gas[25].

Chapter 3
VLE simulation in Aspen Plus

A key step to ensure that the properties of pure components and mixtures are properly estimated when setting up a simulation, is the correct selection of the thermodynamic method. The selection will depend on the present components and their affinity.

In Aspen Plus, it is possible to calculate numerous thermodynamic and transport properties. Aspen Plus has an in-built database that enables the estimation of thermodynamic and transport properties for both pure components or mixtures. The used parameters for these calculations were determined by either fitting experimental data or using theoretical methods.

In this section, the basic concepts of thermodynamic methods in Aspen Plus are reviewed together with the criteria considered for selecting the model.

3.1 Aspen Plus thermodynamic methods

The phase equilibrium, the physical and thermodynamic properties for both pure fluids and mixtures are considerably affected by the strength of inter-molecular forces. The greater the magnitude and the amount of the inter-molecular forces, the more non-ideal behavior the fluids will have[3].

The modeling of systems such as pure fluids and mixtures of non polar molecules (hydrocarbons), where only the "physical" forces of attraction and repulsion between molecules is present, is more appropriately done through equations of state (EOS)[15]. EOS, permit consideration of a wide range of pressures and temperatures in a unified way.

Between polar molecules (organic acids, alcohols, bases, water) hydrogen bonds appear, which lead to chemical forces that can be strong leading to non-ideal behaviors like dimerization in vapor phase, azeotropes in the liquid phase and phase separation. For these systems the liquid activity coefficient methods (LACM) are used for liquid

phase and equations of state (EOS) for vapor phase.

The parameters of the LACM methods are adjusted using experimental data. For blends of non polar and moderately polar substances it is possible to use modified EOS that predict the behavior of the mixture in both vapor and liquid phase well [67].

3.1.1 Phases equilibrium calculation

Fugacity is the basis for the phase equilibrium, and it depends on the temperature, pressure and phase composition. Liquid-vapor equilibrium must be fulfilled for each compound i in both phases:

$$f_i^L = f_i^V \tag{3.1}$$

Where:

f_i^L is the fugacity of compound i in the liquid phase.
f_i^V is the fugacity of compound i in the vapor phase.

The fugacity of the vapor is always calculated with equations of state, whereas for liquids, two methods can be used, equations of state and activity coefficient methods.

Phases equilibrium calculation with EOS

When using EOS, the fugacities may be calculated by:

$$f_i^L = \phi_i^L x_i P \tag{3.2}$$

$$f_i^V = \phi_i^V y_i P \tag{3.3}$$

Where ϕ_i^l and ϕ_i^v are the fugacity coefficients in the liquid and vapor phase respectively, x_i and y_i are the mole fractions in the liquid and vapor phase respectively, and P the system pressure. Both are calculated using equations of state. Balancing both fugacities in the liquid-vapor equilibrium gives us:

$$K_i = \frac{y_i}{x_i} = \frac{\phi_i^L}{\phi_i^V} \tag{3.4}$$

Phases equilibrium calculation with LACM

If the LACM method is used, the following equations apply:

$$f_i^{L,0} = \gamma_i x_i f_i^{L,0} \tag{3.5}$$

$$f_i^{L,0} \approx P_i^{sat} \longrightarrow f_i^L = \gamma_i x_i P_i^{sat} \tag{3.6}$$

Where γ_i is the activity coefficient calculated through LACM and $f_i^{L,0}$ is the fugacity of the liquid pure compound i at the mixture's temperature and pressure.The latter can be approximated by the vapor pressure of component i at moderate pressures. The fugacity in the vapor phase is calculated, using EOS with equation 3.3.

In equilibrium it is fulfilled:

$$\gamma_i x_i P_i^{sat} = \phi_i^V y_i P \longrightarrow K_i = \frac{y_i}{x_i} = \frac{\gamma_i P_i^{sat}}{\phi_i^V P} \tag{3.7}$$

At low to moderate pressures, the vapor phase can be assumed to be ideal $\phi_i^V \approx 1$, according to Dalton's law $P_i = y_i P$, therefore:

$$P = \sum_{i=1} P y_i = \sum_{i=1} \gamma_i x_i P_i^{sat} \tag{3.8}$$

And if ideal behaviour is considered for the liquid phase, then Raoult's law is applicable:

$$\gamma_i \approx 1 \longrightarrow P = \sum_{i=1} P y_i = \sum_{i=1} x_i P_i^{sat} \tag{3.9}$$

In the LACM methods a problem occurs when there are supercritical components in the mixture. Since there is no supercritical P^{sat} component in the mixture, because there is no P for those compounds, it cannot be calculated in a conventional way. It is necessary to treat them by the use of Henry constants. This is only valid if the supercritical concentration of the component in the liquid phase is small (<5% molar)[9].

The LACM are based on the excess Gibbs free energy which is the difference between the Gibbs free energy of the real and the ideal mixtures. Different models have been proposed for excess Gibbs free energy for binary mixtures based on theories of mixtures. The models can be extended to multi component mixtures using only the binary interactions between the components[67].

3.2 Property selection method

In order to select the correct model different criteria have been determined, including the presence of polar compounds such as water and MEG. Since non-ideality is expected, activity coefficient models are used. Other important criteria are the presence of light gases such as nitrogen and finally the presence of non-condensable components such as methane, carbon dioxide and hydrocarbon mixtures in general. These components are treated in Aspen Plus as Henry components in order to characterize their equilibrium with water and MEG[17].

The NRTL (non-random two-liquid) model is recommended for highly non-ideal systems, and can be used for VLE, LLE and VLLE applications[67]. The equation for the NRTL model is shown below[54].

$$ln\gamma_i = \frac{\sum_j x_j \tau_{ji} G_{ji}}{\sum_k x_k G_{ki}} + \sum_j \left(\frac{x_j Gij}{\sum_k x_k G_{kj}} \left(\tau_{ij} - \frac{\sum_m x_m \tau_{mj} G_{mj}}{\sum_k x_k G_{kj}} \right) \right) \tag{3.10}$$

Where

$$\begin{aligned} G_{ij} &= exp(-\alpha_{ij}\tau_{ij}) \\ \tau_{ij} &= a_{ij} + b_{ij}/T + e_{ij} lnT + f_{ij} T \\ \alpha_{ij} &= c_{ij} + d_{ij}(T - 273.15) \\ G_{ii} &= 1 \\ \tau_{ii} &= 0 \end{aligned}$$

The binary parameters a_{ij}, b_{ij}, c_{ij}, d_{ij}, e_{ij} and f_{ij} used by the model can be determined from VLE and/or LLE data regression. For the systems studied in this work, the parameters were available in Aspen Plus.

However, the ELECNRTL model is used in this work to simulate the gas dehydration system in Aspen Plus, since the presence of electrolytes is very common

during rich MEG regeneration, leading to problems such as, salt precipitation and sour water solutions[69].

The ELECNRTL model is an expansion of the NRTL model including a larger amount of interactions in order to include the electrolytes simulation capabilities[67]. This model can handle a wide range of concentrations, as well as aqueous and mixed solvent, and it considers that the excess Gibbs free energy in the electrolyte system is the sum of two contributions. As modeled with the NRTL model[52]:

$$g^{ex^*} = g^{ex^*,LR} + g^{ex^*,local} \tag{3.11}$$

Where

g^{ex^*} is the molar excess Gibbs free energy.
$g^{ex^*,LR}$ is the molar excess Gibbs free energy contribution from long range forces.
$g^{ex^*,local}$ is the molar excess Gibbs free energy contribution from local forces.

The local or short-range forces, are those between all the species that include the local ion-molecule, ion-ion, and molecule-molecule interactions. This local contribution is derived as per the NRTL model.

The long-range forces refer to the electrostatic ion-ion interactions which are modeled by combining the Pitzer-Debye-Huckel formula and the Born expression.

$$g^{ex^*,RL} = g^{ex^*}_{PHD} + g^{ex^*,Born} \tag{3.12}$$

The Pitzer-Debye-Huckel formula is given by Equation

$$g^{ex^*}_{PHD} = -RT\left(\sum_m x_k\right)\left(\frac{100}{M_s}^{\frac{1}{2}}\right)\left(\frac{4A_\phi I_x}{\rho}\right)ln\left(1+\rho I_x^{\frac{1}{2}}\right) \tag{3.13}$$

Where

x_k is the liquid phase mole fraction.
M_s is the solvent molecular weight in kg/kmol.
A_ϕ is the Debye-Huckel parameter.
A_x is the ionic strength on a mole fraction basis.
ρ is the closest approach parameter.

$$A_\phi = \frac{1}{3}\left(\frac{2\pi N_o d}{1000}\right)^{\frac{1}{2}}\left(\frac{e^2}{D_w k_B T}\right)^{1.5} \tag{3.14}$$

Where

N_o is the Avogadro's number.
d is the solvent density.
e is the charge of an electron.
D_w is the dielectric constant for waters.
k_B is the Boltzman constant.
T is temperature in K.

$$I_x = 0.5\sum_k x_k z_k^2 \tag{3.15}$$

Where z_k is the charge on species k.

The Born expression is given by Equation 3.16

$$g^{ex^*,Born} = RT\left(\frac{e^2}{2k_B T}\right)\left(\frac{1}{D_s} - \frac{1}{D_w}\right)\left(\sum_k \frac{x_k z_k^2}{r_k}\right)10^{-2} \tag{3.16}$$

Where D_s is the dielectric constant of the mixed solvent and r_k is the Born radius of species k.

Chapter 4

Vapor-liquid equilibrium validation

To ensure realistic simulation results, it is necessary to compare the values simulated in Aspen Plus against experimental data.

The validation of the model has been done for the relevant binary systems which comprise of compounds that form part of the natural gas stream to be dehydrated (CH_4 and water) and the studied solvent, MEG. From the non-hydrocarbon compounds, CO_2 is the component that is present in the largest quantity, therefore it may be interesting to study its effect on the process, thus the solubility parameters of CO_2 on MEG and water are validated. The gas stream composition and the assumptions made for the simulations will be discussed in more detail in chapter 5.

The pressure range covered in the simulations encompasses pressures close to vacuum up to 115 bar and temperature range from 25°C up to 161°C. Thus, the binary vapor-liquid equilibria sub-models were validated over this pressure and temperature range if experimental data was available.

In this section the VLE validation methodology is described, and the values obtained from simulations are compared against data reported in literature and in-house data.

4.1 Validation methodology

In Aspen Plus flowsheet, the FLASH model was used to perform the vapor-liquid equilibrium calculations because the studied systems only contain one vapor phase and one liquid phase. The setup of the model in the flowsheet is shown in Figure 4.1.

To determine the bubble point pressure, the temperature and the vapor fraction were set as design variables using a FLASH. FLASH uses rigorous vapor-liquid equilibrium calculations to calculate the phase composition of a mixture at a given

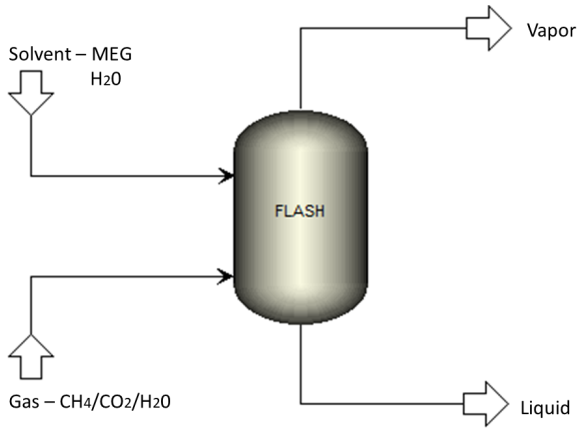

Figure 4.1: Flowsheet used for validations.

pressure and temperature.

The vapor fraction of the FLASH was set to 0.00001, to separate the feed mixture into a vapor stream rich in solute and a liquid stream rich in solvent[58]. The flow rate of the solvent was kept constant and a series of sensitivity analysis were simulated, in which the temperature of the FLASH was specified along with the input feed flow rates of the solute/gas. Different sets of data points were obtained for each system covering different temperatures of interest, by varying the input flow rates of the solute/gas with approximate 200 points per each sensitivity analysis.

Each one of the calculated total pressures were plotted against the mole fraction of the studied component and compared to literature.

For a better quantification of the predictive capacity of the model in Aspen Plus, the relative deviation, absolute relative deviation, average absolute relative deviation and mean absolute deviation were calculated between experimental and simulated data.

Relative deviations $\%\Delta_i$ were calculated with equation 4.1, in order to evaluate whether the model properly predicts the experimental data points.

$$\%\Delta_i = \frac{P_{sim} - P_{exp}}{P_{exp}} \cdot 100\% \tag{4.1}$$

Then the absolute relative deviation ARD for each point was calculated with

equation 4.2 in order to obtain the average absolute relative deviation AARD with equation 4.3. AARD measures how good the model predicts the experimental data points.

$$ARD = |\%\Delta_i| \tag{4.2}$$

$$AARD = \frac{1}{n}\sum_{i=1}^{n}|\%\Delta_i| \tag{4.3}$$

By calculating the mean using equation 4.4, which is the average of all the relative deviations, it is possible to calculate the mean absolute deviation MAD, according to equation 4.5. MAD is the average distance between each data point and the mean, it quantifies the variability in the data points of the model by calculating how much a particular data point deviates from the average relative deviation.

$$\overline{\%\Delta_i} = \frac{1}{n}\sum_{i=1}^{n}\%\Delta_i \tag{4.4}$$

$$MAD = \frac{1}{n}\sum_{i=1}^{n}\left|\%\Delta_i - \overline{\%\Delta_i}\right| \tag{4.5}$$

Due to the fact that the experimental values and the calculated values from Aspen Plus in the sensitivity analysis were not the same, a linear interpolation between the simulated values was done in order to compare the predicted models with the experimental values.

Interpolations were calculated with excel using the "forecast" function, to compare the predicted pressures against experimental pressures, based on the interpolated mole fractions. Since it is of special interest to know the amount of solute absorbed by MEG, mole fractions were also predicted based on interpolated pressures. To ensure that the results obtained with the forecast function were correct, the interpolation intervals were chosen manually for each data point along the entire sensitivity analysis and a quality check for one set was performed according to formulas 4.6 and 4.7.

$$P_{sim} = P_1 + (P_2 - P_1)\Big(\frac{\alpha_{exp} - \alpha_1}{\alpha_2 - \alpha 1}\Big) \tag{4.6}$$

$$\alpha_{sim} = \alpha_1 + (\alpha_2 - \alpha_1)\Big(\frac{P_{exp} - P_1}{P_2 - P_1}\Big) \tag{4.7}$$

The plots showing the results from the different validations will be shown in the following sections of this chapter. Additionally, the simulation results that were interpolated and compared to literature data can be found in Appendix A, including the percentage deviations for each system.

4.2 Literature review - VLE data

In the table 4.1 a summary of the available data used for validation of the vapor-liquid equilibria model are listed..

Table 4.1: Available experimental VLE data for the relevant systems.

	Temperature range °C	**Pressure range KPa**	**Mole fraction range**	**Reference**
H_2O-MEG	60-80	0.22-47.44	0-1	Horstman et al[26]
	60	0.214-19.931	0-1	Villaman et al.[68]
	50	0.316-5.978	0-1	Gonzalez and Van Ness[24]
CH_4-MEG	50-125	0-15490	0.00016-0.0179	Jou et al.[29]
	30-150	0-14000	0.0015-0.0291	Galvao and Francesconi[23]
	50-125	0-39617	0.0005-.0421	Zheng et al.[70]
CH_4-H_2O	25-50	0-19490	0.0006-0.0026	Frost et al.[21]
	25-40	0-18000	0.0002-0.0023	Chapoy et al.[11]
CO_2-MEG	25-125	0-20290	0.000693-0.1388	Jou et al.[30]
	30-150	0-6283	0.0045-0.0538	Galvao and Francesconi[23]
	50-125	0-38400	0.0049-0.1724	Zheng et al.[70]
CO_2-H_2O	40-120	0-445.7	0.000448-0.000687	Blanca[10]
	25-50	105-409	0.00026-0.00293	Serpa et al.[60]

4.3 H_2O pressure validation

The water pressure was predicted with Aspen Plus and compared to literature data from tables[50] and experimental data obtained in previous work[10]. The results are shown in Figure 4.2.

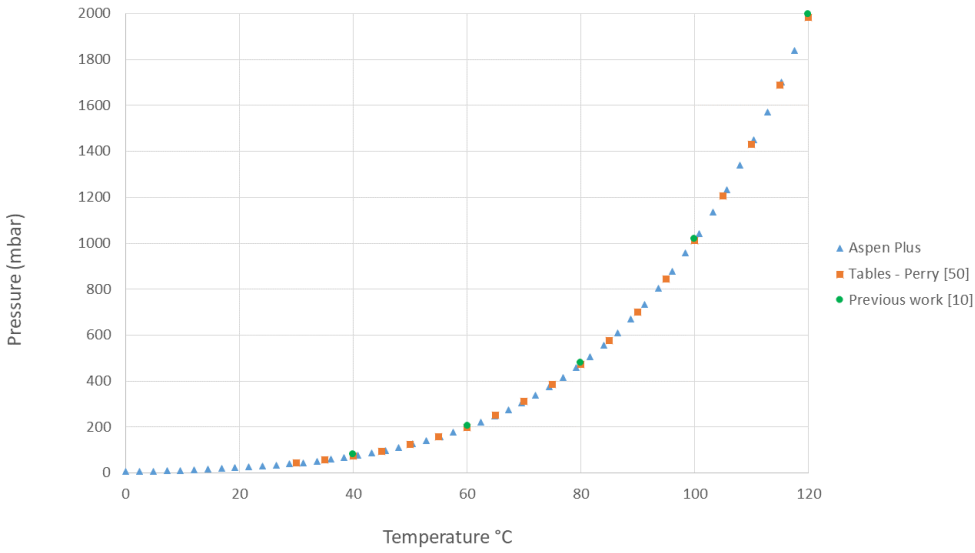

Figure 4.2: Vapor pressure of water in the temperature range of $30 - 120°C$. Triangles represent the models, squares represent literature data and circles represent experimental data from previous work.

It is clear that all the data points fall in the same curve and there are no obvious deviations between the predicted values using Aspen Plus, the literature data and the experimental data.

4.4 Solubility of H_2O in MEG

Since the absorption and regeneration of water-MEG system are important to achieve dry gas and lean MEG specifications, this is a relevant binary system to validate. Water mole fractions were plotted against pressures and compared against available experimental data at 50°C, 60°C and 80°C. No experimental data was available to validate the model at higher temperatures, therefore it was not possible to validate regeneration temperatures of up to 161°C.

Through the visual analysis of Figure 4.3 it is established that the simulated values fall in the same curve as the experimental data points along the entire data set, showing a slightly higher deviation as the pressure increases but without significant differences.

In general, it is observed that the experimental and the simulated data agree well with each other. For example, at 50°C the simulated data was compared against

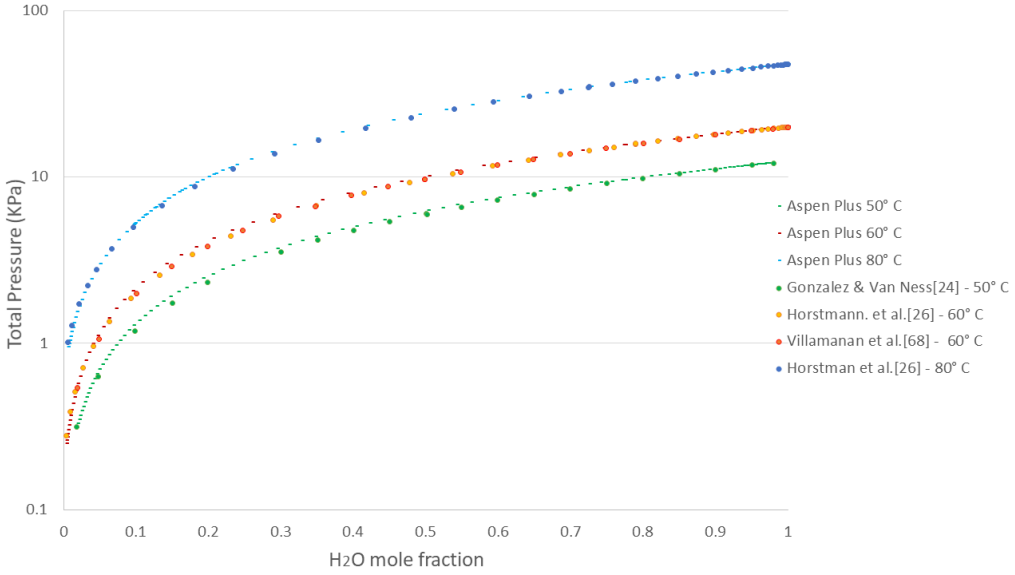

Figure 4.3: Total pressure on a log scale as a function of liquid H_2O mole fraction in MEG, in the temperature range of $50 - 80°C$. The dotted lines represent the models and the circles represent the experimental data.

experimental data from Gonzalez and Van Ness[24], as shown in Appendix Tables A.1 and A.2. Based on the interpolated mole fractions, the pressures predicted by the model showed an average absolute relative deviation (AARD) of only 4% from the pressures in the literature between 0.31 and 12.14 KPa. For absorber simulations at approximately 50°C, the required energy to absorb water can be expected slightly higher compared to reality. The model behaves similarly for the predicted mole fractions at the interpolated pressures with an average absolute relative deviation of 4% from literature data. The ELECNRTL model in Aspen Plus gives an accurate prediction of the amount of water that can be absorbed with MEG.

As the temperature increases the deviations from experimental data decrease. Showing an even better agreement between the simulated and experimental data. At 60°C and 80°C, the simulated data was compared against experimental data from Horstman et al.[26]. The average absolute relative deviation (AARD) results within that temperature range were less than 0.5% for predicted pressures and mole fractions. At 60°C mean absolute deviation was 3%, which is the maximum value observed.

At 60°C the simulated values were also compared with experimental data from

Villaman et al.[68]. The average absolute relative deviation (AARD) results were slightly higher compared to those from Horstman et al. but still very low, less than 2% for both the interpolated pressures and the interpolated mole fractions. The mean absolute deviation (MAD) however was only 2%.

This binary system has a high solubility. Since both water and MEG are polar compounds and can form complexes. These also show a more non-ideal behaviour than other non-polar compounds such as methane. Overall, it can be concluded that the VLE-model used to represent MEG-water -system is accurate and can be used in simulations.

4.5 Solubility of CH_4 in MEG

Because methane is the main component in natural gas, CH_4-MEG is another key system to evaluate. Since the solubility of hydrocarbons decreases as the carbon chain increases, and therefore becoming more hydrophobic, it has been considered that other carbon compounds in natural gas are not imperative to validate.

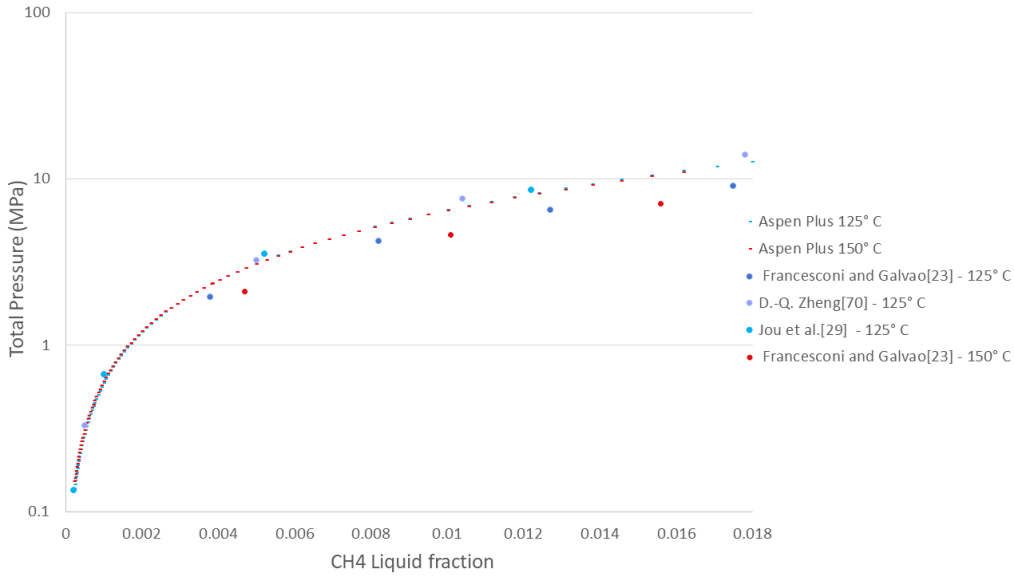

Figure 4.4: Total pressure on a log scale as a function of liquid CH_4 mole fraction in MEG, in the temperature range of $125 - 150°C$. The dotted lines represent the models and the circles represent the experimental data.

The simulated data was compared against experimental data from Francesconi

and Galvao [23]. At 30°C the lower the pressure, the more the model overpredicts the solubility and, as the pressure increases the model starts to under predict the solubility. As the temperature increases the model tends to underpredict the solubility along the entire range of pressures, showing a maximum of 26-29% under prediction at 150°C.

In the absorption column where the gas stream containing mostly methane is fed at the bottom inlet at 50°C and 115 bar, comparing against experimental data from Francesconi and Galvao [23], it can be expected that the model underpredicts absorpion of methane in MEG, meaning that in reality more methane is being absorbed by MEG than what the model predicts. The average absolute relative deviation (AARD) at this temperature, was 12% for the predicted pressures and 13% for the predicted mole fractions. The mean absolute deviation (MAD) was within the same ranges.

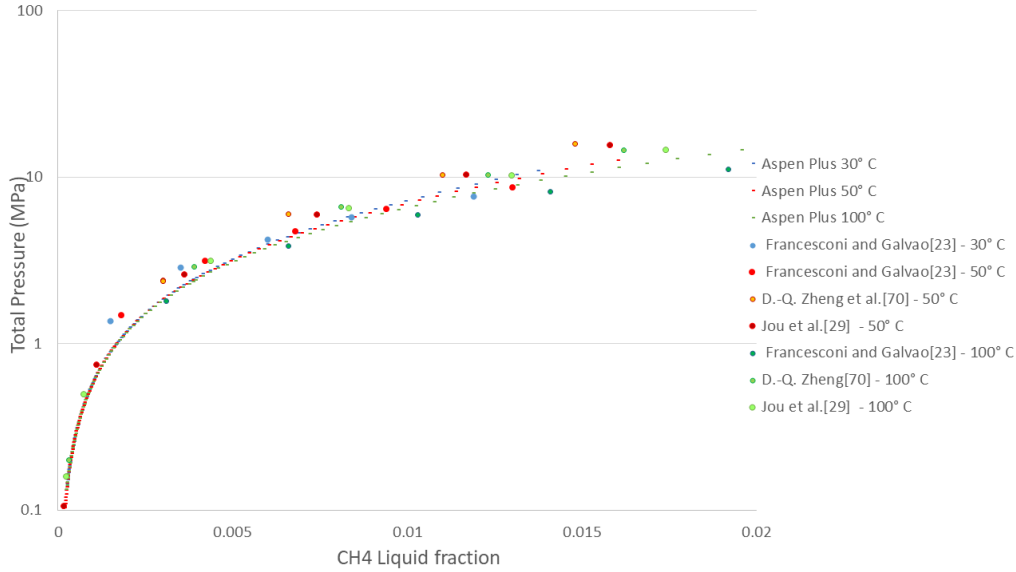

Figure 4.5: Total pressure on a log scale as a function of liquid CH_4 mole fraction in MEG, in the temperature range of $30 - 100$°C. The dotted lines represent the models and the circles represent the experimental data.

However, at 50°C compared against experimental data from D.Q. Zheng et al.[70] and Jou et al.[30], the model overpredicts the absorption of methane in MEG and no underprediction is observed. The average absolute relative deviation (AARD) at this temperature was higher, especially for the deviations from D.Q. Zheng et al.

experimental data which was around 25-27%. The mean absolute deviation (MAD) was as low as 2%, meaning that the model predicts better results when it is compared to experimental data from Francesconi and Galvao. It also shows higher variations from the average relative deviation, which can also be observed with the over- and underpredictions.

As the temperature increases, the deviations tend to increase when comparing the results with experimental data from Francesconi and Galvao[23]. The maximum deviations are observed at 150°C with a maximum average absolute relative deviation (AARD) of 47% for the predicted pressures and 28% for the predicted mole fractions.

On the other hand, when comparing the results against experimental data from D.Q. Zheng et al.[70] and Jou et al.[30] the deviations decrease below 9% at 125°C with mean absolute deviations (MAD) around 2%. Meaning that the model can give good predictions with very low variations from the average solubility, keeping in mind that the model tends to underpredict the results.

In general, it is clearly observed that both graphically and analytically, that the experimental data is not consistent since the different data sources do not agree with each other. Overall, the data fit is good and the model is able to accurately predict the vapor-liquid equilibrium at temperatures 30-150°C.

4.6 Solubility of CH_4 in H_2O

Validation of the binary system CH_4-H_2O has been done considering that CH_4 is the stripping gas for one of the regeneration schemes studied in this work. The simulated isotherms in Aspen Plus and the experimental data from literature were plotted for the temperature range between 25-50°C as shown in Figure 4.7.

From the plot it can clearly be seen that there is a very good agreement between the simulated isotherms and the experimental data. Especially for the isotherm at 25°C, which falls in between all of the experimental data points. The isotherm at 40°C at low pressures shows a good agreement with experimental data from Chapoy et al.[11] but as the pressure increases, the model starts to underpredict the absorption results. Compared to Frost et al.[21], the model overpredicts the absorption of CH_4 but as pressure increases, the model underpredicts the absorption results. At 50°C, the model shows similar results as for the previous isotherms.

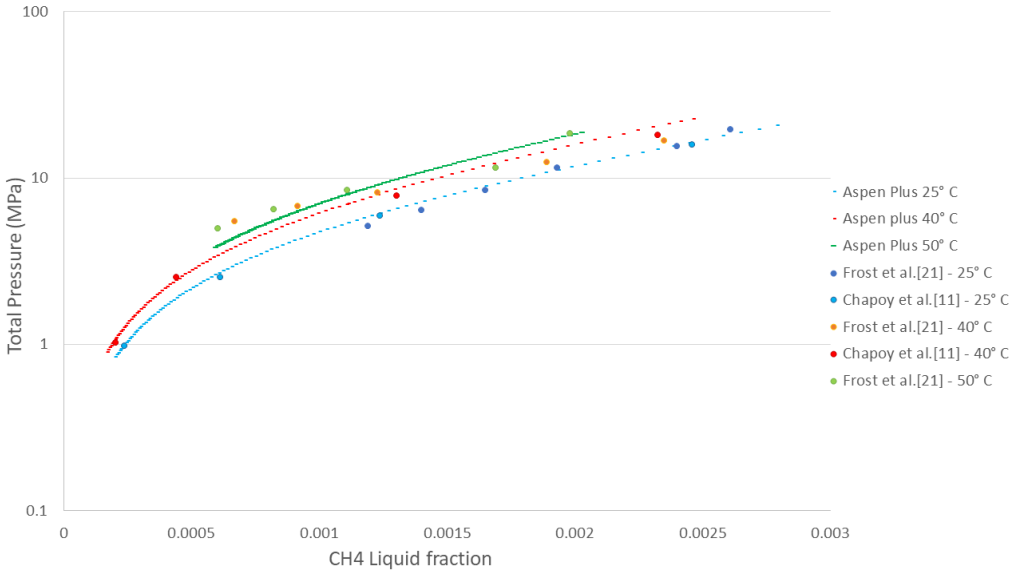

Figure 4.6: Total pressure on a log scale as a function of liquid CH_4 mole fraction in H_2O, in the temperature range of $25-50°C$. The dotted lines represent the models and the circles represent the experimental data.

At 25°C the average absolute relative deviation (AARD) results are less than 7% for both predicted pressures and mole fractions. In comparison with the experimental results of Frost et al. and Chapoy et al. Mean absolute deviation (MAD) is around 9% compared to the experimental data of Frost et al. and less than 2% from Chapoy et al. experimental data. It is clear that the simulated results are more in line with the experimental data from Chapoy et al. and have almost no variation.

At 40°C compared to Chapoy et al. experimental data, the average absolute relative deviation (AARD) is less than 9% and the mean absolute deviation less than 6%, while for Frost et al. the deviations are considerably higher with an average absolute relative deviation and mean absolute deviation of around 18% for the predicted pressures. Better results are observed for the simulated isotherm at 50°C compared to the results at 40°C for Frost et al.

In general it can be said that the Aspen Plus model is able to predict the solubility of the binary system CH_4-H_2O with good results and any expected over- and underpredictions are low.

4.7 Solubility of CO_2 in MEG

It is of interest to validate the binary system CO_2-MEG since MEG can help to separate any remaining CO_2 in the gas stream.

Through the visual analysis of Figures 4.7 and 4.8 it is established that the CO_2-MEG model is in acceptable agreement with the experimental data at low temperatures. At higher temperatures the model deviates more from the experimental data. The biggest differences are given for the experimental data from Francesconi and Galvao[23] at 150°C, as shown in Appendix Tables A.55 and A.56, with a maximum average absolute relative deviation (AARD) of 145% for the predicted pressures and 49% for the predicted mole fractions. The mean absolute deviation (MAD) is as high as 61% which implies that the model would give a poor prediction, and the variations from the average relative deviations will increase with increased pressures and temperatures.

As the pressures and temperatures increase, the model tends to underpredict the solubility of CO_2 in MEG in a greater order than for example the predictions for CH_4 in MEG. The predictions for CO_2 in MEG can be expected to be less accurate, showing bad results and less CO_2 being absorbed in MEG than what it would actually be in reality.

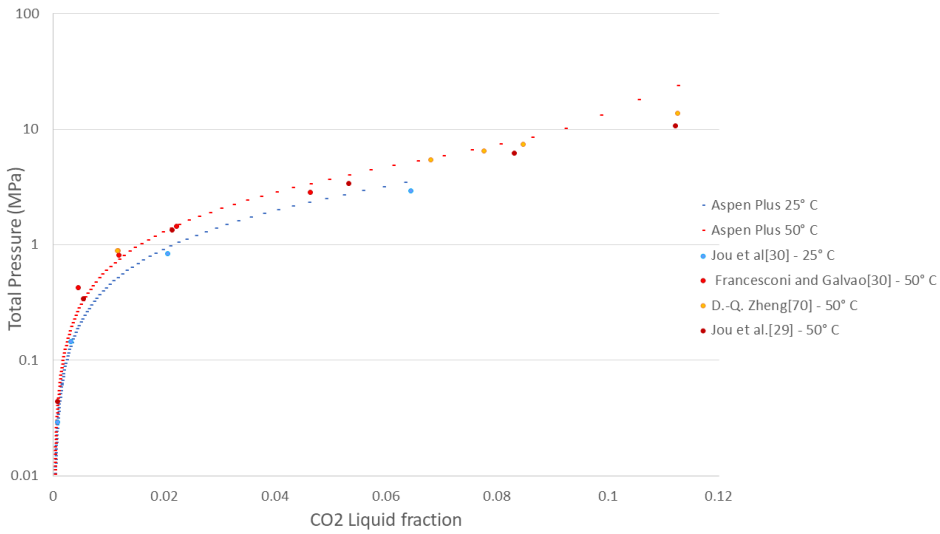

Figure 4.7: Total pressure on a log scale as a function of liquid CO_2 mole fraction in MEG, in the temperature range of $25 - 50$°C. The dotted lines represent the models and the circles represent the experimental data.

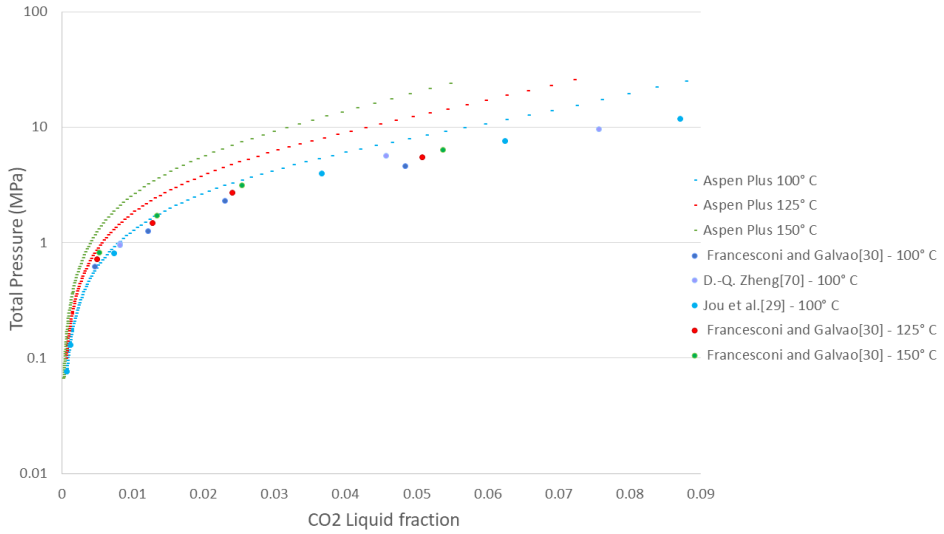

Figure 4.8: Total pressure on a log scale as a function of liquid CO_2 mole fraction in MEG, in the temperature range of $100 - 150°C$. The dotted lines represent the models and the circles represent the experimental data.

4.8 Solubility of CO_2 in H_2O

Figure 4.9 shows the validation for the binary system CO_2- H_2O.

It can be observed that there is a good agreement with the experimental data from Serpa et al.[60] at 25°C, since the predicted values from Aspen Plus fall in between all the experimental data points. The average absolute deviation (AARD) is 28% and the mean absolute deviation (MAD) is 21% for the predicted pressures. The deviations may seem high but it is important to bear in mind that the order of relative magnitude in the fractions is extremely low, especially compared to the other binary systems. Any differences observed between the experimental and simulated data do not have any noteworthy impact.

At 50°C the isotherm predicted with Aspen Plus falls below the experimental data points, meaning that the model underpredicts the absorption, especially at the lowest pressures. As the pressure increases the relative deviation decreases. The average absolute deviation (AARD) is 7% and the mean absolute deviation (MAD) is 4% for the predicted pressures

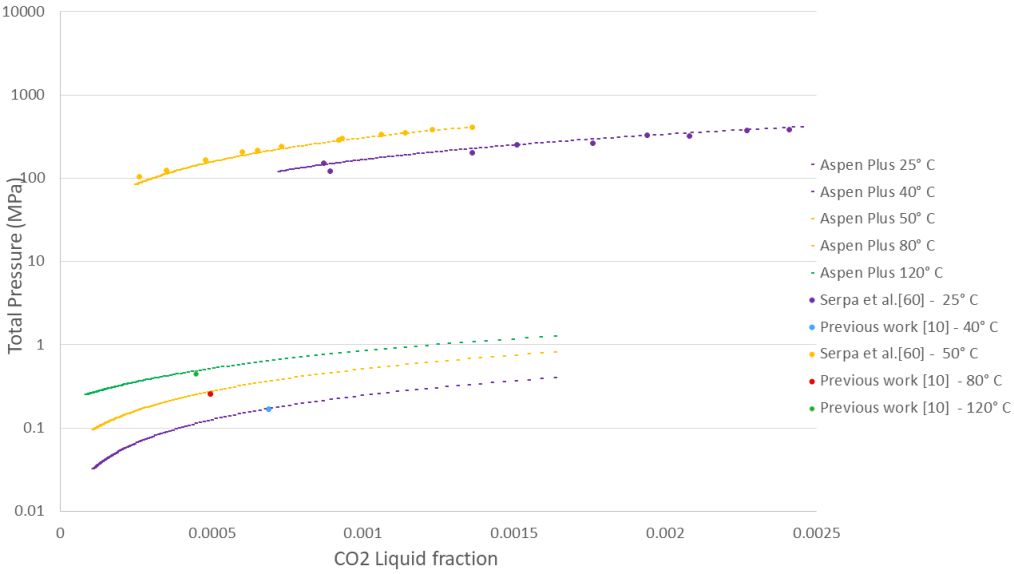

Figure 4.9: Total pressure on a log scale as a function of liquid CO_2 mole fraction in H_2O, in the temperature range of $25 - 120°C$. The dotted lines represent the models and the circles represent the experimental data.

The average absolute deviation AARD at 25°C and 50°C remains below 8% for the predicted mole fractions. The mean absolute deviation is maximum 6%, which is mainly influenced by the high relative deviations at the lowest pressures. As the pressure increases, the relative deviations decrease.

It can be concluded that the proposed model has a very good agreement to the values found experimentally, thus validating the model.

The predicted values were also compared against experimental data obtained as part of previous work[10] and three data points were obtained and compared at 40°C, 80°C and 120°C as shown in Figure 4.9 and reported in Appendix Tables A.67 and A.68. There was a good agreement observed and the maximum average absolute deviation is 8% for the predicted pressure and 13% for the predicted mole fraction, both at 120°C.

Chapter 5
Basis for process simulation

Gas treating operations are commonly used to match technical operation requirements for subsequent processing, keep the reliability of the equipment or to preserve the environment. The type of process or equipment to use will depend on the required gas specifications since the requirements are not the same for pipeline gas, NGL pre-treatment or LNG pre-treatment. For example, the allowed water content in natural gas that is transported in export pipelines is actually lower than for sales gas and this is due to flow assurance issues[45].

In the case of offshore gas processing, the aim is to achieve and maintain the gas operation conditions in order to protect the pipelines. This is done by maintaining a single phase fluid in the pipeline network under normal operations and under shut-in.

This chapter presents the basis for the Aspen Plus simulations and the background for the criteria that have been selected through an extensive literature review. For setting up the absorption and regeneration processes, as well as the assumptions that have been made.

5.1 Problem statement

A typical process for gas treatment offshore is shown in Figure 5.1. where in many cases the stream coming from a well, which in many cases can be a multiphase flow that consists on a gas, aqueous and a condensate phase. MEG is injected directly in the flow stream coming from the the well for hydrate control. The hydrocarbon stream coming from the wellhead goes through a separation and stabilization phase where the hydrocarbon and rich gas specifications are obtained. MEG and water are treated and separated so a solution of MEG can be pumped back to the well. The next stage is the gas sweetening, where CO_2 and H_2S are removed. The sweetened gas is dehydrated using glycol, which in many cases can be TEG, before it is finally compressed and sent onshore as export gas through pipelines[44].

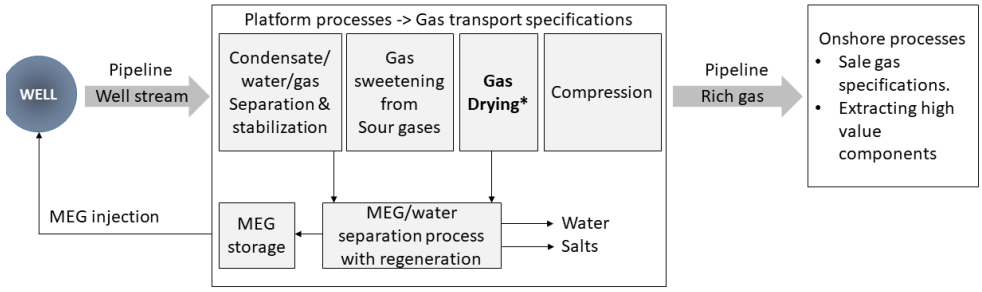

Figure 5.1: Typical offshore gas process from extraction to onshore treatment.

Since this work focuses on offshore gas dehydration (**gas drying*** process in Figure 5.1) and the study of different regeneration schemes by modeling them in Aspen Plus, certain process specifications were fixed throughout the study. Such as the number of stages in the absorber, the feed composition and the absorber process conditions, which will be given in chapter 6. Other process conditions were varied in each regeneration case, to find the range of conditions at which the gas dehydration meets the specified water content. Comparisons of the results obtained are made between the different regeneration methods based on amount of water removed, glycol make-up, glycol loss, methane loss and energy/heat consumption.

5.2 Gas composition and assumptions

Natural gas composition is of vital importance in gas processing plants, especially offshore since it is widely known that natural gas composition varies to a great extent depending on the type of reservoir this is being produced from[39].

The gas dehydration simulations in this study are based on offshore facility dehydration processes. Therefore the water content in the gas stream is considered to be different from the gas composition coming directly from the well.

Most of the technical data including operating conditions and gas compositions is confidential and major operators do not make this information available in open literature. The gas composition and water content has been established as the base of the simulations for this work based on literature review, and it considers that the gas has undergone the separation and stabilization processes. In this specification the gas contains H_2S, however in this work, H_2S removal was not taken into account. A summary of all the gas compositions found in literature is shown in Appendix Table B.2. The gas composition used to build the base case simulations in this work has been taken from literature[53], and it is shown in Table 5.1.

Table 5.1: Base case gas composition used in this work.

Component	**mole%**
N_2	0.10
H_2S	1.55
CO_2	2.84
C_1	89.76
C_2	3.10
C_3	1.48
i-C_4	0.59
n-C_4	0.30
i-C_5	0.10
n-C_5	0.05
H_2O	0.14
MEG	0.00

As mentioned in the problem statement section some specific process specifications were fixed to compare every regeneration process, and those are shown in table 5.2. In addition, all other inlet streams parameters different from the main wet gas stream to be dehydrated (such as make-up MEG, stripping gas, etc.), have been set to 25°C and 1 bar for practical comparison purposes.

Table 5.2: Base case operating conditions

Absorber inlet gas temperature	50° C
Absorber inlet gas pressure	115 bar
Absorber inlet gas flow rate	320,000 kg/h
Lean MEG temperature	54-56° C
Lean MEG pressure	115 bar
Number of stages in absorber	5 (See section 6.1)
Pressure after the depressurization valve	2 Bar

The pressure drop in the pipes has been considered to be to small compared to the pressure drop across the different equipment in the simulations, therefore the pressure drop in the pipes has been neglected.

A pump or a compressor (for gas/vapor) has been situated at the exit of every equipment operating under vacuum, in order to account for the discharge pressure requirement in the pipes and make a more realistic comparison between the different regeneration models in terms of energy utilization. Since the flow rate through the

pumps is not large resulting in a very small required energy, these units have been considered adiabatic, even though a pump is a highly non-adiabatic unit.

Compression is considered a polytropic process, but for this work the compression units are also considered to be an adiabatic process, implying that it is both isentropic and reversible[62]. In Aspen Plus, "isentropic" type of compressor has been used for this purpose.

When calculating pumps and compressors efficiency, the main factors to consider are the unswept volume (also called clearance), any leakage around valves, piston rings, rod packing, friction losses and number of stages. Since the adiabatic assumption becomes less valid at low compression/pumping ratios (time that the valves are open become too large a proportion of the total time)[62], for this work, both pump efficiency and isentropic efficiency (for compressors) was set to 0.8 in Aspen Plus, and the mechanical efficiency was set to 0.9.

For calculating the energy consumption in the different regeneration schemes some special considerations have been taken into account. First, the coolers are not considered since water is used as utility in Aspen Plus to cool down the different streams and the cost of water has been considered negligible. In other words, free unlimited supply of sea water. Second, the equivalent heat has been calculated for the electricity requirement of pumps and compressors assuming that the efficiency of stand-alone steam power generation rarely exceeds 40%, and after the steam has been condensed the majority of the heat is removed in cooling towers. Therefore, the equivalent heat requirement in pumps and compressors is corrected to be "electricity/0.4"[33].

5.3 Water content specification in export gas

When it comes to water content estimation in sour gas it is necessary to consider that H_2S and CO_2 contain more water at saturation, therefore having an effect on the overall water content which makes the water estimation significantly more challenging[65].

As mentioned in section 5.2, a typical gas composition has been taken from literature and typical gas specifications for gas export from the Norwegian continental shelf[20] are given in Appendix Table B.3. The water dew point specification of -18°C at 69 barg is used to calculate the maximum allowable water in export gas for transport, which resulted to be 46 ppm in a molar base. This has been set as the base for the simulations in Aspen Plus. The correlation chart in Appendix Figure 6.1 along with the calculations shown in Appendix B, have been used to calculate the maximum allowable water.

Chapter 6
Process simulation

Models for traditional gas dehydration processes are proposed by the developers of the different simulation programs such as HYSYS, PROSIM, UNISIM and Aspen Plus. Away from this there is not much information about the actual simulation process in the open literature. There is some information based on TEG usage for gas dehydration simulation, but not for MEG.

The gas dehydration process simulation in Aspen Plus for this work incorporates gas dehydration process by absorption, in which water is removed from the gas using MEG and the MEG regeneration before it can be reused for dehydration.

The model *"Radfrac"* was used for rigorous simulation of gas-liquid contactors such as absorbers and strippers. In this chapter the absorption process simulation in Aspen Plus is described together with the different regeneration processes.

6.1 Gas dehydration process description

A typical simplified gas dehydration and MEG regeneration process flow diagram (PFD) is shown in Figure 6.1.

The wet gas stream enters the absorber column inlet at the bottom and the lean MEG enters at the top, flowing downwards through the absorber and gets in contact with the wet gas that flows upwards. Water separation occurs by simple dew point depression.

The rich MEG leaving the absorber from the bottom of the column is sent to the regeneration process, but first a pressure relief valve is used for reducing the pressure to 2 Bar. The main purpose of this pressure reduction is to reduce the required thickness of the pipeline and vessel units walls[63].

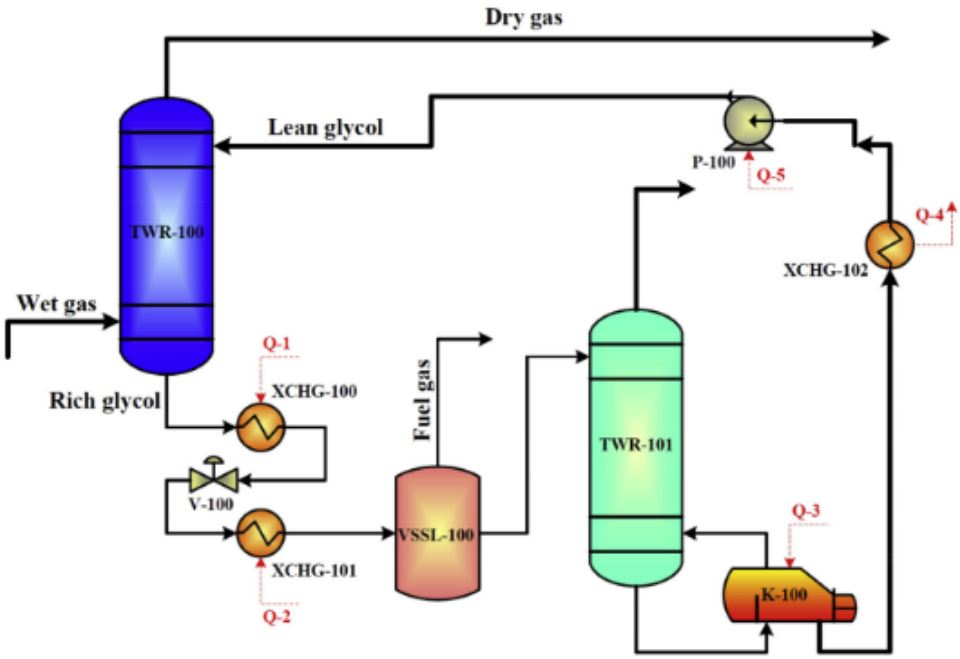

Figure 6.1: Typical simplyfied gas dehydration process[57].

After the pressure reduction valve a 2 phase flash tank separator is used for separating part of the hydrocarbon gas from the rich MEG. The main purposes of this flash tank are to prevent foaming in the regeneration stripper which may lead to higher MEG losses and to prevent sludge formation due to accumulation of solid particles which, over a period of time can turn into formation of black sticky and abrasive gum causing erosion of equipment, specially pumps and valves[25]. Filters are used to remove the solids. This flash tank is also used to regulate the liquid flow in order to avoid pump cavitation.

The heat exchangers are designed to recover the maximum amount of heat possible and in this way optimize the process in terms of heat/energy requirements. By using the lean MEG stream to heat the rich MEG stream while using the rich MEG stream to cool down the lean MEG stream. The heat exchange system includes the stripper overhead condenser where the cold rich MEG is preheated before it enters the regeneration stripping unit.

The MEG regenerator is a stripping column with the main purpose of regenerating MEG to the required purity so it can be re-used in the absorber unit. When the rich

MEG contains high amounts of solid particles or dissolved salts, these have to be separated and sent to disposal before the MEG can be reused. For this it is necessary to include a reclamation system[69].

A simplified diagram of a regeneration and reclamation commercial process is shown in Figure 6.2. The diagram shows the different units used for salt removal, including a brine column where MEG is circulated through, in order to remove salt before MEG is regenerated.

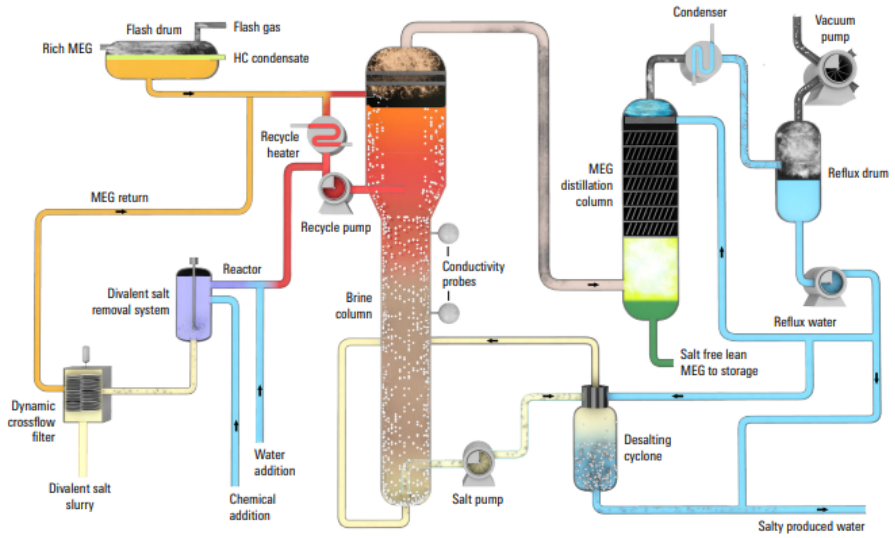

Figure 6.2: MEG regeneration and reclamation offshore system (Picture taken from Schlumberger "PUREMEG" brochure).

The regeneration schemes studied in this work will be explain in more detail in the following subsections, the reclamation system is not part of the scope of this work.

Since the MEG regenerator operates at low pressure or vacuum (depending on the regeneration process), and the absorber operates at high pressure (115 bar), a pump is needed to increase the pressure of the Lean MEG stream before entering the absorber.

6.1.1 Gas dehydration simulation.

The absorption column was simulated in Aspen Plus using the fixed parameters shown in table 6.1.

Table 6.1: Specifications used in Aspen Plus for the absorption column.

Wet gas inlet pressure (atm)	113.5
Lean MEG inlet pressure (atm)	113.5
Lean MEG inlet flow rate (kmol/hr)	235
Wet gas inlet temperature (°C)	50
Lean MEG inlet temperature (°C)	57
Absorber pressure (atm)	108.5

A sensitivity analysis was performed to study the effect of the number of stages in the absorption column by varying the wet gas flow rate. For this analysis 98% MEG solution was used as base case and 3 to 9 stages are simulated. The results are shown in Figure 6.3. It was possible to achieve the required gas purity of 46 ppm with the different number of stages. However, it is observed that with 4 stages the solvent to feed ratio must be higher than 0.018 to achieve the required gas specifications and with only 3 stages even higher solvent to feed ratios would be required. The number of stages was set to 5 in the absorber column as base for all the simulations.

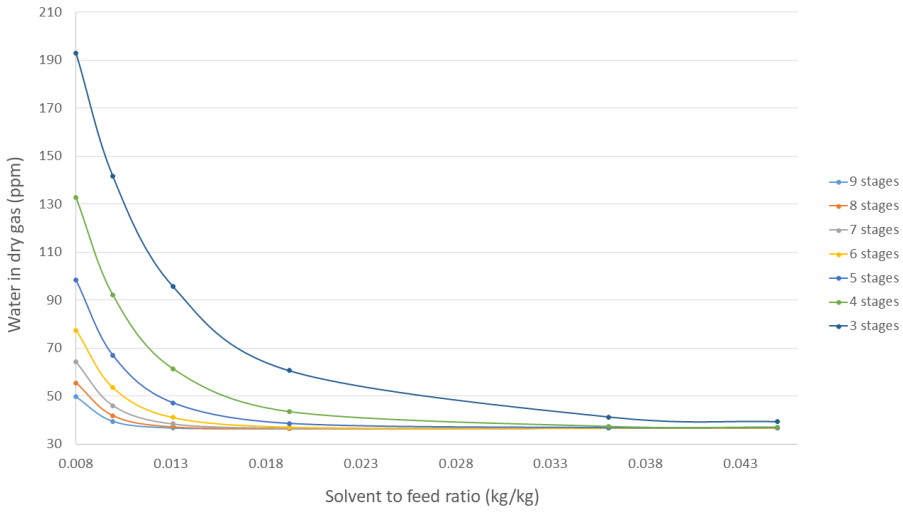

Figure 6.3: Effect of number of stages in absorber on dry gas water content (ppm).

6.2 Regeneration methods

6.2.1 Regeneration under vacuum

The first MEG regeneration method studied in this work, was regeneration under vacuum. After water has been removed from the gas stream, the rich MEG stream is pre-heated and fed to a stripping column working under vacuum, which reduces the processing temperatures required to achieve a higher MEG purity considerably[35]. Lean MEG exiting the stripping column is pumped back to the absorber column.

Vacuum process simulation.

Regeneration with vacuum has been considered the base case simulation in Aspen Plus, the process simulated in Aspen Plus is shown in Figure 6.4.

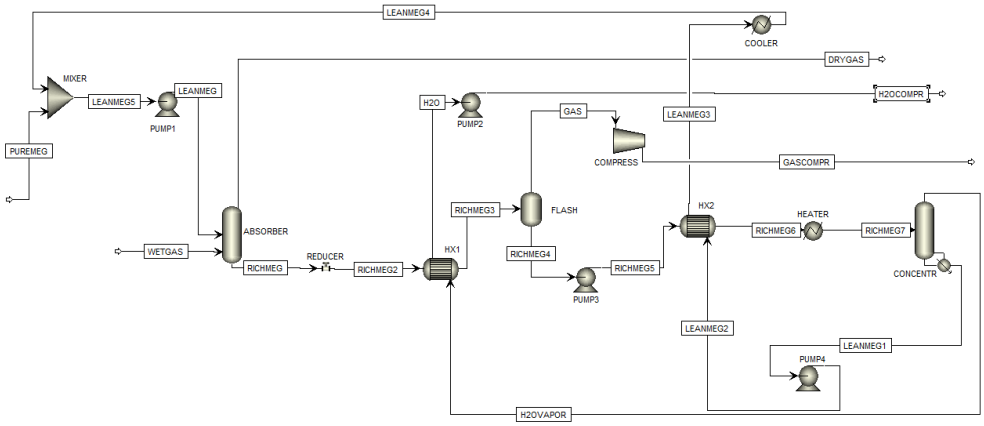

Figure 6.4: Simulation in Aspen Plus of the regeneration process under vacuum.

Rich MEG coming from the ABSORBER column and exiting the REDUCER valve is pre-heated in HX1 to 93°C before it enters the FLASH tank, which works under vacuum conditions. The rich MEG (liquid flow) from the FLASH tank goes through HX2 that recovers heat from the bottoms stream of CONCENTR. The cold stream outlet of HX2 comes out at 140°C, which is the maximum temperature value that can be reached considering a temperature approach of 10°C between the hot and the cold streams. The unit operation HEATER was located to preheat further the mixture to 152°C, because of the molar fraction of MEG, because otherwise the bottoms temperature of CONCENTR would be 167 °C which is above the degradation temperature of MEG (165°C).

The purpose of HEATER is to decrease the molar fraction of MEG on the bottoms so that the temperature is lower. The additional added heat to the feed helps to overcome this issue by decreasing the ΔT between the top of CONCENTR and the bottom. This decreases the difference of the chemical potential, hence CONCENTR performs a less sharp separation, which means that the purity of MEG in the bottoms is not going to be as good as without HEATER.

The LEANMEG1 stream exits the bottom of CONCENTR and is pumped back to the ABSROBER column. Pumps were added after every unit that operates under vacuum, as mentioned in chapter 5. This provides the required increase in pressure for the MEG stream to flow in all the different parts of the process loop. The operating parameters used for the simulation are shown in Table 6.2

Table 6.2: Specifications used in Aspen Plus for the FLASH tank and the CONCENTR column in the regeneration process under vacuum.

FLASH pressure (atm)	0.45
CONCENTR pressure (atm)	0.41
RICHMEG7 temperature (°C)	152
LEANMEG1 temperature (°C)	160
Bottoms to feed ratio mole base	0.829
Number of stages in regenerator (kmol/hr)	5

Through the absorption and MEG regeneration processes there are MEG losses. A MEG make-up mixer is used to account for these losses and in this way achieve the required lean MEG purity that is recirculated to the ABSORBER column. The total MEG loss is calculated along the entire process loop, were HSOCOMPR is the stream were most MEG losses are observed followed by GASCOMPR stream. The make-up MEG and process conditions where always adjusted in order to reach the required water content in the natural gas.

The reflux ratio was set to "bottoms to feed ratio" in Aspen Plus, and since it has a direct effect on the amount of MEG lost in the overhead vapor, the needed make-up MEG was iterated as a function of the reflux ratio, using initially five equilibrium stages.

After convergence was achieved and the new process parameters were set, the effect of equilibrium stages in CONCENTR column was studied by varying the wet gas flow rate and the number of equilibrium stages in the CONCENTR column. The remaining process parameters were kept constant. The number of stages was fixed to five, as it can be observed in Figure 6.5 that increasing the number of stages would not produce a significant decrease in dry gas water content.

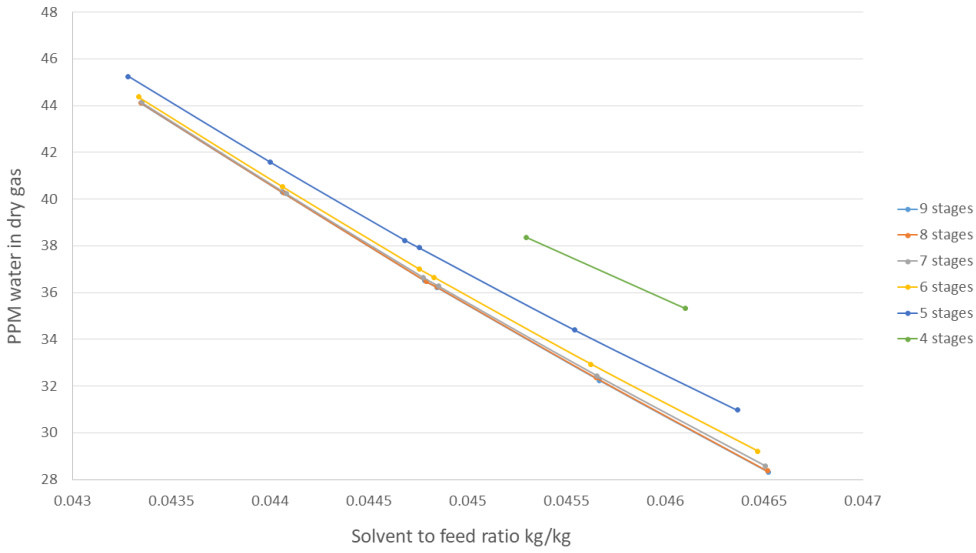

Figure 6.5: Stages effect on regeneration with vacuum.

In terms of energy utilization, the equipment overview and the energy consumption are shown in Table 6.3.

Table 6.3: Energy requirements for MEG regeneration under vacuum.

Unit	**kJ/kg**$_{H_2Oremoved}$
Pump 1	1212
Pump 2	482
Pump 3	15
Pump 4	14
Compressor	176
Total Electricity requirement	**1899**
Heater	1239
Reboiler	4561
Total heat requirement	**5800**
Heat exchanger 1	4313
Heat exchanger 2	5323
Total recoverable energy	**9636**

6.2.2 Regeneration with stripping gas

A way to reduce the amount of water in MEG, is to reduce the partial pressure of the water vapor in the gas (CH_4 process line in Figure 6.6) phase by using stripping gas, which is introduced at the bottom of the stripping column[38]. This stripping gas can be an inert gas such as N_2, or it can also be dehydrated natural gas. In this work, CH_4 has been chosen, since an inert gas is used in very rare cases and CH_4 is often taken from the fuel gas system[56].

Regeneration with stripping gas simulation

The regeneration process using stripping gas, was simulated in Aspen Plus by adding a stream of methane to the inlet bottom of the CONCENTR column as shown in Figure 6.6.

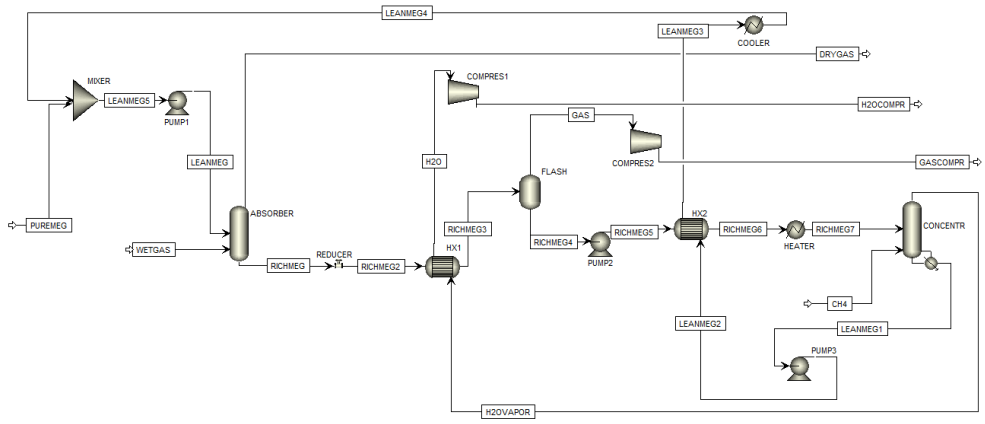

Figure 6.6: Simulation in Aspen Plus of the regeneration process with stripping gas.

It was not possible to achieve the required MEG purity to achieve less than 46 ppm water in the dry gas while keeping the regeneration temperature below 165°C, operating at atmospheric conditions. Therefore the process is simulated with the FLASH tank and the CONCENTR column operating under vacuum, the operating parameters are shown in Table 6.4.

Table 6.4: Specifications used in Aspen Plus for the flash tank and the stripping column in the regeneration process under vacuum.

FLASH tank pressure (atm)	0.5
CONCENTR pressure (atm)	0.7
RICHMEG7 temperature (°C)	152
LEANMEG1 temperature (°C)	158
CONCENTR bottoms rate (kmol/hr)	220
CONCENTR distillate rate (kmol/hr)	65.8
Stripping gas rate (kmol/hr)	20
Number of stages in CONCENTR (kmol/hr)	5

The number of stages in the CONCENTR column was simulated following the same procedure as for the vacuum regeneration process but the reflux ratio in this case was set to "bottoms rate". It can be observed from Figure 6.7, that based on the same solvent to feed ratio as for the regeneration process with vacuum, it is possible to achieve the required dry gas water content with 5 stages. The number of stages was therefore set to 5.

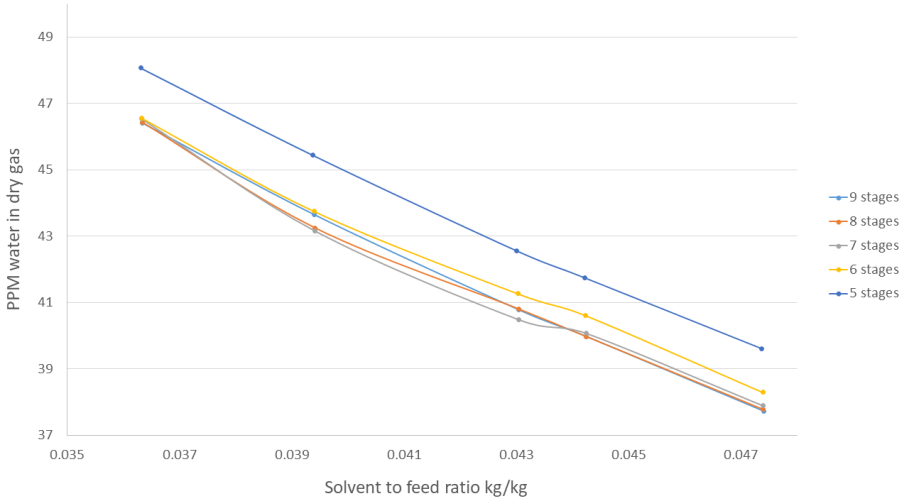

Figure 6.7: Stages effect on regeneration with stripping gas and vacuum.

In terms of energy utilization, the equipment overview and the energy consumption is shown in Table 6.5.

Table 6.5: Energy requirements for MEG regeneration with stripping gas and vacuum.

Unit	**kJ/kg$_{H_2Oremoved}$**
Pump 1	1202
Pump 2	18
Pump 3	3
Compressor 1	907
Compressor 2	133
Total Electricity requirement	**2264**
Heater	1473
Reboiler	4542
Total heat requirement	**6015**
Heat exchanger 1	4283
Heat exchanger 2	5020
Total recoverable energy	**9304**

6.2.3 DRIZO process

DRIZO is a process commonly used for TEG regeneration and it was originally developed by Dow Chemical Company in 1970. In this process the stripping column performance is enhanced by the use of a volatile hydrocarbon liquid which acts as an azeotrope former[38]. In this work, the application of the DRIZO process for MEG regeneration is studied, and compared to the traditional MEG regeneration methods. A simplified DRIZO process diagram is shown in Figure 6.8, which provides a small comparison overview to other conventional glycol processes.

The stripping medium is usually a liquid at ambient conditions and a vapor at reboiler conditions, conformed of a mixture of C_5+ hydrocarbons[56]. The stripping medium can be absorbed from the natural gas as BTEX compounds or it can be introduced externally, e.g. n-heptane.[49].

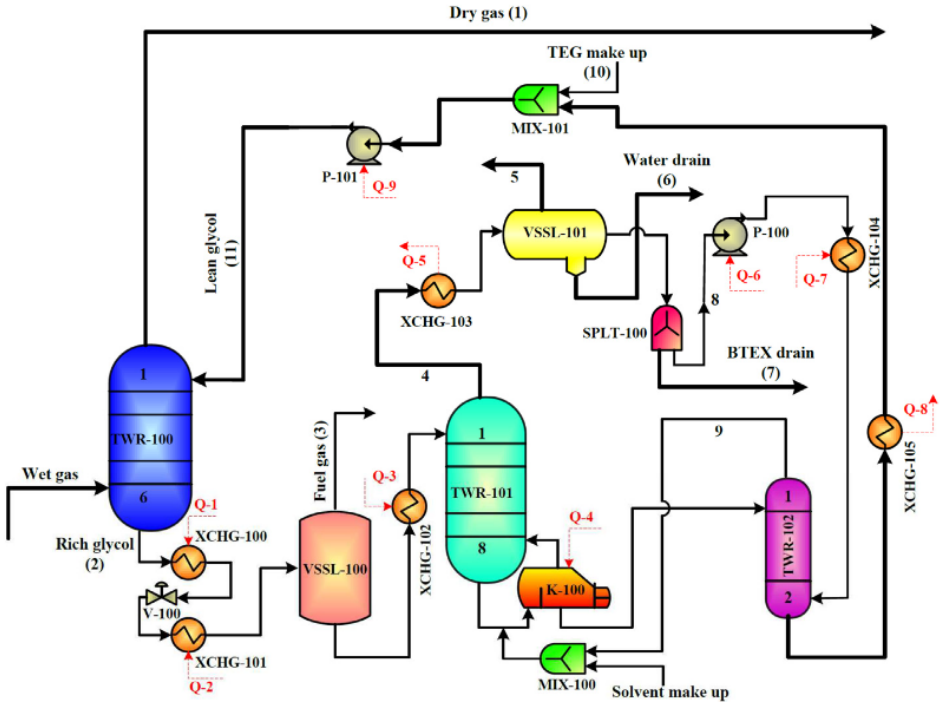

Figure 6.8: DRIZO process diagram[57]

The stripping gas medium exiting the regeneration column overhead is cooled down in the heat exchange system, in the meantime providing heat that can be harnessed. The stripping medium is recovered as a liquid after the regeneration column. The stripping medium is separated in liquid form from the condensed water in a three phase separator (LLV) in which light hydrocarbons exit in form of vapor. The recovered stripping medium is then recycled to a second regeneration column, where lean MEG coming from the first regeneration column is introduced. Having the second regeneration column in this process will allow to achieve MEG purities as high as 99.99 wt%[56].

DRIZO process simulation

In this work pure n-heptane has been used as the stripping medium. Because the commonly used stripping mixtures have similar chemical nature, and can be assumed to behave in a similar way as n-heptane without affecting significantly the accuracy of the results.

The process is shown in Figure 6.9. The rich MEG coming from the ABSORBER column and exiting the REDUCER, recovers heat from the top stream of CONCENT1 in HX1 before it enters the FLASH unit operation at 96°C. The FLASH unit operation in this case works at atmospheric conditions. The rich MEG exiting the FLASH recovers heat from the bottoms stream of CONCENT2 in HX2 and is further preheated to 158°C, for the same reasons as explained in subsection 6.2.1. Preheated Rich MEG and n-heptane are introduced into the CONCENT1 column. LEANMEG1 exiting CONCENT1 is introduced into CONCENT2 column together with N-heptane in order to achieve higher MEG purity.

In order to recirculate n-heptane back to the regeneration columns a new loop was implemented in the simulation. N-heptane is introduced to CONCENT2 column and when it exists the column overhead it is sent to CONCENT1 column. N-heptane exiting the CONCENT1 overhead is condensed in the heat exchangers, HX1 and HX2, before being separated from water and light gases in 3PHASEP. N-heptane is recirculated back to the CONCENT2 column to regenerate MEG.

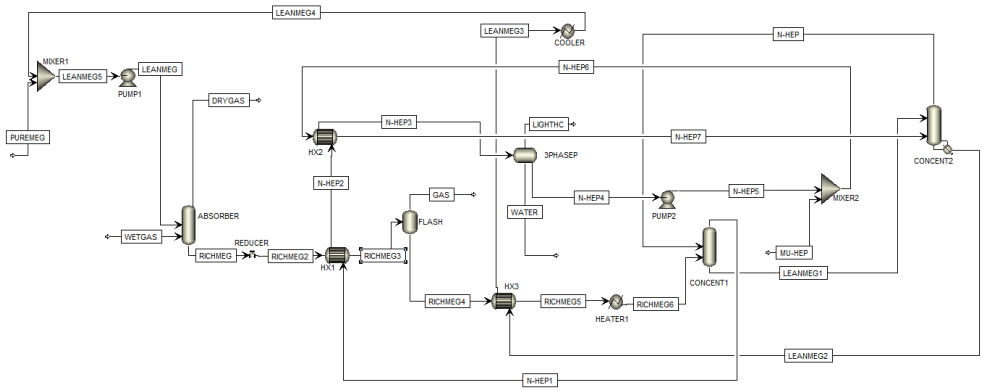

Figure 6.9: Simulation in Aspen Plus of the regeneration process with DRIZO.

It was not possible to make the loop converge using only the ELECNRTL model for the DRIZO process. The 3PHASEP was the only unit, from all the different units in the simulations, that required a different thermodynamic model in Aspen Plus. The three phase separator "3PHASEP" was set to use the SRK equation of state, since it is popular and commonly used to perform calculations of petroleum engineering, in order to predict the phase behavior of petroleum fluids by treating them as a multi-components system of pure and pseudo-components[2].

It can be seen from the process diagram that an extra pump is necessary to recirculate the stripping medium. The operating parameters used for the simulations are shown in Table 6.6.

Table 6.6: Specifications used in Aspen Plus for the flash tank and the different stripping columns used in the DRIZO regeneration process.

FLASH tank pressure (atm)	1.01
CONCENT1 pressure (atm)	1.01
RICHMEG6 temperature (°C)	158
LEANMEG1 temperature (°C)	160
Bottoms to feed ratio mole base	–
CONCENT1 bottoms rate (kmol/hr)	197.7
CONCENT1 distillate rate (kmol/hr)	54.8
Make-up stripping medium rate (kmol/hr)	40
Number of stages in CONCENT1	5
CONCENT2 pressure (atm)	1.01
LEANMEG2 temperature (°C)	146
CONCENT2 bottoms rate (kmol/hr)	220
CONCENT2 distillate rate (kmol/hr)	25.5
Number of stages in CONCENT2	5

The reflux ratio in CONCENT2 was set to "bottoms rate" in Aspen Plus. The number of stages in the CONCENT1 and CONCENT2 column were simulated combining different number of stages in each column and the results are shown in Figures 6.10 and 6.11.

It can be observed from figure 6.10 that by setting 5 stages in both CONCENT1 and CONCENT2, it is possible to achieve less than 46 ppm water in the dry gas stream. Therefore the number of stages was set to 5 for the CONCENT1 column and 5 for the CONCENT2 column.

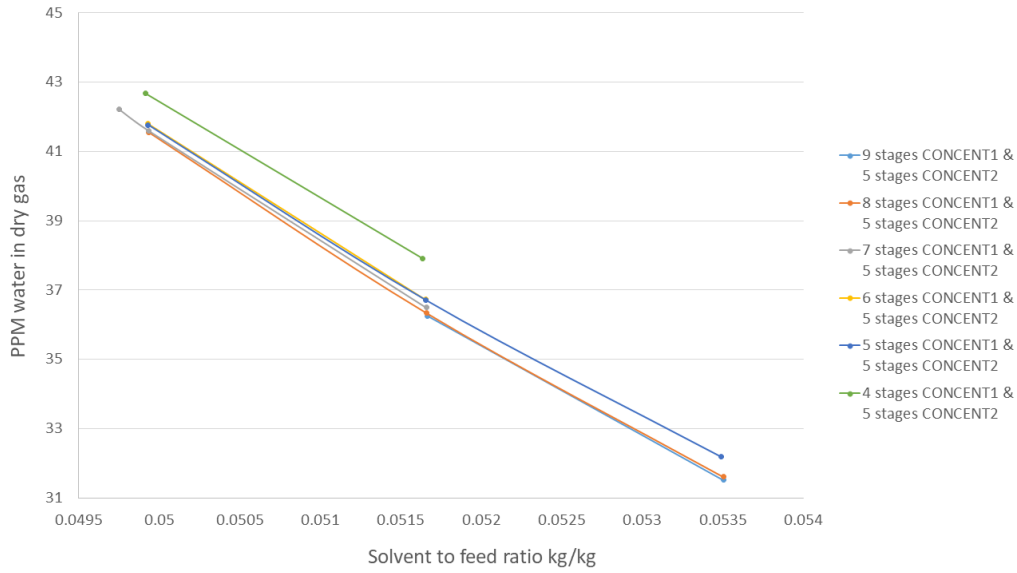

Figure 6.10: Stages effect on CONCENT1 with DRIZO process.

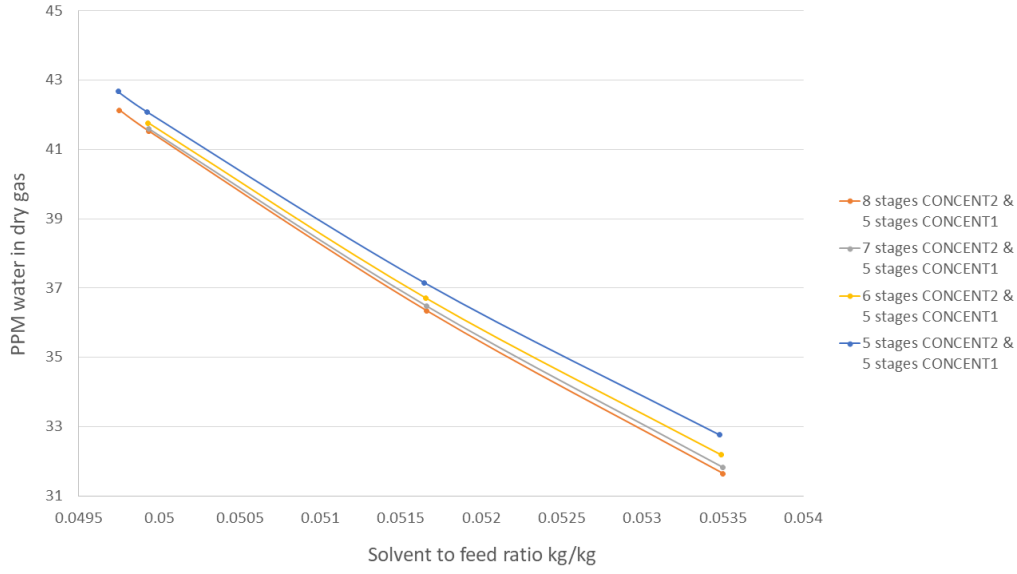

Figure 6.11: Stages effect on CONCENT2 with DRIZO process.

In terms of energy utilization, the equipment overview and the energy consumption are shown in Table 6.7.

Table 6.7: Energy requirements for MEG regeneration with DRIZO process.

Unit	**kJ/kg**$_{H_2Oremoved}$
Pump 1	1574
Pump 2	0
Total Electricity requirement	**1574**
Heater	3594
Reboiler	2072
Total heat requirement	**5667**
Heat exchanger 1	3821
Heat exchanger 2	2699
Heat exchanger 3	4558
Total recoverable energy	**11078**

6.3 Results and regeneration methods comparison

An overview of the results for the different regeneration methods simulated in Aspen Plus is shown in Table 6.8.

In terms of energy consumption the best results are obtained with DRIZO. This process consumes the least amount of energy, while the regeneration with stripping gas shows the worst results, with 8278 kJ per kg of water removed. The heat exchange design in the DRIZO process also results in a higher heat recovery compared to the other two regeneration processes, especially compared to the regeneration with stripping gas.

The required amount of make-up MEG due to losses is preeminent for the DRIZO process with 894 kg/hr, which represents 168 kg/hr more make-up MEG required than the regeneration with stripping gas which shows the lowest requirement from the studied processes. The results obtained from the regeneration process with vacuum are not too different from the results obtained with vacuum and stripping gas regeneration, with only 43 kg/hr difference.

Table 6.8: Results overview for the different regeneration schemes simulated.

	Regeneration with vacuum	**Regeneration with stripping gas**	**Regeneration with DRIZO**
Total energy consummption (kJ/kg water removed)	7700	8278	7241
Total energy recovered in heat exchangers (kJ/kg water removed)	9636	9304	11078
MEG loss/make-up (kg/hr)	770	726	894
Methane loss/make-up (as stripping gas) (kg/hr)	––	321	––
N-heptane loss/make-up (kg/hr)	––	––	4008
Methane loss (not used as stripping gas) (kg/hr)	12.83	12.53	9.45
Water content in dry gas (ppm)	38.27	41.70	42.38
MEG regeneration temperature (°C)	160	158	160

A substantial difference between the different regeneration processes is the stripping gas/liquid injected in the stripping columns, which is not required for the vacuum process. Despite the higher amount of stripping medium required for DRIZO, this process has the advantage that the stripping medium can be absorbed from natural gas as BTEX compounds or recovered as a surplus of aromatics condensed from the same DRIZO process. Consequently DRIZO is an environmentally friendly process which reduces the BTEX emissions to the environment.

The methane loss is the lowest in DRIZO, whereas for the regeneration processes with vacuum and with stripping gas, the losses are very similar and no meaningful difference is observed between them. According to the results obtained, the DRIZO process and regeneration using vacuum were selected to modify each process by implementing a MEG recovery loop in the simulation in order to perform a closer comparison between the two most promising processes.

Chapter 7
Process modification for MEG recovery

In this Chapter the main subject for discussion is the minimization of the losses of MEG in the two processes that showed the best results. Also, to compare how the other parameters and results in each process are influenced by the MEG recovery modification.

7.1 Regeneration with vacuum and MEG recovery

The composition of the distillate stream coming out from the top of the CONCENT1 column is shown in Table 7.1. It can be seen that it contains mainly 22% mass of water and 38% mass of MEG that can be recovered.

Table 7.1: Composition of distillate stream coming from the top of the CONCENT1 column under vacuum.

	% mole	Mole flows (kmol/hr)	% mass	Mass flows (kg/hr)
MEG	0.25	11	0.38	695
H_2O	0.49	23	0.22	406
CO_2	2E-05	1E-03	3E-05	0.05
N_2	2E-09	1E-07	2E-09	3E-06
C_1	7E-06	3E-04	3E-06	5E-03
C_2	2E-07	1E-05	2E-07	3E-04
C_3	5E-08	2E-06	6E-08	1E-04
C_4	9E-09	4E-07	1E-08	2E-05
C_5	0.02	8E-01	0.03	54
H_2S	0	0.01	0	0.20
I-C_4	0.20	9	0.29	531
I-C_5	0.04	2	0.08	146

The simulation in Aspen Plus for the regeneration process with vacuum and MEG recovery is highlighted in yellow in Figure 7.1. The modification of the vacuum process included the addition of an extra loop to recover the MEG from the H2OCOMPR stream exiting PUMP2 at 82°C.

A second stripping column "CONCENT2" which operates under vacuum is included in the new loop to separate water from MEG. An extra heater "HEATER2" preheats the H2OCOMPR stream to 124°C before it enters the CONCENT2 column to achieve a lower lean MEG temperature on the CONCENT2 bottoms, as explained in subsection 6.2.1. A compressor "COMPRESS2" is added at the exit of the CONCENT2 column overhead and an extra pump "PUMP5" is added at the exit of CONCENT2 column bottoms. In addition, an extra cooler "COOLER2" is required to cool down the lean MEG stream to be reused.

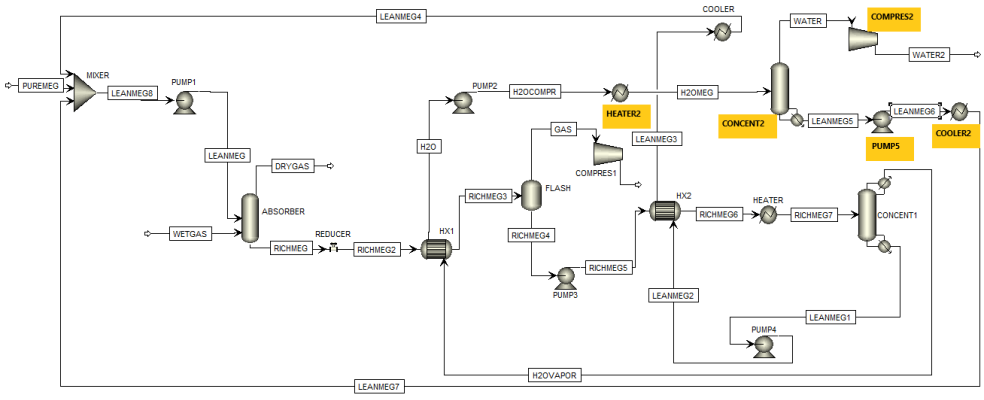

Figure 7.1: Modified vacuum regeneration with MEG recovery.

The implementation was extremely challenging and many iterations were required to achieve convergence in the loop. The main limitation resulted from keeping the temperature below MEG decomposition temperature. The main parameters manipulated were the MEG make-up and the CONCENT2 column specifications. It was not possible to improve the lean MEG purity exiting the bottom of the CONCENT2 column by only varying the reflux ratio, since this parameter is a function of the reboiler temperature. The CONCENT2 column was set to "bottoms rate" in Aspen Plus and the new process parameters are shown in Table 7.2.

Table 7.2: Specifications used in Aspen Plus for the MEG recovery option in the vacuum regeneration process.

CONCENT2 pressure (atm)	0.3
LEANMEG5 temperature (°C)	160
CONCENT2 bottoms rate (kmol/hr)	9.11
CONCENT2 distillate rate (kmol/hr)	36.8
Number of stages in CONCENT2	5
Make-up MEG (kmol/hr)	3.4

The effects of the number of stages in the CONCENT2 column was simulated and is shown in Figure 7.2. It was observed that the highest purity of MEG can be achieved with 5 stages. More than 5 stages in CONCENT2 do not have any significant improvement in the amount of water than can be separated from MEG.

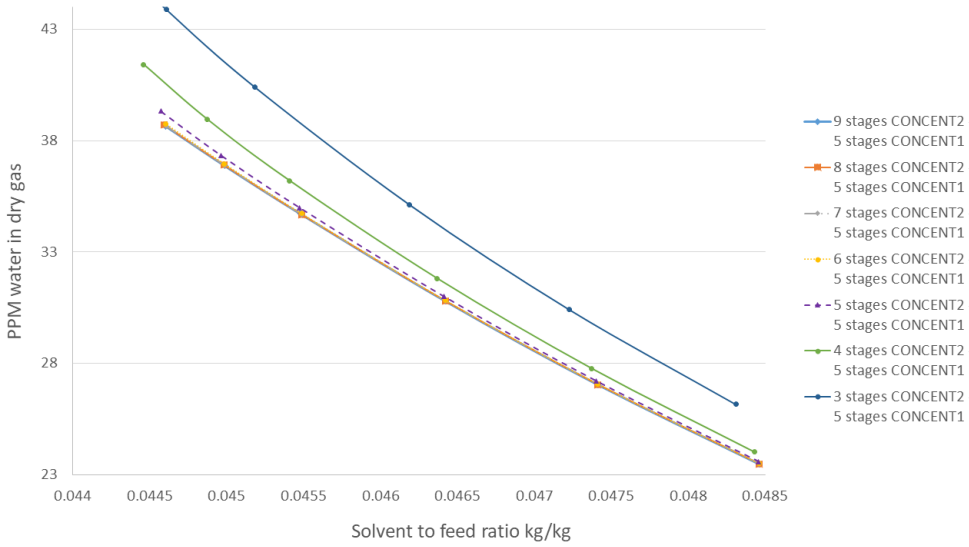

Figure 7.2: CONCENT2 stages effect on the modified vacuum regeneration with MEG recovery, with CONCENT1 set to 5 stages.

The effects of the number of stages in the CONCENT1 column was simulated again, with the CONCENT2 column set to 5 stages. The results are shown in Figure 7.3. It can be clearly seen that it is possible to recover more water from the gas stream with less amount of MEG make-up. In the new simulations there was no significant improvement in the dry gas quality from increasing the number of equilibrium stages, in the CONCENT1 column, over five.

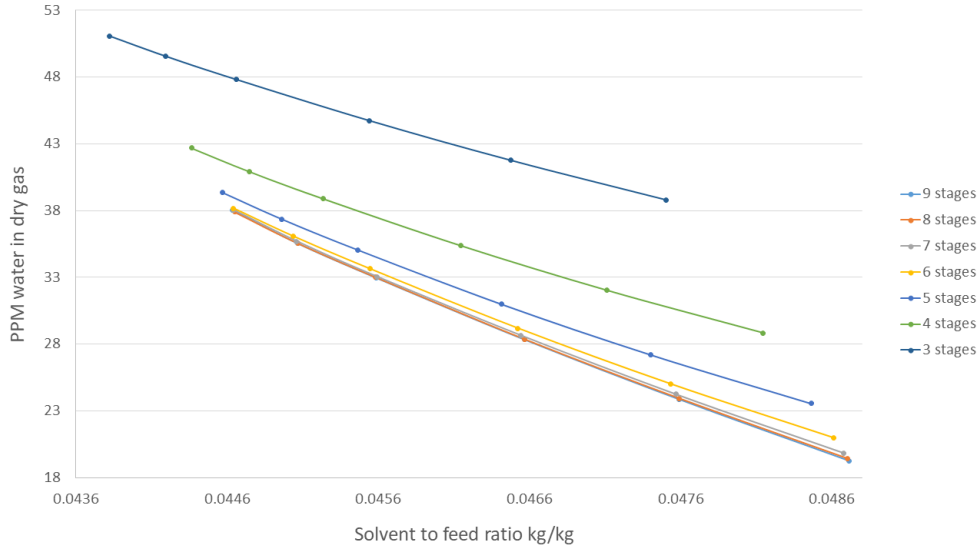

Figure 7.3: CONCENT1 stages effect on the modified vacuum regeneration with MEG recovery and CONCENT2 set to 5 stages.

The new equipment and results overview in terms of energy consumption and recovery are shown in Table 7.3. Compared to the first vacuum process simulation, it can be seen that this new modified process requires more energy. The electricity requirement increased about 1000 kJ per kg H_2O removed after MEG recovery. The heat requirement increased around 2900 kJ per kg H_2O removed. The recoverable energy is almost the same, no significant increase is observed.

Table 7.3: Energy requirements for MEG recovery with the modified vacuum regeneration.

Unit	**Before MEG recovery ($\mathbf{kJ/kg_{H_2Oremoved}}$)**	**After MEG recovery ($\mathbf{kJ/kg_{H_2Oremoved}}$)**
Pump 1	1212	1220
Pump 2	482	494
Pump 3	15	15
Pump 4	14	14
Pump 5	–	–
Compressor 1	176	178
Compressor 2	–	1197
Total Electricity requirement	**1899**	**3119**
Heater 1	1239	1246
Heater 2	–	2288
Reboiler 1	4561	4616
Reboiler 2	–	520
Total heat requirement	**5800**	**8669**
Heat exchanger 1	4313	4339
Heat exchanger 2	5323	5355
Total recoverable energy	**9636**	**9694**

7.2 DRIZO process with MEG recovery

The composition of the water stream coming from the 3PHASEP is shown in Table 7.4. It can be seen that it contains mainly 67% mass of water and 33% mass of MEG that can be recovered.

Table 7.4: Composition of water stream from the 3-phase separator in the DRIZO process.

	% mole	**Mole flows (kmol/hr)**	**% mass**	**Mass flows (kg/hr)**
MEG	0.37	37	0.67	838
H_2O	0.63	14	0.33	419
CO_2	9E-07	23	1E-06	1E-03
N_2	0	3E-05	0	1E-10
C_1	4E-09	5E-12	2E-09	2E-06
C_2	6E-10	1E-07	5E-10	6E-07
C_3	9E-11	2E-08	1E-10	2E-07
C_4	10E-12	3E-09	2E-11	2E-08
C_5	9E-07	4E-10	2E-06	2E-03
H_2S	3E-05	3E-05	3E-05	0.04
I-C_4	2E-05	1E-03	3E-05	0.04
I-C_5	2E-06	7E-04	4E-06	6E-03
N-C_7	7E-09	8E-05	2E-08	3E-05

The simulation in Aspen Plus for the DRIZO regeneration process and MEG recovery is highlighted in yellow in Figure 7.4. The extra loop integrated in this process, recovers the MEG from the condensed WATER stream coming from the 3PHASEP at 11°C.

A third stripping column "CONCENT3" which operates under vacuum is added in the new loop to separate water from MEG. In this process, an extra heater "HEATER2" preheats the WATER stream coming from the 3PHASEP to 133°C, before it enters the CONCENT3 column, to achieve a lower lean MEG temperature on the CONCENT3 bottoms, as explained in subsection 6.2.1. A compressor "COMPRES1" is added at the exit of the CONCENT3 column overhead and an extra pump "PUMP3" is added at the exit of the CONCENT3 column bottoms. In addition, an extra cooler "COOLER3" is required in the new loop, to cool down the lean MEG stream to be reused.

This specific part of the process, or new loop, is identical for both regeneration schemes in terms of equipment requirements.

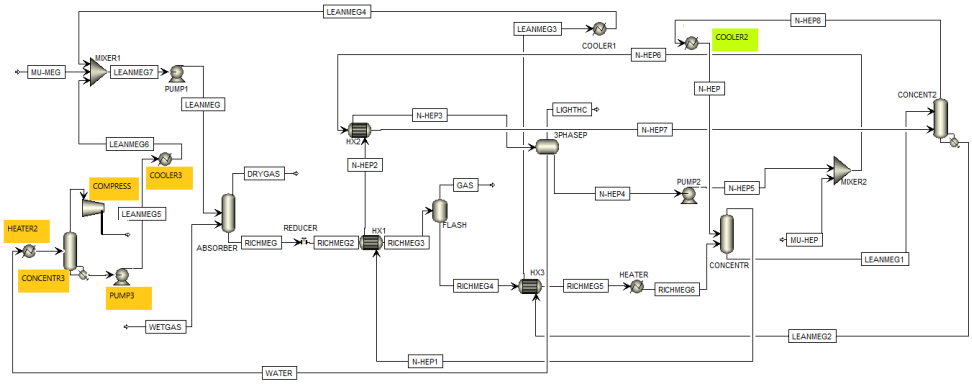

Figure 7.4: Modified DRIZO with MEG recovery.

The simulation of this process was the most challenging of all, and extremely difficult to converge. A substantial number of iterations were required to achieve convergence in the loop, while at the same time keeping the temperature below 165°C in the entire process. The main parameters that were manipulated were the MEG make-up and the CONCENT3 specifications. Especially the reflux ratio, which in this case was set to "bottoms rate" in Aspen Plus. In addition, the reflux ratio of the CONCENT2 column was also manipulated. A new cooler unit "COOLER2" highlighted in green, was implemented in the n-heptane loop. This was done to lower the temperature of the n-heptane introduced in the CONCENT1 column. This helped to control the temperature in the entire process process. The new process parameters are shown in Table 7.5.

Table 7.5: Specifications used in Aspen Plus for the MEG recovery option in the modified DRIZO regeneration process.

CONCENT2 bottoms rate (kmol/hr)	225
CONCENT2 distillate rate (kmol/hr)	73.2
CONCENT3 pressure (atm)	0.3
LEANMEG5 temperature (°C)	161
CONCENT3 bottoms rate (kmol/hr)	14
CONCENT3 distillate rate (kmol/hr)	26.6
Number of stages in CONCENT3	5
Make-up MEG (kmol/hr)	3.7

The effect of equilibrium stages in the different regeneration column was also studied, by varying the wet gas flow rate and the number of equilibrium stages in the CONCENT3 column. Figure 7.5 shows the effect of varying the number of stages in the CONCENT3 and the wet gas flow rate to the absorber. Both CONCENT1 and CONCENT2 were set to 5 equilibrium stages.

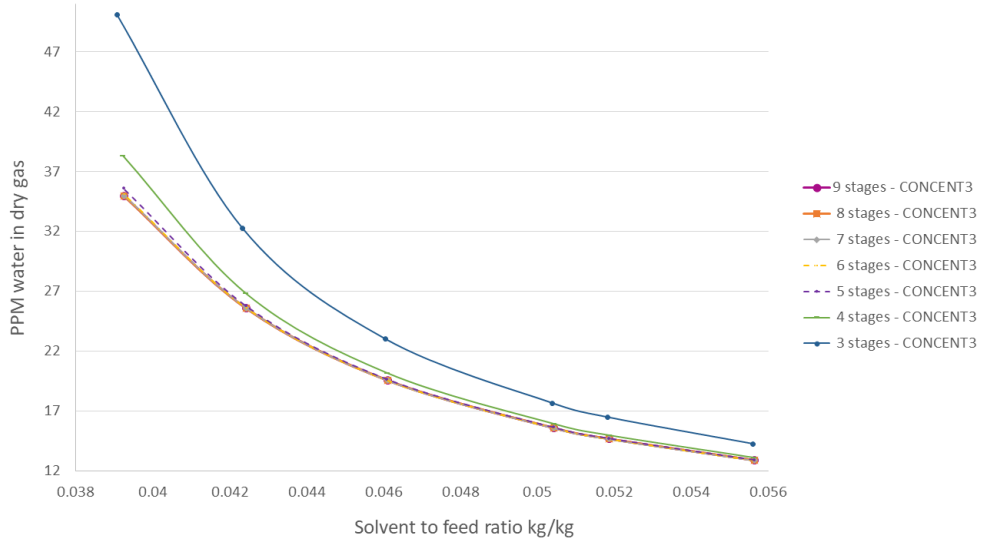

Figure 7.5: DRIZO regeneration with MEG recovery - Stages effect on CONCENT3 column with CONCENT1 and CONCENT2 fixed to 5 stages.

It is clear that at higher flow rates there was no significant improvement in the dry gas quality from increasing the number of equilibrium stages in the CONCENT3 column over five.. The number of stages was therefore set to five.

The effects of the equilibrium stages in the CONCENT1 and CONCENT2 columns were simulated again to study the impact of implementing the CONCENT3 column. From Figure 7.6 it can be seen that dry gas purity is improved and more water can be removed even with 3 stages in CONCENT1. The comparison of varying the equilibrium stages in the CONCENT1 and CONCENT2 columns is shown in Figure 7.7.

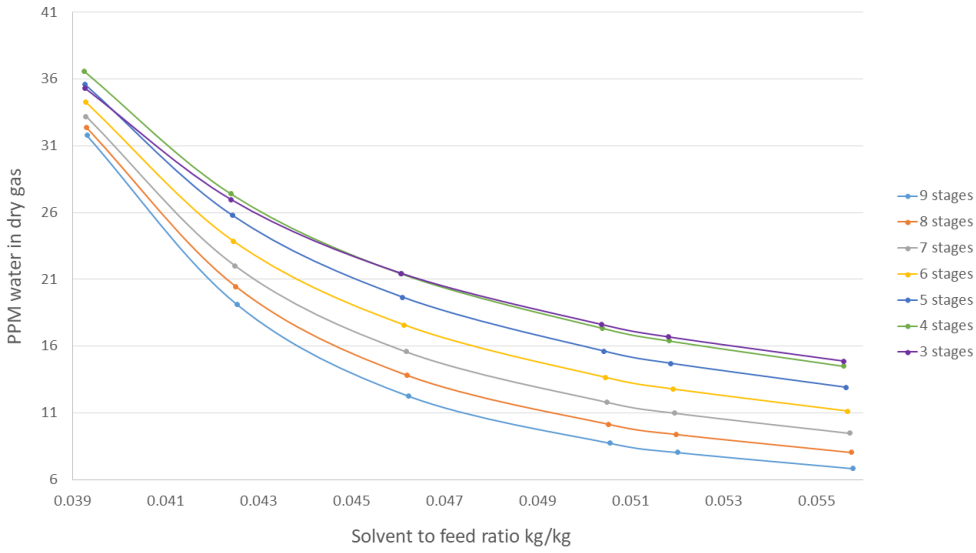

Figure 7.6: DRIZO regeneration with MEG recovery - Stages effect on CONCENT1 with CONCENT2 fixed to 5 stages.

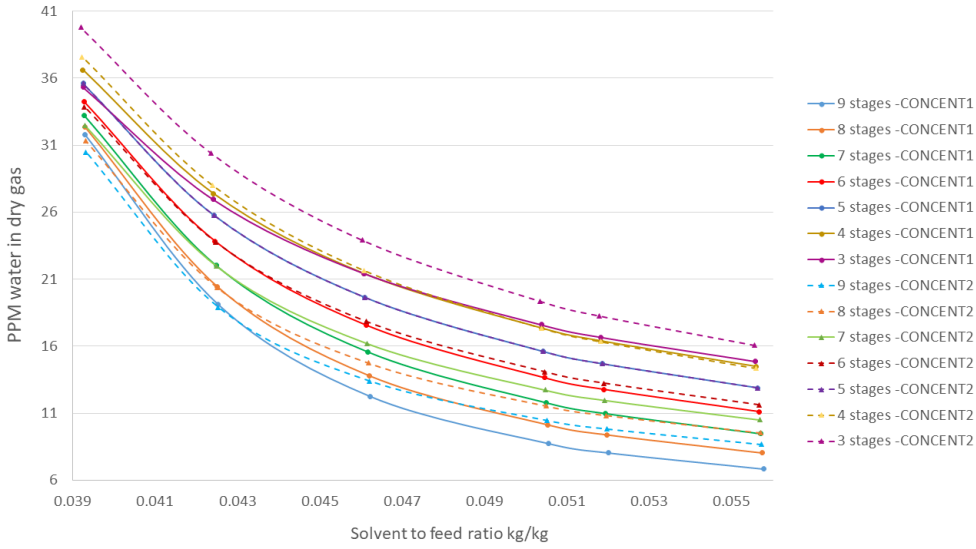

Figure 7.7: DRIZO regeneration with MEG recovery - Stages effect comparison on CONCENT1 with CONCENT2 fixed to 5 stages against CONCENT2 with CONCENT1 fixed to 5 stages.

The new equipment and results overview in terms of energy consumption and recovery are shown in Table 7.6. Compared to the first DRIZO process simulation, it can be seen that recovering MEG requires more energy. The electricity requirement increased around 1000 kJ per kg H_2O removed. The heat requirement increased 7752 kJ per kg H_2O removed. On the other hand, the recoverable energy increased to 12357 kJ per kg H_2O removed.

An increase in heat requirement in the reboiler of the CONCENT2 column can be clearly observed . The increase in energy requirement for the modified DRIZO process can be explained by looking at the total amount of water removed from the treated gas in Table 7.6. Since it is observed from the simulation results that more water is absorbed by MEG, and this increased amount of water needs to be vaporized.

In addition, it is obvious that the extra equipment added in the modified process simulation contributes to the overall increase in the energy requirement.

Table 7.6: Energy requirements for MEG recovery with the modified DRIZO regeneration.

Unit	**Before MEG recovery ($\mathbf{kJ/kg_{H_2Oremoved}}$)**	**After MEG recovery ($\mathbf{kJ/kg_{H_2Oremoved}}$)**
Pump 1	1574	1595
Pump 2	–	–
Pump 3	–	1
Compressor	–	911
Total Electricity requirement	**1574**	**2507**
Heater 1	3594	3438
Heater 2	–	2722
Reboiler 1	2072	6190
Reboiler 2	–	1069
Total heat requirement	**5667**	**13419**
Heat exchanger 1	3821	3955
Heat exchanger 2	2699	3827
Heat exchanger 3	4558	4575
Total recoverable energy	**11078**	**12357**

7.3 Results comparison and discussion

Figure 7.8 shows a comparison between the modified vacuum and DRIZO processes in terms of dry gas purity, and wet gas flow rate for different equilibrium stages. It is clear that with the modified DRIZO process it is possible to recover higher amounts of water from the wet gas while also covering a wider range of wet gas flow rates compared to the modified vacuum process.

Since the concentration of water in the rich MEG is larger for higher wet gas flow rates, vaporizing the water from the rich MEG requires more heat. The stripping medium, in this case n-heptane, increases the volatility of water in the rich MEG solution facilitating it's vaporization in the CONCENT1 column. Afterwards, the n-heptane acts as stripping gas in the CONCENT2 column increasing the purity of the lean MEG that is recirculated back to the ABSORBER column.

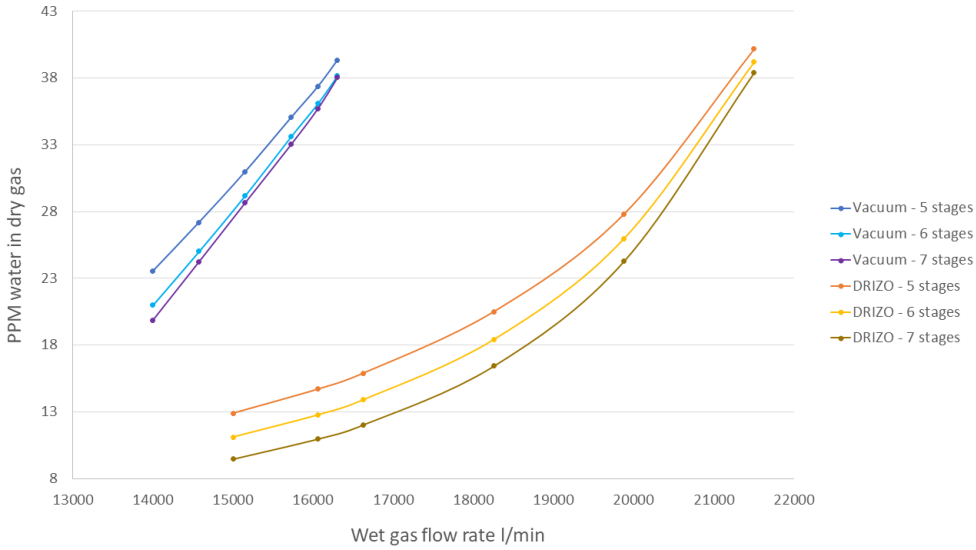

Figure 7.8: Comparison of the vacuum and the DRIZO modified regeneration processes.

Table 7.7 presents a summary of the results obtained and compares the two modified processes. The energy consumption increased in both modified processes as expected, since more energy is required to regenerate the recovered MEG. The energy requirement is clearly higher for the DRIZO process, but more energy is also recovered and is harnessed in the heat exchanger system.

Table 7.7: Results overview for the modified regeneration schemes simulated.

	Regeneration with vacuum	**Regeneration with DRIZO**
Total energy consumption before process modification (kJ/kg water removed)	7700	7241
Total energy consumption after process modification (kJ/kg water removed)	11788	15925
Total energy recovered in heat exchangers (kJ/kg water removed)	9694	12357
MEG loss/make-up before process modification (kg/hr)	770	894
MEG loss/make-up after process modification (kg/hr)	214	227
N-heptane loss/make-up (kg/hr)	–	4008
Methane loss (kg/hr)	13	0.03
Water content in dry gas (ppm)	37	13
Recovered MEG regeneration temperature (°C)	160	161

MEG loss was reduced in both regeneration schemes. By modifying the DRIZO process it was possible to reduce by 667 kg/hr the MEG loss. By modifying the vacuum process MEG loss was reduced by 556 kg/hr. In both cases the MEG make-up amount decreased considerably, making it possible to recover up to 75% of the MEG lost in the non-modified process. At the end, the MEG loss remained the lowest with the modified vacuum process, resulting in 214 kg/hr MEG loss.

The methane loss remained the same for the modified vacuum process. Contrary to the modified DRIZO process, in which a noticeable improvement is observed and it can be considered that almost no methane is being lost.

The achieved water content in dry gas was below 46 ppm for both schemes, fulfilling the gas specifications requirement in each case. However, with the modified DRIZO process the water content in dry gas was further reduced to values as low as 13 ppm. Therefore, it may be possible to reduce the energy consumption in the modified DRIZO process by increasing the water content in dry gas. Otherwise, this can be advantageous for dehydrating gas streams with higher water content or treating larger wet gas flow rates, as observed in Figure 7.8.

It is important to mention, that the MEG regeneration temperature criteria was

met in the two modified processes, by keeping the temperature in the new loop below 165°C to avoid MEG decomposition.

In conclusion, both the water content in dry gas and the methane loss decreased by adding the extra loop in the process simulation, but the energy consumption increased. The process parameters that have a major effect on the losses and energy consumption are the solvent to feed ratio and the use of a stripping medium.

Chapter 8
Concluding remarks

8.1 Conclusions

The ELECNRTL model in Aspen Plus was validated against experimental data from literature for different binary systems that are relevant for the gas dehydration process simulation. The results from the validation showed a good prediction within a wide range of conditions for the different binary systems used in the simulations. The exception was the binary system CO_2-MEG which resulted in very high deviations from the experimental data. However, this system was only of interest for separating any remaining CO_2 in the gas stream but not relevant, since the main objective is to remove water from natural gas.

A total of three regeneration schemes were simulated and compared: vacuum, stripping gas and DRIZO process. For the base case simulations, the processes with vacuum and stripping gas required at least one compressor and more pumps than the DRIZO process, which required only one pump to recirculate the stripping medium.

Comparing the results obtained with the three base case regeneration processes, regeneration with vacuum and DRIZO showed the best results in terms of energy consumption. Therefore, further work was done on these processes in order to modify them by recovering the MEG losses through the addition of an extra regeneration column in a new loop.

It can be concluded that the regeneration process with vacuum and MEG recovery was more efficient in terms of energy consumption for the gas stream composition and flow rate used in this study. However, since the resulting amount of water in dry gas was much lower for the DRIZO process with MEG recovery, it may be possible to extend the use of this regeneration scheme in the following cases:

– To treat larger wet gas flow rates if high reservoir pressures are expected.

– To treat larger amounts of water in the gas stream, during the decline period of a producer well in which the gas-water ratio changes as the reservoir is depleted and more water is being produced.

In terms of minimizing MEG losses during the dehydration process, DRIZO is preferred, which would be an advantage to reduce transportation and storage of MEG. The DRIZO regeneration process also showed the best results in terms of methane losses, reducing losses almost entirely.

Another advantage is the stripping medium required for the DRIZO process, that can be absorbed from natural gas as BTEX compounds and in this way reduce the BTEX emissions to the environment at the same time as reducing the cost of using other valuable gases for stripping gas, such as methane.

In the end a robust gas dehydration simulation was obtained with Aspen Plus. The different MEG regeneration processes were compared, reaching the required water content transport specifications (46 ppm water content) by keeping the temperature of the process below the MEG degradation temperature (165°C).

8.1.1 Further work

The simulations implemented in this work were done using the ELECNRTL model in Aspen Plus, a model that has been validated for the specific dehydration process with MEG. This model introduces the electrolyte capabilities in Aspen Plus. In order to complement the gas dehydration process with MEG, some work that can be done in Aspen Plus is to extend the scope of this work to the simulation of the MEG reclaiming system, including:

– Removal of dissolved salt or other chemicals by MEG and water evaporation.

– Centrifugal separation of solids.

– Study of the impurities that must be removed depending on the different fluids present, such as formation water or completion fluids.

– Study of the various types of salts and the removal requirements according to their solubility.

– Simulation loop including other equipment commonly used offshore, such as particle separators or slug catchers.

References

[1] (2015). Chapter 13 - gas hydrate control. In Fink, J., editor, *Petroleum Engineer's Guide to Oil Field Chemicals and Fluids (Second Edition)*, pages 405 – 443. Gulf Professional Publishing, Boston, second edition edition.

[2] Al-Jawad, M. S., Hassan, O. F., et al. (2012). Comprehensive model for flash calculations of heavy oils using the soave-redlich-kwong equation of state. In *North Africa Technical Conference and Exhibition*. Society of Petroleum Engineers.

[3] Al-Malah, K. I. (2016). *Aspen plus: chemical engineering applications*. John Wiley & Sons.

[4] Arne Fredheim, E. S. (2017). Gas processing - part i "offshore gas processing for rich gas transport". *Lecture in TEP4185.*, pages 16–20.

[5] Bahadori, A., Vuthaluru, H. B., and Mokhatab, S. (2008). Analyzing solubility of acid gas and light alkanes in triethylene glycol. *Journal of Natural Gas Chemistry*, 17(1):51–58.

[6] Braek, A., Almehaideb, R., Darwish, N., and Hughes, R. (2001). Optimization of process parameters for glycol unit to mitigate the emission of btex/vocs. *Process Safety and Environmental Protection*, 79(4):218–232.

[7] Brustad, S., Løken, K.-P., Waalmann, J. G., et al. (2005). Hydrate prevention using meg instead of meoh: Impact of experience from major norwegian developments on technology selection for injection and recovery of meg. In *Offshore Technology Conference*. Offshore Technology Conference.

[8] Campbell, J. (1992). The equipment modules. *Gas Conditioning and Processing. Norman, Okla*, 7:361–362.

[9] Carlson, E. C. (1996). Don't gamble with physical properties. *Chem. Eng. Prog.*, 92(10):35.

[10] Cervantes, B. (2018). Vapor liquid equilibrium of co_2 in mdea/meg/h_2o solutions. *Specialization Project*.

[11] Chapoy, A., Mohammadi, A. H., Richon, D., and Tohidi, B. (2004). Gas solubility measurement and modeling for methane–water and methane–ethane–n-butane–water systems at low temperature conditions. *Fluid phase equilibria*, 220(1):111–119.

[12] Crabtree, M., Eslinger, D., Fletcher, P., Miller, M., Johnson, A., and King, G. (1999). Fighting scale—removal and prevention. *Oilfield review*, 11(3):30–45.

[13] Dalane, K., Hillestad, M., and Deng, L. (2019). Subsea natural gas dehydration with membrane processes: Simulation and process optimization. *Chemical Engineering Research and Design*, 142:257–267.

[14] Darwish, N. A., Al-Mehaideb, R. A., Braek, A. M., and Hughes, R. (2004). Computer simulation of btex emission in natural gas dehydration using pr and rks equations of state with different predictive mixing rules. *Environmental Modelling & Software*, 19(10):957–965.

[15] Dimian, A. C., Bildea, C. S., and Kiss, A. A. (2014). *Integrated design and simulation of chemical processes*, volume 13. Elsevier, pages 140-141, 196-203.

[16] Dugstad, A., Seiersten, M., Nyborg, R., et al. (2003). Flow assurance of ph stabilized wet gas pipelines. In *CORROSION 2003*. NACE International.

[17] Eden, M. R. (2012). Introduction to aspen plus simulation. *Chemical Engineering Department, Auburn University, CHEN*, 4460:1–11.

[18] Encyclopaedia Britannica, I. (1969). *Encyclopædia britannica*. Encyclopaedia Britannica, Incorporated.

[19] Esmaeili, A. (2016). Supersonic separation of natural gas liquids by twister technology. *Chemical Engineering Transactions*, 52:7–12.

[20] Fredheim Arne, S. E. (2017). Lecture in natural gas technology. *Department of energy and process engineering*.

[21] Frost, M., Karakatsani, E., von Solms, N., Richon, D., and Kontogeorgis, G. M. (2013). Vapor–liquid equilibrium of methane with water and methanol. measurements and modeling. *Journal of Chemical & Engineering Data*, 59(4):961–967.

[22] Fu, S., Cenegy, L., Neff, C., et al. (2001). A summary of successful field applications of a kinetic hydrate inhibitor. In *SPE International Symposium on Oilfield Chemistry*. Society of Petroleum Engineers.

[23] Galvão, A. and Francesconi, A. (2010). Solubility of methane and carbon dioxide in ethylene glycol at pressures up to 14 mpa and temperatures ranging from (303 to 423) k. *The Journal of Chemical Thermodynamics*, 42(5):684–688.

[24] Gonzalez, C. and Van Ness, H. C. (1983). Excess thermodynamic functions for ternary systems. 9. total-pressure data and ge for water/ethylene glycol/ethanol at 50. degree. c. *Journal Of Chemical And Engineering Data*, 28(4):410–412.

[25] Haque, M. E. (2012). Ethylene glycol regeneration plan: a systematic approach to troubleshoot the common problems. *Journal of Chemical Engineering*, 27:21–26.

[26] Horstmann, S., Gardeler, H., Wilken, M., Fischer, K., and Gmehling, J. (2004). Isothermal vapor- liquid equilibrium and excess enthalpy data for the binary systems water+ 1, 2-ethanediol and propene+ acetophenone. *Journal of Chemical & Engineering Data*, 49(6):1508–1511.

[27] Hydro, S. (2008). Gas treating. hammerfest lng process. *Guest leture in TPG4230.*

[28] Jokar, S. M., Rahimpour, H. R., Momeni, H., Rahimpour, M. R., and Abbasfard, H. (2014). Simulation and feasibility analysis of structured packing replacement in absorption column of natural gas dehydration process: A case study for farashband gas processing plant, iran. *Journal of Natural Gas Science and Engineering*, 18:336–350.

[29] Jou, F., Otto, F., and Mather, A. (1994). Solubility of methane in glycols at elevated pressures. *Canadian journal of chemical engineering*, 72:130–130.

[30] Jou, F.-Y., Deshmukh, R., Otto, F., and Mather, A. (1990). Vapor-liquid equilibria of H_2S and CO_2 and ethylene glycol at elevated pressures. *Chemical engineering communications*, 87(1):223–231.

[31] Kasiri, N. and Hormozdi, S. (2004). Improving performance of absorption tower in natural gas dehydration process. *Technology*, 23:25.

[32] KATZ, T., SIEDER, G., and HEARN, J. (2013). How glycols affect acid gas removal. *Petroleum technology quarterly*, 18(5).

[33] Kemp, I. C. (2007). 5 - utilities, heat and power systems. In Kemp, I. C., editor, *Pinch Analysis and Process Integration (Second Edition)*, pages 161 – 211. Butterworth-Heinemann, Oxford, second edition edition.

[34] Kidnay, A. J., Parrish, W. R., and McCartney, D. G. (2011). *Fundamentals of natural gas processing, chapter 6.* CRC press.

[35] Kim, H., Lim, Y., Seo, Y., and Ko, M. (2017). Life cycle cost analysis of meg regeneration process incorporating a modified slip stream concept. *Chemical Engineering Science*, 166:181–192.

[36] Knepper, S., Wieneke, M., and Morrissey, C. (2009). Subsea control fluids: Avoidance of hydrate formation. *Measurement and Control*, 42(5):140–144.

[37] Koh, C. A., Sloan, E. D., Sum, A. K., and Wu, D. T. (2011). Fundamentals and applications of gas hydrates. *Annual review of chemical and biomolecular engineering*, 2:237–257.

[38] Kohl, A. L. and Nielsen, R. (1997). Gas purification. (5):946–988.

[39] Kotarba, M. J. and Nagao, K. (2008). Composition and origin of natural gases accumulated in the polish and ukrainian parts of the carpathian region: Gaseous hydrocarbons, noble gases, carbon dioxide and nitrogen. *Chemical Geology*, 255(3-4):426–438.

[40] Latosov, E., Loorits, M., Maaten, B., Volkova, A., and Soosaar, S. (2017). Corrosive effects of h2s and nh3 on natural gas piping systems manufactured of carbon steel. *Energy Procedia*, 128:316–323.

[41] Li, X. (2016). Hydrate control - still a major flow assurance challenge. *Guest lecture in TPG4230.*

[42] McMullen, N. (2011). Chapter four - how hydrate plugs are remediated. In Sloan, D., Koh, C., Sum, A. K., Ballard, A. L., Creek, J., Eaton, M., Lachance, J., Mcmullen, N., Palermo, T., Shoup, G., and Talley, L., editors, *Natural Gas Hydrates in Flow Assurance*, pages 49 – 86. Gulf Professional Publishing, Boston.

[43] Mokhatab, Saeid, M. M. and Northrop, S. (2017). Controlling the hydrocarbon dew point of pipeline gas.

[44] Mokhatab, S. and Bloemendal, G. (2017). Optimal processing scheme for producing pipeline quality gas. pages 323–364.

[45] Mokhatab, S. and Poe, W. A. (2012). *Handbook of natural gas transmission and processing*. Gulf professional publishing.

[46] Neagu, M. and Cursaru, D. L. (2017). Technical and economic evaluations of the triethylene glycol regeneration processes in natural gas dehydration plants. *Journal of Natural Gas Science and Engineering*, 37:327–340.

[47] Nordsveen, M. (2018). Flow assurance for Åsgard subsea compression. *Guest lecture in TPG4230.*

[48] O'Donoghue, A. (2005). Pigging as a flow assurance solution–avoiding slug catcher overflow. *Pipeline Research Limited*.

[49] Øi, L. E. and Tyvand Selstø, E. (2002). Process simulation of glycol regeneration. In *GPA Europe's meeting in Bergen< www. escet. urjc. es/˜ sop/alumnos/proyectos/descargas/propuesta06. pdf>*.

[50] Perry, R. H., Green, D. W., and Maloney, J. O. (2015). *Perry's chemical engineers' handbook*. McGraw-Hill New York.

[51] Piemonte, V., Maschietti, M., and Gironi, F. (2012). A triethylene glycol–water system: A study of the teg regeneration processes in natural gas dehydration plants. *Energy Sources, Part A: Recovery, Utilization, and Environmental Effects*, 34(5):456–464.

[52] Plus, A. (V10). Physical property methods and models - steady state simulation. *Reference Manual*.

[53] Ranjbar, H., Ahmadi, H., Sheshdeh, R. K., and Ranjbar, H. (2015). Application of relative sensitivity function in parametric optimization of a tri-ethylene glycol dehydration plant. *Journal of Natural Gas Science and Engineering*, 25:39–45.

[54] Renon, H. and Prausnitz, J. M. (1968). Local compositions in thermodynamic excess functions for liquid mixtures. *AIChE journal*, 14(1):135–144.

[55] Ruppel, C. (2008). Gas hydrates offshore southeastern united states. *World Wide Web Address: http://oceanexplorer. noaa. gov/explorations/03windows/background/hydrates/hydrates. html*.

[56] Russell, F., Adler, S., Albaugh, L., and Aldana, G. (2004). Gpsa engineering data book. *Gas Process. Suppliers Assoc*, 821.

[57] Saidi, M., Parhoudeh, M., and Rahimpour, M. R. (2014). Mitigation of btex emission from gas dehydration unit by application of drizo process: a case study in farashband gas processing plant; iran. *Journal of Natural Gas Science and Engineering*, 19:32–45.

[58] Sandler, S. I. (2015). *Using Aspen Plus in thermodynamics instruction: a step-by-step guide*. John Wiley & Sons.

[59] Scholes, C. A., Stevens, G. W., and Kentish, S. E. (2012). Membrane gas separation applications in natural gas processing. *Fuel*, 96:15–28.

[60] Serpa, F. S., Vidal, R. S., Filho, J., Dariv, E., Santos, Alexandre, C., and Franceschi, E. (2013). Solubility and thermodynamic properties of carbon dioxide in meg/water mixtures. *III Iberoamerican Conference on Supercritical Fluids Cartagena de Indias (Colombia)*.

[61] Siažik, J. and Malcho, M. (2017). Accumulation of primary energy into natural gas hydrates. *Procedia engineering*, 192:782–787.

[62] Simpson, D. A. (2017a). Chapter eight - gas compression. In Simpson, D. A., editor, *Practical Onshore Gas Field Engineering*, pages 513 – 571. Gulf Professional Publishing.

[63] Simpson, D. A. (2017b). Chapter six - gas gathering systems. In Simpson, D. A., editor, *Practical Onshore Gas Field Engineering*, pages 349 – 460. Gulf Professional Publishing.

[64] Sloan, E., Koh, C., Sum, A., Ballard, A., Shoup, G., McMullen, N., Creek, J., Palermo, T., et al. (2009). Hydrates: state of the art inside and outside flowlines. *Journal of petroleum technology*, 61(12):89–94.

[65] Terrigeol, A., Coquelet, C., and Chapoy, A. (2015). Water content assessment in acid gas. *GPA Europe, Annual Conference, Florence, Italy 16th -18th September*.

[66] Tohidi, B. (2005). *Gas Hydrates: Friend or Foe?* Society of Petroleum Engineers.

[67] V11.1, A. P. (2001). Aspen physical property system - physical property methods and models physical property methods and models. *Chapter 2: Property method descriptions*, pages 40–62.

[68] Villamanan, M. A., Gonzalez, C., and Van Ness, H. C. (1984). Excess thermodynamic properties for water/ethylene glycol. *Journal of Chemical and Engineering Data*, 29(4):427–429.

[69] Zaboon, S., Soames, A., Ghodkay, V., Gubner, R., and Barifcani, A. (2017). Recovery of mono-ethylene glycol by distillation and the impact of dissolved salts evaluated through simulation of field data. *Journal of Natural Gas Science and Engineering*, 44:214–232.

[70] Zheng, D.-Q., Ma, W.-D., Wei, R., and Guo, T.-M. (1999). Solubility study of methane, carbon dioxide and nitrogen in ethylene glycol at elevated temperatures and pressures. *Fluid phase equilibria*, 155(2):277–286.

Chapter A
Appendix

A.1 VLE validation deviations

Table A.1: Aspen Plus pressures obtained by interpolation at 50° C for the system H_2O-MEG and their respective calculated deviations from literature

Gonzalez and Van Ness[24] H_2O-MEG - 50° C		**Interpolated Pressure KPa**	**Absolute Relative Deviation**	**Relative Deviation $\%\Delta_i$**	**Distance from RD mean**
Mole fraction X	**Total pressure KPa**				
0.0185	0.316	0.3178	0.58 %	0.58 %	3.48 %
0.0479	0.634	0.6788	7.06 %	7.06 %	3.00 %
0.0991	1.185	1.3074	10.33 %	10.33 %	6.26 %
0.15	1.753	1.9324	10.23 %	10.23 %	6.17 %
0.199	2.315	2.5341	9.47 %	9.47 %	5.40 %
0.3006	3.524	3.7821	7.32 %	7.32 %	3.26 %
0.3506	4.157	4.3964	5.76 %	5.76 %	1.70 %
0.4009	4.758	5.0145	5.39 %	5.39 %	1.33 %
0.4506	5.411	5.6252	3.96 %	3.96 %	0.10 %
0.5006	6.023	6.2398	3.60 %	3.60 %	0.46 %
0.502	5.978	6.2570	4.67 %	4.67 %	0.61 %
0.5494	6.589	6.8396	3.80 %	3.80 %	0.26 %
0.5994	7.224	7.4543	3.19 %	3.19 %	0.87 %
0.6494	7.858	8.0691	2.69 %	2.69 %	1.38 %
0.6995	8.494	8.6852	2.25 %	2.25 %	1.81 %
0.7498	9.156	9.3038	1.61 %	1.61 %	2.45 %
0.8	9.798	9.9213	1.26 %	1.26 %	2.80 %
0.8501	10.44	10.5376	0.94 %	0.94 %	3.13 %
0.8999	11.094	11.1503	0.51 %	0.51 %	3.55 %
0.9502	11.745	11.7693	0.21 %	0.21 %	3.85 %
0.9803	12.082	12.1397	0.48 %	0.48 %	3.58 %
		AARD	**4.06 %**	**MAD**	**2.64 %**

Table A.2: Aspen Plus water mole fractions obtained by interpolation at 50° C for the system H_2O-MEG and their respective calculated deviations from literature

Gonzalez and Van Ness[24] H_2O-MEG - 50° C		**Interpolated H_2O mole fraction**	**Absolute Relative Deviation**	**Relative Deviation $\%\Delta_i$**	**Distance from RD mean**
Mole fraction X	**Total Pressure KPa**				
0.0185	0.316	0.0184	0.81 %	-0.81 %	3.17 %
0.0479	0.634	0.0443	7.61 %	-7.61 %	3.63 %
0.0991	1.185	0.0891	10.06 %	-10.06 %	6.08 %
0.15	1.753	0.1354	9.74 %	-9.74 %	5.76 %
0.199	2.315	0.1812	8.97 %	-8.97 %	4.99 %
0.3006	3.524	0.2796	6.99 %	-6.99 %	3.01 %
0.3506	4.157	0.3311	5.56 %	-5.56 %	1.58 %
0.4009	4.758	0.3800	5.21 %	-5.21 %	1.23 %
0.4506	5.411	0.4332	3.87 %	-3.87 %	0.11 %
0.5006	6.023	0.4830	3.52 %	-3.52 %	0.45 %
0.502	5.978	0.4793	4.52 %	-4.52 %	0.54 %
0.5494	6.589	0.5290	3.71 %	-3.71 %	0.27 %
0.5994	7.224	0.5807	3.13 %	-3.13 %	0.85 %
0.6494	7.858	0.6322	2.64 %	-2.64 %	1.33 %
0.6995	8.494	0.6840	2.22 %	-2.22 %	1.76 %
0.7498	9.156	0.7378	1.60 %	-1.60 %	2.38 %
0.8	9.798	0.7900	1.25 %	-1.25 %	2.72 %
0.8501	10.44	0.8422	0.93 %	-0.93 %	3.04 %
0.8999	11.094	0.8953	0.51 %	-0.51 %	3.47 %
0.9502	11.745	0.9482	0.21 %	-0.21 %	3.77 %
0.9803	12.082	0.9756	0.48 %	-0.48 %	3.50 %
		AARD	**3.98 %**	**MAD**	**2.55 %**

Table A.3: Aspen Plus pressures obtained by interpolation at 60° C for the system H_2O-MEG and their respective calculated deviations from literature

Horstmann. et al.[26] H_2O-MEG - 60° C		**Interpolated Pressure KPa**	**Absolute Relative Deviation**	**Relative Deviation $\%\Delta_i$**	**Distance from RD mean**
Mole fraction X	**Total Pressure KPa**				
0.0033	0.28	0.2506	10.51 %	-10.51 %	12.08 %
0.0095	0.39	0.3734	4.25 %	-4.25 %	5.81 %
0.0163	0.51	0.5088	0.24 %	-0.24 %	1.81 %
0.0272	0.71	0.7239	1.96 %	1.96 %	0.39 %
0.0414	0.96	1.0042	4.61 %	4.61 %	3.04 %
0.0634	1.35	1.4385	6.56 %	6.56 %	4.99 %
0.0928	1.87	2.0187	7.95 %	7.95 %	6.39 %
0.1322	2.58	2.7977	8.44 %	8.44 %	6.87 %
0.1783	3.43	3.7087	8.13 %	8.13 %	6.56 %
0.231	4.42	4.7514	7.50 %	7.50 %	5.93 %
0.2889	5.52	5.8963	6.82 %	6.82 %	5.25 %
0.3488	6.69	7.0799	5.83 %	5.83 %	4.26 %
0.4146	7.99	8.3816	4.90 %	4.90 %	3.34 %
0.4777	9.27	9.6311	3.89 %	3.89 %	2.33 %
0.5378	10.49	10.8206	3.15 %	3.15 %	1.59 %
0.5926	11.61	11.9050	2.54 %	2.54 %	0.98 %
0.642	12.64	12.8844	1.93 %	1.93 %	0.37 %
0.6863	13.55	13.7606	1.55 %	1.55 %	0.01 %
0.7254	14.37	14.5361	1.16 %	1.16 %	0.41 %
0.7594	15.09	15.2099	0.79 %	0.79 %	0.77 %
0.7892	15.72	15.7777	0.37 %	0.37 %	1.20 %
0.7898	15.81	15.8116	0.01 %	0.01 %	1.55 %
0.8201	16.42	16.4113	0.05 %	-0.05 %	1.62 %
0.8482	16.99	16.9431	0.28 %	-0.28 %	1.84 %
0.8739	17.5	17.4788	0.12 %	-0.12 %	1.69 %
0.8972	17.94	17.9402	0.00 %	0.00 %	1.56 %
0.918	18.38	18.3528	0.15 %	-0.15 %	1.71 %
0.936	18.74	18.6840	0.30 %	-0.30 %	1.86 %
0.9515	19.04	19.0178	0.12 %	-0.12 %	1.68 %
0.9633	19.22	19.2518	0.17 %	0.17 %	1.40 %
0.973	19.43	19.4439	0.07 %	0.07 %	1.49 %
0.9808	19.58	19.5970	0.09 %	0.09 %	1.48 %
0.9867	19.7	19.7144	0.07 %	0.07 %	1.49 %
0.9911	19.78	19.8030	0.12 %	0.12 %	1.45 %
0.9941	19.83	19.8607	0.15 %	0.15 %	1.41 %
0.996	19.87	19.8988	0.14 %	0.14 %	1.42 %
0.9974	19.92	19.9272	0.04 %	0.04 %	1.53 %
0.9984	19.89	19.9472	0.29 %	0.29 %	1.28 %
0.9992	19.88	19.9619	0.41 %	0.41 %	1.15 %
0.9997	19.92	19.9724	0.26 %	0.26 %	1.30 %
1	19.93	19.9787	0.24 %	0.24 %	1.32 %
		AARD	**0.19 %**	**MAD**	**2.55 %**

Table A.4: Aspen Plus water mole fractions obtained by interpolation at 60° C for the system H_2O-MEG and their respective calculated deviations from literature

Horstmann. et al.[26] H_2O-MEG - 60° C		**Interpolated H_2O Mole Fraction**	**Absolute Relative Deviation**	**Relative Deviation $\%\Delta_i$**	**Distance from RD mean**
Mole fraction X	**Total Pressure KPa**				
0.0033	0.28	0.0049	45.58 %	45.58 %	46.20 %
0.0095	0.39	0.0105	8.84 %	8.84 %	9.46 %
0.0163	0.51	0.0165	0.39 %	0.39 %	1.01 %
0.0272	0.71	0.0266	2.58 %	-2.58 %	1.96 %
0.0414	0.96	0.0393	5.41 %	-5.41 %	4.78 %
0.0634	1.35	0.0590	7.07 %	-7.07 %	6.44 %
0.0928	1.87	0.0853	8.11 %	-8.11 %	7.49 %
0.1322	2.58	0.1212	8.33 %	-8.33 %	7.71 %
0.1783	3.43	0.1642	7.91 %	-7.91 %	7.29 %
0.231	4.42	0.2143	7.26 %	-7.26 %	6.63 %
0.2889	5.52	0.2699	6.59 %	-6.59 %	5.96 %
0.3488	6.69	0.3290	5.65 %	-5.65 %	5.03 %
0.4146	7.99	0.3948	4.77 %	-4.77 %	4.15 %
0.4777	9.27	0.4594	3.82 %	-3.82 %	3.19 %
0.5378	10.49	0.5211	3.11 %	-3.11 %	2.48 %
0.5926	11.61	0.5777	2.51 %	-2.51 %	1.89 %
0.642	12.64	0.6297	1.92 %	-1.92 %	1.30 %
0.6863	13.55	0.6756	1.55 %	-1.55 %	0.92 %
0.7254	14.37	0.7170	1.16 %	-1.16 %	0.53 %
0.7594	15.09	0.7534	0.80 %	-0.80 %	0.17 %
0.7892	15.72	0.7852	0.51 %	-0.51 %	0.11 %
0.7898	15.81	0.7897	0.01 %	-0.01 %	0.61 %
0.8201	16.42	0.8205	0.05 %	0.05 %	0.68 %
0.8482	16.99	0.8493	0.13 %	0.13 %	0.75 %
0.8739	17.5	0.8750	0.12 %	0.12 %	0.75 %
0.8972	17.94	0.8972	0.00 %	0.00 %	0.62 %
0.918	18.38	0.9194	0.15 %	0.15 %	0.77 %
0.936	18.74	0.9375	0.16 %	0.16 %	0.79 %
0.9515	19.04	0.9527	0.12 %	0.12 %	0.74 %
0.9633	19.22	0.9617	0.17 %	-0.17 %	0.46 %
0.973	19.43	0.9723	0.07 %	-0.07 %	0.55 %
0.9808	19.58	0.9799	0.09 %	-0.09 %	0.54 %
0.9867	19.7	0.9859	0.07 %	-0.07 %	0.55 %
0.9911	19.78	0.9900	0.12 %	-0.12 %	0.51 %
0.9941	19.83	0.9925	0.16 %	-0.16 %	0.47 %
0.996	19.87	0.9945	0.15 %	-0.15 %	0.48 %
0.9974	19.92	0.9970	0.04 %	-0.04 %	0.59 %
0.9984	19.89	0.9955	0.29 %	-0.29 %	0.34 %
0.9992	19.88	0.9950	0.41 %	-0.41 %	0.21 %
0.9997	19.92	0.9970	0.26 %	-0.26 %	0.36 %
1	19.93	0.9975	0.25 %	-0.25 %	0.38 %
		AARD	**0.18 %**	**MAD**	**3.31 %**

Table A.5: Aspen Plus pressures obtained by interpolation at 60° C for the system H_2O-MEG and their respective calculated deviations from literature

Villamanan et al.[68] H_2O-MEG - 60° C		**Interpolated Pressure KPa**	**Absolute Relative Deviation**	**Relative Deviation $\%\Delta_i$**	**Distance from RD mean**
Mole fraction X	**Total Pressure KPa**				
0.0188	0.543	0.55735	2.64 %	2.64 %	0.95 %
0.0487	1.058	1.14807	8.51 %	8.51 %	4.92 %
0.1008	1.997	2.17755	9.04 %	9.04 %	5.45 %
0.1497	2.892	3.14399	8.71 %	8.71 %	5.12 %
0.1989	3.813	4.11655	7.96 %	7.96 %	4.37 %
0.2479	4.76	5.08534	6.83 %	6.83 %	3.24 %
0.2973	5.79	6.06223	4.70 %	4.70 %	1.11 %
0.3477	6.678	7.05909	5.71 %	5.71 %	2.12 %
0.3975	7.724	8.04427	4.15 %	4.15 %	0.56 %
0.4478	8.718	9.03954	3.69 %	3.69 %	0.10 %
0.4982	9.721	10.03698	3.25 %	3.25 %	0.34 %
0.4987	9.717	10.04688	3.39 %	3.39 %	0.20 %
0.5487	10.713	11.03661	3.02 %	3.02 %	0.57 %
0.5989	11.751	12.03049	2.38 %	2.38 %	1.21 %
0.6489	12.746	13.02061	2.15 %	2.15 %	1.44 %
0.6988	13.757	14.00895	1.83 %	1.83 %	1.76 %
0.7489	14.836	15.00144	1.12 %	1.12 %	2.47 %
0.8003	15.88	16.01988	0.88 %	0.88 %	2.71 %
0.8504	16.879	17.01277	0.79 %	0.79 %	2.80 %
0.9001	17.906	17.99793	0.51 %	0.51 %	3.08 %
0.9495	18.923	18.97733	0.29 %	0.29 %	3.30 %
0.9797	19.428	19.57616	0.76 %	0.76 %	2.83 %
1	19.931	19.97873	0.24 %	0.24 %	3.35 %
		AARD	**1.59 %**	**MAD**	**2.00 %**

Table A.6: Aspen Plus water mole fraction obtained by interpolation at 60° C for the system H_2O-MEG and their respective calculated deviations from literature

Villamanan et al.[68] H_2O-MEG - 60° C		**Interpolated H_2O Mole Fraction**	**Absolute Relative Deviation**	**Relative Deviation $\%\Delta_i$**	**Distance from RD mean**
Mole fraction X	**Total Pressure KPa**				
0.0188	0.543	0.018074	3.86 %	-3.86 %	-0.23 %
0.0487	1.058	0.044141	9.36 %	-9.36 %	-5.73 %
0.1008	1.997	0.091663	9.06 %	-9.06 %	-5.43 %
0.1497	2.892	0.136951	8.52 %	-8.52 %	-4.89 %
0.1989	3.813	0.183545	7.72 %	-7.72 %	-4.09 %
0.2479	4.76	0.231446	6.64 %	-6.64 %	-3.01 %
0.2973	5.79	0.283535	4.63 %	-4.63 %	-1.00 %
0.3477	6.678	0.328434	5.54 %	-5.54 %	-1.91 %
0.3975	7.724	0.381312	4.07 %	-4.07 %	-0.44 %
0.4478	8.718	0.431551	3.63 %	-3.63 %	0.00 %
0.4982	9.721	0.482235	3.20 %	-3.20 %	0.42 %
0.4987	9.717	0.482033	3.34 %	-3.34 %	0.29 %
0.5487	10.713	0.532353	2.98 %	-2.98 %	0.65 %
0.5989	11.751	0.584784	2.36 %	-2.36 %	1.27 %
0.6489	12.746	0.635033	2.14 %	-2.14 %	1.49 %
0.6988	13.757	0.686080	1.82 %	-1.82 %	1.81 %
0.7489	14.836	0.740550	1.12 %	-1.12 %	2.51 %
0.8003	15.88	0.793241	0.88 %	-0.88 %	2.75 %
0.8504	16.879	0.843651	0.79 %	-0.79 %	2.84 %
0.9001	17.906	0.895463	0.52 %	-0.52 %	3.11 %
0.9495	18.923	0.946760	0.29 %	-0.29 %	3.34 %
0.9797	19.428	0.972228	0.76 %	-0.76 %	2.87 %
1	19.931	0.997593	0.24 %	-0.24 %	3.39 %
		AARD	**1.57 %**	**MAD**	**2.06 %**

Table A.7: Aspen Plus pressures obtained by interpolation at 80° C for the system H_2O-MEG and their respective calculated deviations from literature

Horstmann. et al.[26] H_2O-MEG - 80° C		**Interpolated Pressure KPa**	**Absolute Relative Deviation**	**Relative Deviation $\%\Delta_i$**	**Distance from RD mean**
Mole fraction X	**Total Pressure KPa**				
0.0059	1.02	0.9517	6.69 %	-6.69 %	7.05 %
0.0115	1.28	1.2120	5.31 %	-5.31 %	5.67 %
0.0217	1.72	1.6889	1.81 %	-1.81 %	2.17 %
0.0331	2.22	2.2193	0.03 %	-0.03 %	0.39 %
0.0454	2.76	2.7908	1.11 %	1.11 %	0.76 %
0.0668	3.7	3.7876	2.37 %	2.37 %	2.01 %
0.0963	4.99	5.1643	3.49 %	3.49 %	3.13 %
0.1359	6.71	7.0061	4.41 %	4.41 %	4.05 %
0.1816	8.76	9.1398	4.34 %	4.34 %	3.98 %
0.2346	11.15	11.6107	4.13 %	4.13 %	3.77 %
0.2919	13.81	14.2856	3.44 %	3.44 %	3.08 %
0.3516	16.6	17.0684	2.82 %	2.82 %	2.46 %
0.417	19.7	20.1262	2.16 %	2.16 %	1.80 %
0.4797	22.7	23.0550	1.56 %	1.56 %	1.21 %
0.5393	25.58	25.8394	1.01 %	1.01 %	0.66 %
0.5936	28.22	28.3791	0.56 %	0.56 %	0.20 %
0.6428	30.61	30.6816	0.23 %	0.23 %	0.13 %
0.6868	32.75	32.7425	0.02 %	-0.02 %	0.38 %
0.7248	34.59	34.5194	0.20 %	-0.20 %	0.56 %
0.7258	34.65	34.5662	0.24 %	-0.24 %	0.60 %
0.758	36.16	36.0781	0.23 %	-0.23 %	0.59 %
0.7898	37.66	37.5655	0.25 %	-0.25 %	0.61 %
0.82	39.1	38.9828	0.30 %	-0.30 %	0.66 %
0.8481	40.4	40.2992	0.25 %	-0.25 %	0.61 %
0.8738	41.61	41.5054	0.25 %	-0.25 %	0.61 %
0.8971	42.69	42.5946	0.22 %	-0.22 %	0.58 %
0.9179	43.67	43.5692	0.23 %	-0.23 %	0.59 %
0.9358	44.5	44.4130	0.20 %	-0.20 %	0.55 %
0.9513	45.15	45.1387	0.02 %	-0.02 %	0.38 %
0.9631	45.72	45.6919	0.06 %	-0.06 %	0.42 %
0.9728	46.2	46.1456	0.12 %	-0.12 %	0.48 %
0.9804	46.56	46.5051	0.12 %	-0.12 %	0.48 %
0.9863	46.78	46.7782	0.00 %	0.00 %	0.36 %
0.9909	47.02	46.9940	0.06 %	-0.06 %	0.41 %
0.9938	47.16	47.1330	0.06 %	-0.06 %	0.42 %
0.9958	47.26	47.2259	0.07 %	-0.07 %	0.43 %
0.9973	47.32	47.2944	0.05 %	-0.05 %	0.41 %
0.9982	47.36	47.3371	0.05 %	-0.05 %	0.41 %
0.9991	47.4	47.3803	0.04 %	-0.04 %	0.40 %
0.9997	47.41	47.4070	0.01 %	-0.01 %	0.37 %
1	47.44	47.4235	0.03 %	-0.03 %	0.39 %
		AARD	**0.12 %**	**MAD**	**1.32 %**

Table A.8: Aspen Plus water mole fraction obtained by interpolation at 80° C for the system H_2O-MEG and their respective calculated deviations from literature

Horstmann. et al.[26] H_2O-MEG - 80° C		**Interpolated H_2O Mole Fraction**	**Absolute Relative Deviation**	**Relative Deviation $\%\Delta_i$**	**Distance from RD mean**
Mole fraction X	**Total Pressure KPa**				
0.0059	1.02	0.0074	24.91 %	24.90 %	24.64 %
0.0115	1.28	0.0129	12.74 %	12.72 %	12.46 %
0.0217	1.72	0.0224	3.08 %	3.08 %	2.83 %
0.0331	2.22	0.0331	0.05 %	0.05 %	0.21 %
0.0454	2.76	0.0447	1.45 %	-1.46 %	1.71 %
0.0668	3.7	0.0649	2.81 %	-2.82 %	3.07 %
0.0963	4.99	0.0926	3.87 %	-3.88 %	4.14 %
0.1359	6.71	0.1295	4.65 %	-4.68 %	4.93 %
0.1816	8.76	0.1735	4.44 %	-4.49 %	4.74 %
0.2346	11.15	0.2247	4.15 %	-4.21 %	4.46 %
0.2919	13.81	0.2817	3.41 %	-3.49 %	3.74 %
0.3516	16.6	0.3415	2.75 %	-2.86 %	3.11 %
0.417	19.7	0.4079	2.06 %	-2.19 %	2.44 %
0.4797	22.7	0.4721	1.43 %	-1.58 %	1.84 %
0.5393	25.58	0.5337	0.85 %	-1.03 %	1.28 %
0.5936	28.22	0.5902	0.37 %	-0.57 %	0.83 %
0.6428	30.61	0.6412	0.01 %	-0.24 %	0.49 %
0.6868	32.75	0.6870	0.27 %	0.02 %	0.23 %
0.7248	34.59	0.7263	0.47 %	0.21 %	0.05 %
0.7258	34.65	0.7275	0.51 %	0.25 %	0.01 %
0.758	36.16	0.7598	0.51 %	0.23 %	0.02 %
0.7898	37.66	0.7918	0.54 %	0.26 %	0.00 %
0.82	39.1	0.8225	0.60 %	0.30 %	0.05 %
0.8481	40.4	0.8503	0.56 %	0.25 %	0.00 %
0.8738	41.61	0.8761	0.58 %	0.26 %	0.00 %
0.8971	42.69	0.8991	0.56 %	0.23 %	0.03 %
0.9179	43.67	0.9200	0.57 %	0.23 %	0.02 %
0.9358	44.5	0.9377	0.54 %	0.20 %	0.06 %
0.9513	45.15	0.9515	0.38 %	0.03 %	0.23 %
0.9631	45.72	0.9637	0.42 %	0.06 %	0.19 %
0.9728	46.2	0.9739	0.48 %	0.12 %	0.13 %
0.9804	46.56	0.9816	0.48 %	0.12 %	0.13 %
0.9863	46.78	0.9863	0.37 %	0.00 %	0.25 %
0.9909	47.02	0.9914	0.42 %	0.06 %	0.20 %
0.9938	47.16	0.9944	0.43 %	0.06 %	0.20 %
0.9958	47.26	0.9965	0.44 %	0.07 %	0.18 %
0.9973	47.32	0.9978	0.42 %	0.05 %	0.20 %
0.9982	47.36	0.9986	0.42 %	0.05 %	0.20 %
0.9991	47.4	0.9995	0.41 %	0.04 %	0.21 %
0.9997	47.41	0.9997	0.38 %	0.01 %	0.25 %
1	47.44	1.0004	0.41 %	0.04 %	0.22 %
		AARD	**0.47 %**	**MAD**	**1.95 %**

Table A.9: Aspen Plus pressures obtained by interpolation at 30° C for the system CH_4-MEG and their respective calculated deviations from literature

Francesconi and Galvao[23] CH_4-MEG - 30° C		**Interpolated Pressure KPa**	**Absolute Relative Deviation**	**Relative Deviation $\%\Delta_i$**	**Distance from RD mean**
Mole fraction X	**Total Pressure KPa**				
0.0015	1.3674	0.9044	33.86 %	-33.86 %	24.78 %
0.0035	2.8614	2.1920	23.39 %	-23.39 %	14.32 %
0.006	4.244	3.9559	6.79 %	-6.79 %	2.28 %
0.0084	5.77772	5.8452	1.17 %	1.17 %	10.24 %
0.0119	7.7024	9.0509	17.51 %	17.51 %	26.58 %
		AARD	**16.54 %**	**MAD**	**15.64 %**

Table A.10: Aspen Plus methane mole fraction obtained by interpolation at 30° C for the system CH_4-MEG and their respective calculated deviations from literature

Francesconi and Galvao[23] CH_4-MEG - 30° C		**Interpolated CH_4 mole fraction**	**Absolute Relative Deviation**	**Relative Deviation $\%\Delta_i$**	**Distance from RD mean**
Mole fraction X	**Total Pressure KPa**				
0.0015	1.3674	0.0022	49.13 %	49.13 %	34.95 %
0.0035	2.8614	0.0045	28.00 %	28.00 %	13.82 %
0.006	4.244	0.0064	6.40 %	6.40 %	7.78 %
0.0084	5.77772	0.0083	0.97 %	-0.97 %	15.14 %
0.0119	7.7024	0.0105	11.67 %	-11.67 %	25.85 %
		AARD	**19.24 %**	**MAD**	**19.51 %**

Table A.11: Aspen Plus pressures obtained by interpolation at 50° C for the system CH_4-MEG and their respective calculated deviations from literature

Francesconi and Galvao[23] CH_4-MEG - 50° C		**Interpolated Pressure MPa**	**Absolute Relative Deviation**	**Relative Deviation $\%\Delta_i$**	**Distance from RD mean**
Mole fraction X	**Total Pressure KPa**				
0.0018	1.4894	1.0862	27.07 %	-27.07 %	19.40 %
0.0042	3.1514	2.6346	16.40 %	-16.40 %	8.73 %
0.0068	4.722	4.4617	5.51 %	-5.51 %	2.16 %
0.0094	6.4692	6.4728	0.06 %	0.06 %	7.72 %
0.013	8.7064	9.6277	10.58 %	10.58 %	18.25 %
		AARD	**11.92 %**	**MAD**	**11.25 %**

Table A.12: Aspen Plus methane mole fraction obtained by interpolation at 50° C for the system CH_4-MEG and their respective calculated deviations from literature

Francesconi and Galvao[23] CH_4-MEG - 50° C		**Interpolated CH_4 mole fraction**	**Absolute Relative Deviation**	**Relative Deviation $\%\Delta_i$**	**Distance from RD mean**
Mole fraction X	**Total Pressure MPa**				
0.0018	1.4894	0.0024	36.11 %	35.74 %	25.48 %
0.0042	3.1514	0.0050	18.09 %	18.09 %	7.84 %
0.0068	4.722	0.0072	5.17 %	5.17 %	5.09 %
0.0094	6.4692	0.0094	0.05 %	-0.05 %	10.30 %
0.013	8.7064	0.0120	7.66 %	-7.66 %	17.92 %
		AARD	**13.42 %**	**MAD**	**13.33 %**

Table A.13: Aspen Plus pressures obtained by interpolation at 100° C for the system CH_4-MEG and their respective calculated deviations from literature

Francesconi and Galvao[23] CH_4-MEG - 100° C		**Interpolated Pressure MPa**	**Absolute Relative Deviation**	**Relative Deviation $\%\Delta_i$**	**Distance from RD mean**
Mole fraction X	**Total Pressure MPa**				
0.0031	1.7944	1.9098	6.43 %	6.43 %	11.11 %
0.0066	3.8764	4.3150	11.32 %	11.32 %	6.22 %
0.0103	5.917	7.2182	21.99 %	21.99 %	4.45 %
0.0141	8.1992	10.6925	30.41 %	30.41 %	12.87 %
0.0192	11.2164	16.3698	41.67 %	45.95 %	28.41 %
		AARD	**22.36 %**	**MAD**	**12.61 %**

Table A.14: Aspen Plus methane mole fraction obtained by interpolation at 100° C for the system CH_4-MEG and their respective calculated deviations from literature

Francesconi and Galvao[23] CH_4-MEG - 100° C		**Interpolated CH_4 mole fraction**	**Absolute Relative Deviation**	**Relative Deviation $\%\Delta_i$**	**Distance from RD mean**
Mole fraction X	**Total Pressure MPa**				
0.0031	1.7944	0.0029	5.77 %	-5.77 %	8.86 %
0.0066	3.8764	0.0060	9.20 %	-9.20 %	5.44 %
0.0103	5.917	0.0087	15.47 %	-15.47 %	0.83 %
0.0141	8.1992	0.0114	18.89 %	-18.89 %	4.26 %
0.0192	11.2164	0.0146	23.84 %	-23.84 %	9.21 %
		AARD	**14.63 %**	**MAD**	**5.72 %**

Table A.15: Aspen Plus pressures obtained by interpolation at 125° C for the system CH_4-MEG and their respective calculated deviations from literature

Francesconi and Galvao[23] CH_4-MEG - 125° C		**Interpolated Pressure MPa**	**Absolute Relative Deviation**	**Relative Deviation $\%\Delta_i$**	**Distance from RD mean**
Mole fraction X	**Total Pressure MPa**				
0.0038	1.9469	2.3106	18.68 %	19.14 %	10.06 %
0.0082	4.2389	5.2010	22.70 %	22.98 %	6.22 %
0.0127	6.5145	8.4267	29.35 %	29.60 %	0.40 %
0.0175	9.0642	12.2059	34.91 %	34.91 %	5.71 %
0.0237	12.4714	17.3820	39.38 %	39.38 %	10.18 %
		AARD	**29.00 %**	**MAD**	**6.51 %**

Table A.16: Aspen Plus methane mole fraction obtained by interpolation at 125° C for the system CH_4-MEG and their respective calculated deviations from literature

Francesconi and Galvao[23] CH_4-MEG - 125° C		**Interpolated CH_4 mole fraction**	**Absolute Relative Deviation**	**Relative Deviation $\%\Delta_i$**	**Distance from RD mean**
Mole fraction X	**Total Pressure MPa**				
0.0038	1.9469	0.0032	15.28 %	-15.28 %	4.69 %
0.0082	4.2389	0.0068	17.36 %	-17.36 %	2.61 %
0.0127	6.5145	0.0101	20.62 %	-20.62 %	0.65 %
0.0175	9.0642	0.0135	22.61 %	-22.61 %	2.64 %
0.0237	12.4714	0.0181	23.52 %	-23.97 %	4.00 %
		AARD	**19.88 %**	**MAD**	**2.92 %**

Table A.17: Aspen Plus pressures obtained by interpolation at 150° C for the system CH_4-MEG and their respective calculated deviations from literature

Francesconi and Galvao[23] CH_4-MEG - 150° C		**Interpolated Pressure MPa**	**Absolute Relative Deviation**	**Relative Deviation $\%\Delta_i$**	**Distance from RD mean**
Mole fraction X	**Total Pressure MPa**				
0.0047	2.0994	2.8929	37.80 %	37.80 %	8.81 %
0.0101	4.6014	6.4819	40.87 %	40.87 %	5.74 %
0.0156	7.112	10.4953	47.57 %	47.57 %	0.97 %
0.0215	9.9292	14.9449	50.51 %	50.51 %	3.91 %
0.0291	13.7264	21.4517	56.28 %	56.28 %	9.68 %
		AARD	**46.61 %**	**MAD**	**5.82 %**

Table A.18: Aspen Plus methane mole fraction obtained by interpolation at 150° C for the system CH_4-MEG and their respective calculated deviations from literature

Francesconi and Galvao[23] CH_4-MEG- 150° C		**Interpolated CH_4 mole fraction**	**Absolute Relative Deviation**	**Relative Deviation $\%\Delta_i$**	**Distance from RD mean**
Mole fraction X	**Total Pressure MPa**				
0.0047	2.0994	0.0035	26.03 %	-26.03 %	2.09 %
0.0101	4.6014	0.0074	26.96 %	-26.96 %	1.16 %
0.0156	7.112	0.0111	29.16 %	-29.16 %	1.04 %
0.0215	9.9292	0.0152	29.17 %	-29.17 %	1.05 %
0.0291	13.7264	0.0206	29.29 %	-29.29 %	1.17 %
		AARD	**28.12 %**	**MAD**	**1.30 %**

Table A.19: Aspen Plus pressures obtained by interpolation at 50° C for the system CH_4-MEG and their respective calculated deviations from literature

D.-Q. Zheng[70] CH_4-MEG - 50° C		**Interpolated Pressure MPa**	**Absolute Relative Deviation**	**Relative Deviation $\%\Delta_i$**	**Distance from RD mean**
Mole fraction X	**Total Pressure MPa**				
0.003	2.39	1.8452	22.80 %	-22.80 %	2.25 %
0.003	2.37	1.8452	22.14 %	-22.14 %	2.90 %
0.0066	5.98	4.3150	27.84 %	-27.84 %	2.80 %
0.011	10.3	7.8167	24.11 %	-24.11 %	0.93 %
0.0148	15.9	11.3969	28.32 %	-28.32 %	3.28 %
		AARD	**25.04 %**	**MAD**	**2.43 %**

Table A.20: Aspen Plus methane mole fractions obtained by interpolation at 50° C for the system CH_4-MEG and their respective calculated deviations from literature

D.-Q. Zheng[70] CH_4-MEG - 50° C		**Interpolated CH_4 mole fraction**	**Absolute Relative Deviation**	**Relative Deviation $\%\Delta_i$**	**Distance from RD mean**
Mole fraction X	**Total Pressure MPa**				
0.003	2.39	0.0039	27.78 %	27.78 %	0.10 %
0.003	2.37	0.0038	26.77 %	26.77 %	1.11 %
0.0066	5.98	0.0088	33.13 %	33.13 %	5.25 %
0.011	10.3	0.0137	24.55 %	24.55 %	3.33 %
0.0148	15.9	0.0188	27.15 %	27.15 %	0.72 %
		AARD	**27.88 %**	**MAD**	**2.10 %**

Table A.21: Aspen Plus pressures obtained by interpolation at 100° C for the system CH_4-MEG and their respective calculated deviations from literature

D.-Q. Zheng[70] CH_4-MEG - 100° C		**Interpolated Pressure MPa**	**Absolute Relative Deviation**	**Relative Deviation $\%\Delta_i$**	**Distance from RD mean**
Mole fraction X	**Total Pressure MPa**				
0.0003	0.2	0.1770	11.51 %	-11.51 %	0.91 %
0.0039	2.91	2.4342	16.35 %	-16.35 %	3.94 %
0.0081	6.63	5.4423	17.91 %	-17.91 %	5.50 %
0.0123	10.38	8.9763	13.52 %	-13.52 %	1.11 %
0.0162	14.625	12.8744	2.78 %	-2.78 %	9.63 %
		AARD	**12.42 %**	**MAD**	**4.22 %**

Table A.22: Aspen Plus methane mole fractions obtained by interpolation at 100° C for the system CH_4-MEG and their respective calculated deviations from literature

D.-Q. Zheng[70] CH_4-MEG - 100° C		**Interpolated CH_4 mole fraction**	**Absolute Relative Deviation**	**Relative Deviation $\%\Delta_i$**	**Distance from RD mean**
Mole fraction X	**Total Pressure MPa**				
0.0003	0.2	0.0003	12.94 %	12.94 %	1.35 %
0.0039	2.91	0.0046	18.14 %	18.14 %	3.85 %
0.0081	6.63	0.0096	18.43 %	18.43 %	4.13 %
0.0123	10.38	0.0138	12.05 %	12.05 %	2.24 %
0.0162	14.625	0.0044	9.90 %	9.90 %	4.39 %
		AARD	**14.29 %**	**MAD**	**3.19 %**

Table A.23: Aspen Plus pressures obtained by interpolation at 125° C for the system CH_4-MEG and their respective calculated deviations from literature

D.-Q. Zheng[70] CH_4-MEG - 125° C		**Interpolated Pressure MPa**	**Absolute Relative Deviation**	**Relative Deviation $\%\Delta_i$**	**Distance from RD mean**
Mole fraction X	**Total Pressure MPa**				
0.0005	0.33	0.2949	8.41 %	-10.63 %	1.80 %
0.0005	0.33	0.3022	8.41 %	-8.41 %	0.43 %
0.005	3.25	3.0845	5.09 %	-5.09 %	3.75 %
0.0104	7.6	6.7556	11.11 %	-11.11 %	2.27 %
0.0178	13.95	12.4522	10.74 %	-10.74 %	1.90 %
		AARD	**8.75 %**	**MAD**	**2.03 %**

Table A.24: Aspen Plus methane mole fractions obtained by interpolation at 125° C for the system CH_4-MEG and their respective calculated deviations from literature

D.-Q. Zheng[70] CH_4-MEG- 125° C		**Interpolated CH_4 mole fraction**	**Absolute Relative Deviation**	**Relative Deviation $\%\Delta_i$**	**Distance from RD mean**
Mole fraction X	**Total Pressure MPa**				
0.0005	0.33	0.0005	9.36 %	9.36 %	0.47 %
0.0005	0.33	0.0005	9.36 %	9.36 %	0.47 %
0.005	3.25	0.0053	5.12 %	5.12 %	3.77 %
0.0104	7.6	0.0116	11.20 %	11.20 %	2.31 %
0.0178	13.95	0.0196	9.89 %	9.89 %	1.00 %
		AARD	**8.98 %**	**MAD**	**1.60 %**

Table A.25: Aspen Plus pressures obtained by interpolation at 50° C for the system CH_4-MEG and their respective calculated deviations from literature

Jou et al.[30] CH_4-MEG - 50° C		**Interpolated Pressure MPa**	**Absolute Relative Deviation**	**Relative Deviation $\%\Delta_i$**	**Distance from RD mean**
Mole fraction X	**Total Pressure MPa**				
0.000164	0.105	0.0966	8.01 %	-8.01 %	5.44 %
0.00112	0.749	0.6687	10.72 %	-10.72 %	2.73 %
0.00362	2.59	2.2491	13.16 %	-13.16 %	0.28 %
0.00741	5.92	4.9158	16.96 %	-16.96 %	3.52 %
0.0117	10.33	8.4332	18.36 %	-18.36 %	4.92 %
0.0158	15.49	12.4446	19.66 %	-19.66 %	6.22 %
		AARD	**14.48 %**	**MAD**	**3.85 %**

Table A.26: Aspen Plus methane mole fraction obtained by interpolation at 50° C for the system CH_4-MEG and their respective calculated deviations from literature

Jou et al.[30] CH_4-MEG - 50° C		**Interpolated CH_4 mole fraction**	**Absolute Relative Deviation**	**Relative Deviation $\%\Delta_i$**	**Distance from RD mean**
Mole fraction X	**Total Pressure MPa**				
0.000164	0.105	0.0002	8.69 %	8.69 %	5.22 %
0.00112	0.749	0.0013	11.77 %	11.77 %	2.14 %
0.00362	2.59	0.0044	14.18 %	14.18 %	0.27 %
0.00741	5.92	0.0087	17.56 %	17.56 %	3.65 %
0.0117	10.33	0.0137	17.36 %	17.36 %	3.45 %
0.0158	15.49	0.0185	16.96 %	16.96 %	3.05 %
		AARD	**14.42 %**	**MAD**	**2.96 %**

Table A.27: Aspen Plus pressures obtained by interpolation at 100° C for the system CH_4-MEG and their respective calculated deviations from literature

Jou et al.[30] CH_4-MEG - 100° C		**Interpolated Pressure MPa**	**Absolute Relative Deviation**	**Relative Deviation $\%\Delta_i$**	**Distance from RD mean**
Mole fraction X	**Total Pressure MPa**				
0.00023	0.158	0.1375	12.98 %	-12.98 %	2.16 %
0.00075	0.497	0.4454	10.39 %	-10.39 %	0.43 %
0.00438	3.12	2.7558	11.67 %	-11.67 %	0.85 %
0.00833	6.46	5.6208	12.99 %	-12.99 %	2.17 %
0.013	10.25	9.6278	6.07 %	-6.07 %	4.75 %
0.0174	14.59	14.2100	0.0260	-2.60 %	8.22 %
		AARD	**9.45 %**	**MAD**	**3.10 %**

Table A.28: Aspen Plus methane mole fractions obtained by interpolation at 100° C for the system CH_4-MEG and their respective calculated deviations from literature

Jou et al.[30] CH_4-MEG - 100° C		**Interpolated CH_4 mole fraction**	**Absolute Relative Deviation**	**Relative Deviation $\%\Delta_i$**	**Distance from RD mean**
Mole fraction X	**Total Pressure MPa**				
0.00023	0.158	0.0003	16.49 %	16.49 %	4.93 %
0.00075	0.497	0.0008	11.45 %	11.45 %	0.11 %
0.00438	3.12	0.0049	12.20 %	12.20 %	0.64 %
0.00833	6.46	0.0094	12.65 %	12.65 %	1.10 %
0.013	10.25	0.0136	4.99 %	4.99 %	6.56 %
0.0174	14.59	0.0051	1.86 %	1.86 %	9.70 %
		AARD	**9.94 %**	**MAD**	**3.84 %**

Table A.29: Aspen Plus pressures obtained by interpolation at 125° C for the system CH_4-MEG and their respective calculated deviations from literature

Jou et al.[30] CH_4-MEG - 125° C		**Interpolated Pressure MPa**	**Absolute Relative Deviation**	**Relative Deviation $\%\Delta_i$**	**Distance from RD mean**
Mole fraction X	**Total Pressure MPa**				
0.00021	0.135	0.1307	3.15 %	-3.15 %	3.66 %
0.00101	0.666	0.6060	9.00 %	-9.00 %	2.19 %
0.00521	3.53	3.2202	8.78 %	-8.78 %	1.97 %
0.0122	8.58	8.0693	5.95 %	-5.95 %	0.86 %
0.0179	13.52	12.5505	7.17 %	-7.17 %	0.36 %
		AARD	**6.81 %**	**MAD**	**1.81 %**

Table A.30: Aspen Plus CH_4 mole fraction obtained by interpolation at 125° C for the system CH_4-MEG and their respective calculated deviations from literature

Jou et al.[30] CH_4-MEG - 125° C		**Interpolated CH_4 mole fraction**	**Absolute Relative Deviation**	**Relative Deviation $\%\Delta_i$**	**Distance from RD mean**
Mole fraction X	**Total Pressure MPa**				
0.00021	0.135	0.0002	3.43 %	3.43 %	3.46 %
0.00101	0.666	0.0011	9.91 %	9.91 %	3.01 %
0.00521	3.53	0.0057	9.14 %	9.14 %	2.25 %
0.0122	8.58	0.0129	5.59 %	5.59 %	1.30 %
0.0179	13.52	0.0190	6.40 %	6.40 %	0.49 %
		AARD	**6.90 %**	**MAD**	**2.10 %**

Table A.31: Aspen Plus pressures obtained by interpolation at 25° C for the system CH_4-H_2O and their respective calculated deviations from literature

Frost et al.[21] CH_4-H_2O - 25° C		**Interpolated Pressure MPa**	**Absolute Relative Deviation**	**Relative Deviation $\%\Delta_i$**	**Distance from RD mean**
Mole fraction X	**Total Pressure MPa**				
0.00119	5.11	5.8231	13.95 %	13.95 %	18.77 %
0.0014	6.41	7.1433	11.44 %	11.44 %	16.25 %
0.00165	8.45	8.8864	5.16 %	5.16 %	9.98 %
0.00193	11.46	11.1122	3.04 %	-3.04 %	1.78 %
0.0024	15.48	15.7051	1.45 %	1.45 %	6.27 %
0.00261	19.49	18.1943	6.65 %	-6.65 %	1.83 %
		AARD	**6.95 %**	**MAD**	**9.15 %**

Table A.32: Aspen Plus CH_4 mole fraction obtained by interpolation at 25° C for the system CH_4-H_2O and their respective calculated deviations from literature

Frost et al.[21] CH_4-H_2O - 25° C		**Interpolated CH_4 mole fraction**	**Absolute Relative Deviation**	**Relative Deviation $\%\Delta_i$**	**Distance from RD mean**
Mole fraction X	**Total Pressure MPa**				
0.00119	5.11	0.00086	10.22 %	-10.22 %	16.89 %
0.0014	6.41	0.00104	8.16 %	-8.16 %	14.83 %
0.00165	8.45	0.00129	3.63 %	-3.63 %	10.30 %
0.00193	11.46	0.00161	2.08 %	2.08 %	4.59 %
0.0024	15.48	0.00197	0.84 %	-0.84 %	7.51 %
0.00261	19.49	0.00228	3.84 %	3.84 %	2.83 %
		AARD	**4.80 %**	**MAD**	**9.49 %**

Table A.33: Aspen Plus pressures obtained by interpolation at 40° C for the system CH_4-H_2O and their respective calculated deviations from literature

Frost et al.[21] CH_4-H_2O - 40° C		**Interpolated Pressure MPa**	**Absolute Relative Deviation**	**Relative Deviation $\%\Delta_i$**	**Distance from RD mean**
Mole fraction X	**Total Pressure MPa**				
0.000671	5.48	3.8622	29.52 %	-29.52 %	24.71 %
0.000915	6.78	5.5241	18.52 %	-18.52 %	13.71 %
0.001230	8.15	7.9510	2.44 %	-2.44 %	2.37 %
0.001890	12.46	14.5113	16.46 %	16.46 %	21.28 %
0.002350	16.78	20.8304	24.14 %	24.14 %	28.95 %
		AARD	**18.22 %**	**MAD**	**18.20 %**

Table A.34: Aspen Plus CH_4 mole fraction obtained by interpolation at 40° C for the system CH_4-H_2O and their respective calculated deviations from literature

Frost et al.[21] CH_4-H_2O - 40° C		**Interpolated CH_4 mole fraction**	**Absolute Relative Deviation**	**Relative Deviation $\%\Delta_i$**	**Distance from RD mean**
Mole fraction X	**Total Pressure MPa**				
0.000671	5.48	0.00091	35.44 %	35.44 %	28.77 %
0.000915	6.78	0.00108	18.44 %	18.44 %	11.77 %
0.001230	8.15	0.00125	1.94 %	1.94 %	4.73 %
0.001890	12.46	0.00171	9.60 %	-9.60 %	16.27 %
0.002350	16.78	0.00207	11.90 %	-11.90 %	18.57 %
0.00261	19.49	0.00228	3.84 %	3.84 %	2.83 %
		AARD	**15.46 %**	**MAD**	**16.02 %**

Table A.35: Aspen Plus pressures obtained by interpolation at 50° C for the system CH_4-H_2O and their respective calculated deviations from literature

Frost et al.[21] CH_4-H_2O - 50° C		**Interpolated Pressure MPa**	**Absolute Relative Deviation**	**Relative Deviation $\%\Delta_i$**	**Distance from RD mean**
Mole fraction X	**Total Pressure MPa**				
0.0006	4.98	0.00010	24.66 %	24.66 %	17.99 %
0.00082	6.49	0.00016	14.56 %	14.56 %	7.89 %
0.00111	8.48	0.00026	5.38 %	5.38 %	1.29 %
0.00169	11.49	0.00041	13.04 %	-13.04 %	19.71 %
0.00198	18.48	0.00079	1.79 %	1.79 %	4.88 %
		AARD	**13.70 %**	**MAD**	**11.60 %**

Table A.36: Aspen Plus CH_4 mole fraction obtained by interpolation at 50° C for the system CH_4-H_2O and their respective calculated deviations from literature

Frost et al.[21] CH_4-H_2O - 50° C		**Interpolated CH_4 mole fraction**	**Absolute Relative Deviation**	**Relative Deviation $\%\Delta_i$**	**Distance from RD mean**
Mole fraction X	**Total Pressure MPa**				
0.0006	4.98	0.00075	24.66 %	24.66 %	17.99 %
0.00082	6.49	0.00094	14.56 %	14.56 %	7.89 %
0.00111	8.48	0.00117	5.38 %	5.38 %	1.29 %
0.00169	11.49	0.00147	13.04 %	-13.04 %	19.71 %
0.00198	18.48	0.00202	1.79 %	1.79 %	4.88 %
0.00261	19.49	0.00228	3.84 %	3.84 %	2.83 %
		AARD	**11.88 %**	**MAD**	**10.35 %**

Table A.37: Aspen Plus pressures obtained by interpolation at 25° C for the system CH_4-H_2O and their respective calculated deviations from literature

Chapoy et al.[11] CH_4-H_2O - 25° C		**Interpolated Pressure MPa**	**Absolute Relative Deviation**	**Relative Deviation $\%\Delta_i$**	**Distance from RD mean**
Mole fraction X	**Total Pressure MPa**				
0.000238	0.977	0.9961	1.95 %	1.95 %	1.46 %
0.000613	2.542	2.6917	5.89 %	5.89 %	2.48 %
0.001238	5.922	6.1052	3.09 %	3.09 %	0.32 %
0.002459	15.907	16.3385	2.71 %	2.71 %	0.70 %
		AARD	**3.41 %**	**MAD**	**1.24 %**

Table A.38: Aspen Plus CH_4 mole fraction obtained by interpolation at 25° C for the system CH_4-H_2O and their respective calculated deviations from literature

Chapoy et al.[11] CH_4-H_2O - 25° C		**Interpolated CH_4 mole fraction**	**Absolute Relative Deviation**	**Relative Deviation $\%\Delta_i$**	**Distance from RD mean**
Mole fraction X	**Total Pressure MPa**				
0.000238	0.977	0.00023	1.92 %	-1.92 %	0.56 %
0.000613	2.542	0.00058	5.76 %	-5.76 %	3.29 %
0.001238	5.922	0.00123	0.99 %	-0.99 %	1.49 %
0.002459	15.907	0.00243	1.24 %	-1.24 %	1.24 %
		AARD	**2.48 %**	**MAD**	**1.64 %**

Table A.39: Aspen Plus pressures obtained by interpolation at 40° C for the system CH_4-H_2O and their respective calculated deviations from literature

Chapoy et al.[11] CH_4-H_2O - 40° C		**Interpolated Pressure MPa**	**Absolute Relative Deviation**	**Relative Deviation $\%\Delta_i$**	**Distance from RD mean**
Mole fraction X	**Total Pressure MPa**				
0.000204	1.025	1.0866	6.01 %	6.01 %	0.56 %
0.000443	2.534	2.4484	3.38 %	-3.38 %	9.95 %
0.001305	7.798	8.5852	10.09 %	10.09 %	3.52 %
0.002325	17.998	20.4406	13.57 %	13.57 %	7.00 %
		AARD	**8.26 %**	**MAD**	**5.26 %**

Table A.40: Aspen Plus CH_4 mole fraction obtained by interpolation at 40° C for the system CH_4-H_2O and their respective calculated deviations from literature

Chapoy et al.[11] CH_4-H_2O - 40° C		**Interpolated CH_4 mole fraction**	**Absolute Relative Deviation**	**Relative Deviation $\%\Delta_i$**	**Distance from RD mean**
Mole fraction X	**Total Pressure MPa**				
0.000204	1.025	0.00019	5.54 %	-5.54 %	1.39 %
0.000443	2.534	0.00046	3.25 %	3.25 %	7.39 %
0.001305	7.798	0.00121	7.17 %	-7.17 %	3.03 %
0.002325	17.998	0.00216	7.12 %	-7.12 %	2.98 %
		AARD	**5.77 %**	**MAD**	**3.70 %**

Table A.41: Aspen Plus pressures obtained by interpolation at 25° C for the system CO_2-MEG and their respective calculated deviations from literature

Jou et al.[30] CO_2-MEG - 25° C		**Interpolated Pressure MPa**	**Absolute Relative Deviation**	**Relative Deviation $\%\Delta_i$**	**Distance from RD mean**
Mole fraction X	**Total Pressure MPa**				
0.000693	0.0293	0.0302	3.01 %	3.01 %	5.13 %
0.00321	0.145	0.1407	2.96 %	-2.96 %	11.10 %
0.02057	0.84	0.9480	12.86 %	12.86 %	4.72 %
0.0645	2.94	3.5175	19.64 %	19.64 %	11.50 %
		AARD	**9.62 %**	**MAD**	**8.11 %**

Table A.42: Aspen Plus CO_2 mole fraction obtained by interpolation at 25° C for the system CO_2-MEG and their respective calculated deviations from literature

Jou et al.[30] CO_2-MEG - 25° C		**Interpolated CO_2 mole fraction**	**Absolute Relative Deviation**	**Relative Deviation $\%\Delta_i$**	**Distance from RD mean**
Mole fraction X	**Total Pressure MPa**				
0.000693	0.0293	0.000673	2.92 %	-2.92 %	8.86 %
0.00321	0.145	0.003307	3.03 %	3.03 %	8.97 %
0.02057	0.84	0.018350	10.79 %	-10.79 %	16.73 %
0.0645	2.94	0.056550	13.08 %	-13.08 %	19.02 %
		AARD	**7.45 %**	**MAD**	**13.39 %**

Table A.43: Aspen Plus pressures obtained by interpolation at 50° C for the system CO_2-MEG and their respective calculated deviations from literature

Jou et al.[30] CO_2-MEG- 50° C		**Interpolated Pressure MPa**	**Absolute Relative Deviation**	**Relative Deviation $\%\Delta_i$**	**Distance from RD mean**
Mole fraction X	**Total Pressure MPa**				
0.000794	0.044	0.0488	10.94 %	10.94 %	0.67 %
0.005397	0.343	0.3360	2.05 %	-2.05 %	13.67 %
0.02144	1.35	1.4093	4.39 %	4.39 %	7.22 %
0.0533	3.38	4.0220	18.99 %	18.99 %	7.38 %
0.08309	6.2	7.7997	25.80 %	25.80 %	14.19 %
0.1122	10.74	23.4164	118.03 %	118.03 %	106.41 %
0.1226	14.78	33.0255	123.45 %	123.45 %	111.83 %
		AARD	**43.38 %**	**MAD**	**37.34 %**

Table A.44: Aspen Plus CO_2 mole fraction obtained by interpolation at 50° C for the system CO_2-MEG and their respective calculated deviations from literature

Jou et al.[30] CO_2-MEG - 50° C		**Interpolated CO_2 mole fraction**	**Absolute Relative Deviation**	**Relative Deviation $\%\Delta_i$**	**Distance from RD mean**
Mole fraction X	**Total Pressure MPa**				
0.000794	0.044	0.000716	9.86 %	-9.86 %	2.42 %
0.005397	0.343	0.005508	2.06 %	2.06 %	9.50 %
0.02144	1.35	0.020600	3.92 %	-3.92 %	3.52 %
0.0533	3.38	0.046372	13.00 %	-13.00 %	5.56 %
0.08309	6.2	0.072710	12.49 %	-12.49 %	5.05 %
0.1122	10.74	0.097538	13.07 %	-13.07 %	5.63 %
0.1226	14.78	0.103885	15.27 %	-15.27 %	7.82 %
		AARD	**9.95 %**	**MAD**	**5.64 %**

Table A.45: Aspen Plus pressures obtained by interpolation at 100° C for the system CO_2-MEG and their respective calculated deviations from literature

Jou et al.[30] CO_2-MEG - 100° C		**Interpolated Pressure MPa**	**Absolute Relative Deviation**	**Relative Deviation $\%\Delta_i$**	**Distance from RD mean**
Mole fraction X	**Total Pressure MPa**				
0.000723	0.076	0.0901	18.60 %	18.60 %	10.79 %
0.001273	0.129	0.1574	22.05 %	22.05 %	7.34 %
0.00742	0.802	0.9326	16.29 %	16.29 %	13.10 %
0.03664	3.95	5.3919	36.50 %	36.50 %	7.12 %
0.06252	7.51	11.5282	53.50 %	53.50 %	24.11 %
0.08721	11.69	24.5123	109.69 %	109.69 %	80.30 %
		AARD	**42.77 %**	**MAD**	**23.79 %**

Table A.46: Aspen Plus CO_2 mole fraction obtained by interpolation at 100° C for the system CO_2-MEG and their respective calculated deviations from literature

Jou et al.[30] CO_2-MEG - 100° C		**Interpolated CO_2 mole fraction**	**Absolute Relative Deviation**	**Relative Deviation $\%\Delta_i$**	**Distance from RD mean**
Mole fraction X	**Total Pressure MPa**				
0.000723	0.076	0.0006	16.01 %	-16.01 %	3.02 %
0.001273	0.129	0.0010	18.23 %	-18.23 %	0.80 %
0.00742	0.802	0.0064	13.64 %	-13.64 %	5.39 %
0.03664	3.95	0.0283	22.84 %	-22.84 %	3.80 %
0.06252	7.51	0.0472	24.44 %	-24.44 %	5.41 %
0.08721	11.69	0.0630	27.74 %	-27.74 %	8.71 %
		AARD	**20.48 %**	**MAD**	**4.52 %**

Table A.47: Aspen Plus pressures obtained by interpolation at 125° C for the system CO_2-MEG and their respective calculated deviations from literature

Jou et al.[30] CO_2-MEG - 125° C		**Interpolated Pressure MPa**	**Absolute Relative Deviation**	**Relative Deviation $\%\Delta_i$**	**Distance from RD mean**
Mole fraction X	**Total Pressure MPa**				
0.001162	0.13	0.2070	59.27 %	59.27 %	9.72 %
0.006998	0.826	1.2494	51.26 %	51.26 %	17.73 %
0.02428	2.84	4.8055	69.21 %	69.21 %	0.22 %
0.04978	6.31	12.3810	96.21 %	96.21 %	27.23 %
0.07409	10.11	13.6826	35.34 %	35.34 %	33.65 %
0.09925	14.49	54.8031	278.21 %	278.21 %	209.23 %
		AARD	**98.25 %**	**MAD**	**49.63 %**

Table A.48: Aspen Plus CO_2 mole fraction obtained by interpolation at 125° C for the system CO_2-MEG and their respective calculated deviations from literature

Jou et al.[30] CO_2-MEG - 125° C		**Interpolated CO_2 mole fraction**	**Absolute Relative Deviation**	**Relative Deviation $\%\Delta_i$**	**Distance from RD mean**
Mole fraction X	**Total Pressure MPa**				
0.001162	0.13	0.0007158	38.40 %	-38.40 %	1.96 %
0.006998	0.826	0.0046719	33.24 %	-33.24 %	3.20 %
0.02428	2.84	0.0152118	37.35 %	-37.35 %	0.91 %
0.04978	6.31	0.0338821	31.94 %	-31.94 %	4.50 %
0.07409	10.11	0.0435204	41.26 %	-41.26 %	4.82 %
0.09925	14.49	0.0547279	44.86 %	-44.86 %	8.42 %
		AARD	**37.84 %**	**MAD**	**3.97 %**

Table A.49: Aspen Plus pressures obtained by interpolation at 50° C for the system CO_2-MEG and their respective calculated deviations from literature

Francesconi and Galvao[23] CO_2-MEG - 50° C		**Interpolated Pressure MPa**	**Absolute Relative Deviation**	**Relative Deviation $\%\Delta_i$**	**Distance from RD mean**
Mole fraction X	**Total Pressure MPa**				
0.0045	0.4255	0.2793	34.35 %	-34.35 %	28.77 %
0.0118	0.8128	0.7500	7.73 %	-7.73 %	2.14 %
0.0222	1.4579	1.4633	0.37 %	0.37 %	5.96 %
0.0464	2.8335	3.3823	19.37 %	19.37 %	24.95 %
		AARD	**15.45 %**	**MAD**	**15.45 %**

Table A.50: Aspen Plus CO_2 obtained by interpolation at 50° C for the system CO_2-MEG and their respective calculated deviations from literature

Francesconi and Galvao[23] CO_2-MEG - 50° C		**Interpolated CO_2 mole fraction**	**Absolute Relative Deviation**	**Relative Deviation $\%\Delta_i$**	**Distance from RD mean**
Mole fraction X	**Total Pressure MPa**				
0.0045	0.4255	0.0068	51.22 %	51.22 %	39.93 %
0.0118	0.8128	0.0127	8.03 %	8.03 %	3.26 %
0.0222	1.4579	0.0221	0.34 %	-0.34 %	11.63 %
0.0464	2.8335	0.0400	13.75 %	-13.75 %	25.04 %
		AARD	**18.33 %**	**MAD**	**19.96 %**

Table A.51: Aspen Plus pressures obtained by interpolation at 100° C for the system CO_2-MEG and their respective calculated deviations from literature

Francesconi and Galvao[23] CO_2-MEG - 100° C		**Interpolated Pressure MPa**	**Absolute Relative Deviation**	**Relative Deviation $\%\Delta_i$**	**Distance from RD mean**
Mole fraction X	**Total Pressure MPa**				
0.0047	0.6205	0.5843	5.83 %	-5.83 %	37.49 %
0.0122	1.2578	1.5668	24.57 %	24.57 %	7.09 %
0.0231	2.2879	3.1348	37.02 %	37.02 %	5.36 %
0.0485	4.5585	7.7896	70.88 %	70.88 %	39.22 %
		AARD	**34.57 %**	**MAD**	**22.29 %**

Table A.52: Aspen Plus CO_2 mole fraction obtained by interpolation at 100° C for the system CO_2-MEG and their respective calculated deviations from literature

Francesconi and Galvao[23] CO_2-MEG - 100° C		**Interpolated CO_2 mole fraction**	**Absolute Relative Deviation**	**Relative Deviation $\%\Delta_i$**	**Distance from RD mean**
Mole fraction X	**Total Pressure MPa**				
0.0047	0.6205	0.0050	6.08 %	6.08 %	24.02 %
0.0122	1.2578	0.0099	18.87 %	-18.87 %	0.92 %
0.0231	2.2879	0.0174	24.80 %	-24.80 %	6.85 %
0.0485	4.5585	0.0319	34.18 %	-34.18 %	16.24 %
		AARD	**20.98 %**	**MAD**	**12.01 %**

Table A.53: Aspen Plus pressures obtained by interpolation at 125° C for the system CO_2-MEG and their respective calculated deviations from literature

Francesconi and Galvao[23] CO_2-MEG - 125° C		**Interpolated Pressure MPa**	**Absolute Relative Deviation**	**Relative Deviation $\%\Delta_i$**	**Distance from RD mean**
Mole fraction X	**Total Pressure MPa**				
0.005	0.718	0.8851	23.27 %	23.27 %	50.38 %
0.0128	1.4803	2.3563	59.18 %	59.18 %	14.47 %
0.0241	2.7029	4.7640	76.26 %	76.26 %	2.60 %
0.0508	5.421	12.7881	135.90 %	135.90 %	62.25 %
		AARD	**73.65 %**	**MAD**	**32.43 %**

Table A.54: Aspen Plus CO_2 mole fraction obtained by interpolation at 125° C for the system CO_2-MEG and their respective calculated deviations from literature

Francesconi and Galvao[23] CO_2-MEG - 125° C		**Interpolated CO_2 mole fraction**	**Absolute Relative Deviation**	**Relative Deviation $\%\Delta_i$**	**Distance from RD mean**
Mole fraction X	**Total Pressure MPa**				
0.0041	18.62 %	-18.62 %	16.63 %	23.27 %	50.38 %
0.0082	35.62 %	-35.62 %	0.37 %	59.18 %	14.47 %
0.0145	39.69 %	-39.69 %	4.44 %	76.26 %	2.60 %
0.0269	47.07 %	-47.07 %	11.82 %	135.90 %	62.25 %
		AARD	**35.25 %**	**MAD**	**8.31 %**

Table A.55: Aspen Plus pressures obtained by interpolation at 150° C for the system CO_2-MEG and their respective calculated deviations from literature

Francesconi and Galvao[23] CO_2-MEG - 150° C		**Interpolated Pressure MPa**	**Absolute Relative Deviation**	**Relative Deviation $\%\Delta_i$**	**Distance from RD mean**
Mole fraction X	**Total Pressure MPa**				
0.0053	0.8155	1.3928	64.76 %	64.76 %	80.68 %
0.0135	1.7028	3.5948	111.11 %	111.11 %	34.33 %
0.0254	3.1179	7.4565	139.15 %	139.15 %	6.29 %
0.0538	6.2835	23.0438	266.73 %	266.73 %	121.30 %
		AARD	**145.44 %**	**MAD**	**60.65 %**

Table A.56: Aspen Plus CO_2 mole fraction obtained by interpolation at 150° C for the system CO_2-MEG and their respective calculated deviations from literature

Francesconi and Galvao[23] CO_2-MEG - 150° C		**Interpolated CO_2 mole fraction**	**Absolute Relative Deviation**	**Relative Deviation $\%\Delta_i$**	**Distance from RD mean**
Mole fraction X	**Total Pressure MPa**				
0.0053	0.8155	0.0032	39.08 %	-39.08 %	9.85 %
0.0135	1.7028	0.0067	50.55 %	-50.55 %	1.63 %
0.0254	3.1179	0.0134	47.05 %	-47.05 %	1.87 %
0.0538	6.2835	0.0221	59.01 %	-59.01 %	10.08 %
		AARD	**48.92 %**	**MAD**	**5.86 %**

Table A.57: Aspen Plus pressures obtained by interpolation at 50° C for the system CO_2-MEG and their respective calculated deviations from literature

D.-Q. Zheng[70] CO_2-MEG - 50° C		**Interpolated Pressure MPa**	**Absolute Relative Deviation**	**Relative Deviation $\%\Delta_i$**	**Distance from RD mean**
Mole fraction X	**Total Pressure MPa**				
0.0117	0.895	0.7434	16.94 %	-16.94 %	7.49 %
0.0116	0.894	0.7368	17.58 %	-17.58 %	8.13 %
0.068	5.46	5.6024	2.61 %	2.61 %	12.06 %
0.0776	6.542	4.9792	23.89 %	-23.89 %	14.44 %
0.0847	7.474	8.1123	8.54 %	8.54 %	17.99 %
0.1126	13.84	23.7623	71.69 %	71.69 %	81.15 %
		AARD	**23.54 %**	**MAD**	**23.54 %**

Table A.58: Aspen Plus CO_2 mole fraction obtained by interpolation at 50° C for the system CO_2-MEG and their respective calculated deviations from literature

D.-Q. Zheng[70] CO_2-MEG - 50° C		**Interpolated CO_2 mole fraction**	**Absolute Relative Deviation**	**Relative Deviation $\%\Delta_i$**	**Distance from RD mean**
Mole fraction X	**Total Pressure MPa**				
0.0140	19.47 %	19.47 %	13.27 %	-16.94 %	7.49 %
0.0140	20.50 %	20.50 %	14.30 %	-17.58 %	8.13 %
0.0668	1.76 %	-1.76 %	7.96 %	2.61 %	12.06 %
0.0673	3.09 %	-3.09 %	9.29 %	-23.89 %	14.44 %
0.0697	4.11 %	-4.11 %	10.31 %	8.54 %	17.99 %
0.0996	11.58 %	-11.58 %	17.78 %	71.69 %	81.15 %
		AARD	**10.09 %**	**MAD**	**12.15 %**

Table A.59: Aspen Plus pressures obtained by interpolation at 100° C for the system CO_2-MEG and their respective calculated deviations from literature

D.-Q. Zheng[70] CO_2-MEG - 100° C		**Interpolated Pressure MPa**	**Absolute Relative Deviation**	**Relative Deviation $\%\Delta_i$**	**Distance from RD mean**
Mole fraction X	**Total Pressure MPa**				
0.0083	0.967	1.0472	8.30 %	8.30 %	48.01 %
0.0083	0.95	1.0472	10.23 %	10.23 %	46.07 %
0.0457	5.65	7.1766	27.02 %	27.02 %	29.29 %
0.0757	9.58	16.9827	77.27 %	77.27 %	20.97 %
0.104	15.36	39.7372	158.71 %	158.71 %	102.40 %
		AARD	**68.51 %**	**MAD**	**49.35 %**

Table A.60: Aspen Plus CO_2 mole fraction obtained by interpolation at 100° C for the system CO_2-MEG and their respective calculated deviations from literature

D.-Q. Zheng[70] CO_2-MEG - 100° C		**Interpolated CO_2 mole fraction**	**Absolute Relative Deviation**	**Relative Deviation $\%\Delta_i$**	**Distance from RD mean**
Mole fraction X	**Total Pressure MPa**				
0.0083	0.967	0.0077	7.41 %	-7.41 %	6.13 %
0.0083	0.95	0.0078	6.49 %	-6.49 %	6.49 %
0.0457	5.65	0.0380	16.77 %	-16.77 %	3.22 %
0.0757	9.58	0.0706	6.73 %	-6.73 %	6.82 %
0.104	15.36	0.0724	30.34 %	-30.34 %	16.79 %
		AARD	**13.55 %**	**MAD**	**7.89 %**

Table A.61: Aspen Plus pressures obtained by interpolation at 125° C for the system CO_2-MEG and their respective calculated deviations from literature

D.-Q. Zheng[70] CO_2-MEG - 125° C		**Interpolated Pressure MPa**	**Absolute Relative Deviation**	**Relative Deviation $\%\Delta_i$**	**Distance from RD mean**
Mole fraction X	**Total Pressure MPa**				
0.0049	0.96	0.8670	9.68 %	-9.68 %	104.24 %
0.0381	5.55	8.4059	51.46 %	51.46 %	43.09 %
0.0654	9.8	20.5016	109.20 %	109.20 %	14.65 %
0.0959	15.46	50.5901	227.23 %	227.23 %	132.68 %
		AARD	**99.39 %**	**MAD**	**73.66 %**

Table A.62: Aspen Plus CO_2 mole fraction obtained by interpolation at 125° C for the system CO_2-MEG and their respective calculated deviations from literature

D.-Q. Zheng[70] CO_2-MEG - 125° C		**Interpolated CO_2 mole fraction**	**Absolute Relative Deviation**	**Relative Deviation $\%\Delta_i$**	**Distance from RD mean**
Mole fraction X	**Total Pressure MPa**				
0.0049	0.96	0.0054	10.50 %	10.50 %	33.83 %
0.0381	5.55	0.0274	28.03 %	-28.03 %	4.70 %
0.0654	9.8	0.0426	34.89 %	-34.89 %	11.56 %
0.0959	15.46	0.0567	40.90 %	-40.90 %	17.57 %
		AARD	**28.58 %**	**MAD**	**16.91 %**

Table A.63: Aspen Plus pressure obtained by interpolation at 25° C for the system CO_2-H_2O and their respective calculated deviations from literature

Serpa et al.[60] CO_2-H_2O - 25° C		**Interpolated pressure KPa**	**Absolute Relative Deviation**	**Relative Deviation $\%\Delta_i$**	**Distance from RD mean**
Mole fraction X	**Total Pressure KPa**				
0.00089	121	148.23	22.51 %	22.51 %	4.50 %
0.00087	153.5	144.93	5.58 %	-5.58 %	32.59 %
0.00136	201	226.37	12.62 %	12.62 %	14.38 %
0.00151	252.9	251.53	0.54 %	-0.54 %	27.54 %
0.00176	265.3	292.72	10.33 %	10.33 %	16.67 %
0.00208	320.9	508.38	58.42 %	58.42 %	31.42 %
0.00194	325.9	473.63	45.33 %	45.33 %	18.33 %
0.00227	378.3	555.79	46.92 %	46.92 %	19.92 %
0.00241	381.1	496.43	53.02 %	53.02 %	26.02 %
		AARD	**28.36 %**	**MAD**	**21.26 %**

Table A.64: Aspen Plus CO_2 mole fraction obtained by interpolation at 25° C for the system CO_2-H_2O and their respective calculated deviations from literature

Serpa et al.[60] CO_2-H_2O - 25° C		**Interpolated CO_2 mole fraction**	**Absolute Relative Deviation**	**Relative Deviation $\%\Delta_i$**	**Distance from RD mean**
Mole fraction X	**Total Pressure KPa**				
0.00089	121	0.00073	18.48 %	-18.48 %	13.55 %
0.00087	153.5	0.00092	6.12 %	6.12 %	11.05 %
0.00136	201	0.00121	11.01 %	-11.01 %	6.07 %
0.00151	252.9	0.00152	0.74 %	0.74 %	5.67 %
0.00176	265.3	0.00160	9.37 %	-9.37 %	4.44 %
0.00208	320.9	0.00192	7.46 %	-7.46 %	2.52 %
0.00194	325.9	0.00196	0.77 %	0.77 %	5.71 %
0.00227	378.3	0.00226	0.31 %	-0.31 %	4.63 %
0.00241	381.1	0.00228	5.42 %	-5.42 %	0.48 %
		AARD	**6.63 %**	**MAD**	**6.01 %**

Table A.65: Aspen Plus pressure obtained by interpolation at 50° C for the system CO_2-H_2O and their respective calculated deviations from literature

Serpa et al.[60] CO_2-H_2O - 50° C		**Interpolated pressure KPa**	**Absolute Relative Deviation**	**Relative Deviation $\%\Delta_i$**	**Distance from RD mean**
Mole fraction X	**Total Pressure KPa**				
0.00026	105.3	87.22	17.17 %	-17.17 %	10.61 %
0.00035	125	113.26	9.39 %	-9.39 %	2.83 %
0.00048	167.3	151.01	9.74 %	-9.74 %	3.17 %
0.0006	206.2	186.00	9.80 %	-9.80 %	3.24 %
0.00065	215.4	200.61	6.87 %	-6.87 %	0.30 %
0.00073	243.8	224.05	8.10 %	-8.10 %	1.54 %
0.00092	288.7	279.94	3.03 %	-3.03 %	3.53 %
0.00093	302	281.56	6.77 %	-6.77 %	0.21 %
0.00106	335.9	321.35	4.33 %	-4.33 %	2.23 %
0.00114	348.6	345.09	1.01 %	-1.01 %	5.55 %
0.00123	383.9	371.88	3.13 %	-3.13 %	3.43 %
0.00136	408.3	410.70	0.59 %	0.59 %	7.15 %
		AARD	**6.66 %**	**MAD**	**3.65 %**

Table A.66: Aspen Plus CO_2 mole fraction obtained by interpolation at 50° C for the system CO_2-H_2O and their respective calculated deviations from literature

Serpa et al.[60] CO_2-H_2O - 50° C		**Interpolated CO_2 mole fraction**	**Absolute Relative Deviation**	**Relative Deviation $\%\Delta_i$**	**Distance from RD mean**
Mole fraction X	**Total Pressure KPa**				
0.00026	105.3	0.00032	24.04 %	24.04 %	16.18 %
0.00035	125	0.00039	11.57 %	11.57 %	3.70 %
0.00048	167.3	0.00054	11.65 %	11.65 %	3.79 %
0.0006	206.2	0.00067	11.52 %	11.52 %	3.65 %
0.00065	215.4	0.00070	7.77 %	7.77 %	0.09 %
0.00073	243.8	0.00080	9.22 %	9.22 %	1.36 %
0.00092	288.7	0.00095	3.23 %	3.23 %	4.63 %
0.00093	302	0.00099	6.95 %	6.95 %	0.91 %
0.00106	335.9	0.00111	4.63 %	4.63 %	3.23 %
0.00114	348.6	0.00115	1.04 %	1.04 %	6.82 %
0.00123	383.9	0.00127	3.28 %	3.28 %	4.58 %
0.00136	408.3	0.00135	0.56 %	-0.56 %	8.42 %
		AARD	**7.96 %**	**MAD**	**4.78 %**

Table A.67: Aspen Plus CO_2 mole fraction obtained by interpolation at 40, 80 and 120° C for the system CO_2-H_2O and their respective calculated deviations from literature

Blanca CO_2-H_2O		**Temperature °C**	**Interpolated CO_2 mole fraction**	**Average absolute deviation (AD)**	**Percentage deviation $\%\Delta_i$**
Mole fraction X	**Total Pressure MPa**				
0.0006873	0.16721793	40	0.169420	1.32 %	1.32 %
0.000496	0.256415	80	0.273610	6.71 %	6.71 %
0.000448	0.445688	120	0.482830	8.33 %	8.33 %

Table A.68: Aspen Plus pressure obtained by interpolation at 40, 80 and 120° C for the system CO_2-H_2O and their respective calculated deviations from literature

Blanca CO_2-H_2O		**Temperature °C**	**Interpolated Pressure MPa**	**Average absolute deviation (AD)**	**Percentage deviation $\%\Delta_i$**
Mole fraction X	**Total Pressure MPa**				
0.0006873	0.16721793	40	0.0006781	1.35 %	-1.35 %
0.000496	0.256415	80	0.0004582	7.54 %	-7.54 %
0.000448	0.445688	120	0.0003902	12.98 %	-12.98 %

Chapter B Appendix

B.1 Basis for process simulation

B.1.1 Glycols Properties

Table B.1: Properties of glycols. Source: Union Carbide 1971, Worley 1966.

Property	Ethylene Glycol (EG)	Diethylene Glycol (DEG)	Triethylene Glycol (TEG)
Formula	$C_2H_6O_2$	$C_4H_{10}O_3$	$C_6H_{14}O_4$
Molecular weight	62.1	106.1	150.2
Boiling point at 760 mm Hg °C (°F)	197.6 (387.7)	245.8 (474.4)	288 (550.4)
Initial Decomposition Temp. °C (°F)	165 (329)	164.4 (328)	206.7 (404)
Density at 25°C, g/ml	1.110	1.113	1.119
Freezing point °C (°F)	-12.7 (9.1)	-7.8 (17.6)	-7.2 (19.04)
Viscosity abs. @ 25° C, cp	16.5	28.2	37.3
Surface tension @ 25 °C, dyne/cm	47	44	45
Specific heat at 25 °C, Btu/lb°F	0.58	0.55	0.53
Heat of vaporization (760 mm Hg), Btu/lb	364	232	174
Flash Point, °F (C.O.C[1])	240	280	320
Heat of solution of water in infinite amount of glycol (approx. 80°F) Btu/lb	-	58	86

[1] Cleveland open cup method

B.1.2 Gas composition and assumptions.

Table B.2: Different gas compositions obtained from literature review.

Component	M.Seyyed [28]	V. Piemonte [51]	N. Kasiri [31]	N. Darwish [14]	A. Braek [6]	Ranjbar [53]	M. Neagu [46]
	% mass		% mole [ppm]				
C_1	0.8026	0.3853	0.853	0.636	0.63314	0.8976	0.949
C_2	0.0258	0.2408	0.0554	0.114	0.1115	0.031	0.025
C_3	0.0087	0.1948	0.0235	0.095	0.09088	0.0148	0.002
i-C_4	0.0004	0.0325	0.0046	0.023	0.02501	0.0059	0.00003
n-C_4	0.0048	0.0687	0.00669	0.044	0.04217	0.003	0.00003
i-C_5	0.0028	-	0.00189	0.012	0.01536	0.001	0.00001
n-C_5	0.0024	0.0592	0.001762	0.012	0.01469	0.0005	0.00001
cyc-C_6	-	-	-	[590]	-	-	-
i-C_6	-	-	-	0.002	-	-	-
n-C_6	0.0028	-	0.00392	-	0.00721		0.00001
n-C_7	0.0033	-	-	[270]	-	-	-
i-C_7	-	-	-	[390]	-	-	-
c-C_7	-	-	-	[590]	-	-	-
i-C_8	-	-	-	[100]	-	-	-
c-C_8	-	-	-	[190]	-	-	-
CO_2	0.0191	0.0021	0.0132	0.05	0.04957	0.0284	0.007
O_2	-	-	-	-	-	-	0.0002
N_2	0.1112	0.0122	0.0352	0.005	0.0062	0.001	0.016
water	0.0007	0.0044	0.00142	0.003	0.004	0.0014	0.001264
H_2S	-	-	0.000001	-	0.00027	0.0155	-
Benzene	0.0004	-	0.000045	[290]	-	-	-
Toluene	0.0005	-	0.00003	[200]	-	-	-
o-Xylene	0.0045	-	-	[100]	-	-	-
Ethyl-benzene	0.001	-	-	[10]	-	-	-

B.1.3 Calculation method for water specification.

Table B.3: Typical rich gas transport specifications[20].

Designation and unit	**Specification**
Max. operating pressure (barg)	210
Min. operating pressure (barg)	112
Max operating temperature (°C)	60
Min operating temperature (°C)	-10
Max cricondetherm temperature (°C)	105
Max cricondetherm temperature (°C)	40
Max water dew point (°C at 69 barg)	-18
Max carbon dioxide (mole%)	2
Max hydrogen sulphide and COS (ppmv)	2
Max O_2 (ppmv)	2
Max daily average methanol content (ppmv)	2.5
Max peak methanol content (ppmv)	20
Max daily average glycol content (litres/MSm3)	8

To calculate the maximum ppm of water in sweet gas, the molar volume at standard conditions was calculated using Equation B.1.

$$V_{m,std} = \left(\frac{RT}{P}\right)_{std} \tag{B.1}$$

Where

$V_{m,std}$ is the molar volume at standard conditions (101.325 kPa and 15°C).

R is the ideal gas constant in $M^3Pa/Kmol$.

T is the temperature in K.

P is the pressure in Pa.

According to the gas specifications for Norwegian transport pipelines, the maximum water dew point at 69 barg is -18°C, at this conditions and using the chart in Figure B.1, a maximum water content of 35 $kg/10^6$ has been estimated at standard conditions (marked with yellow lines).

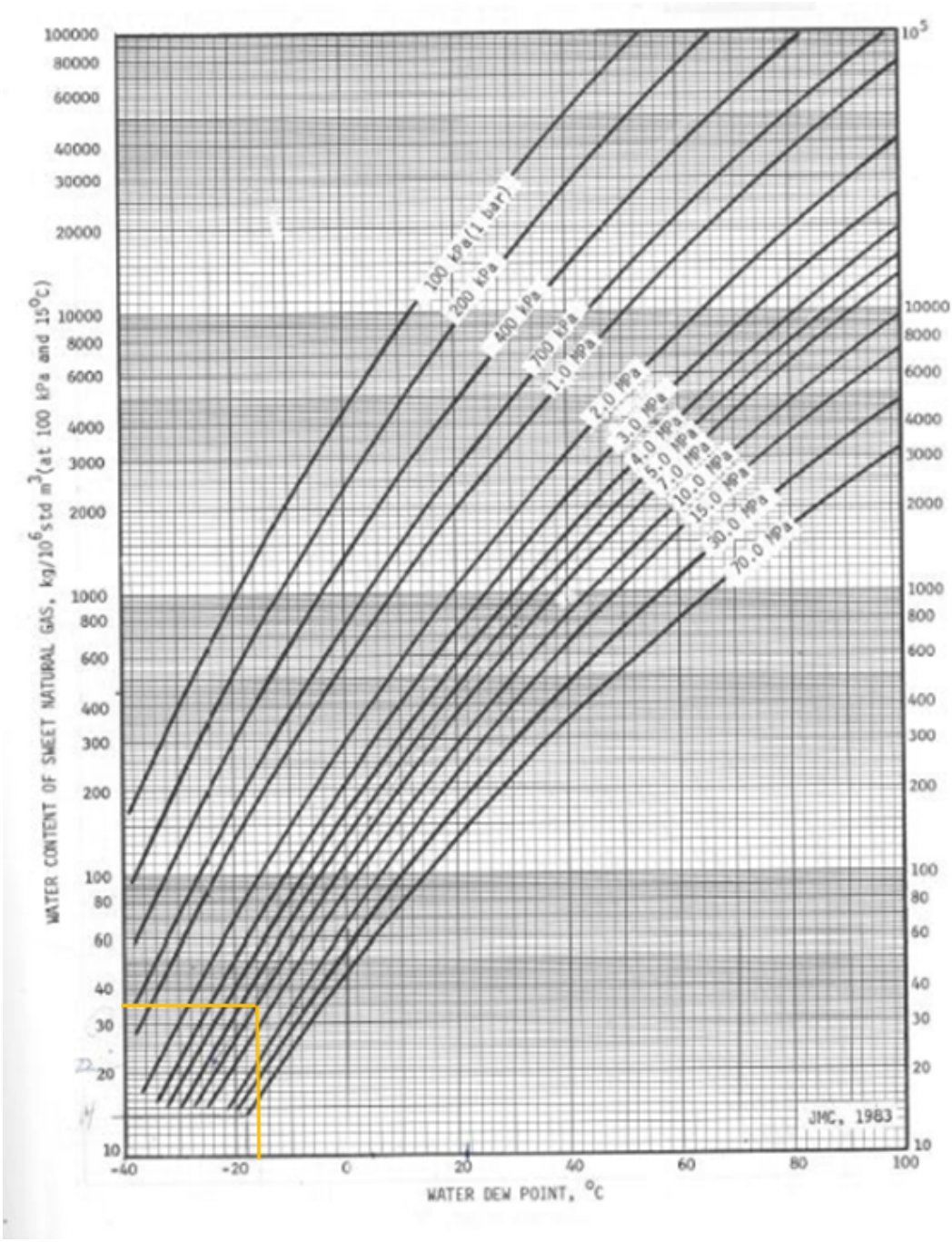

Figure B.1: Water content of sweet natural gas at standard conditions at different pressures and water dewpoints.[8].

The number of moles in 10^6 natural gas and the molar water specification were calculated using Equations B.2 and B.3.

$$n_{gas} = \frac{10^6 m^3}{V_{m.std}} \tag{B.2}$$

$$n_{water,spec} = \frac{35 kg/10^6 stdm^3}{Mm_{water}} \tag{B.3}$$

Where the molar mass of water is 18.02 kg/kmol. According to the calculated amount of moles, the maximum allowable water content for gas transport has been calculated to be 46 ppm in a molar basis.

Chapter C
Appendix

C.1 Process simulation diagrams

In this appendix, the process diagrams for each regeneration method including the processes with MEG recovery are listed, showing the pressures and temperatures in all the streams.

C.1.1 Gas dehydration with vacuum regeneration

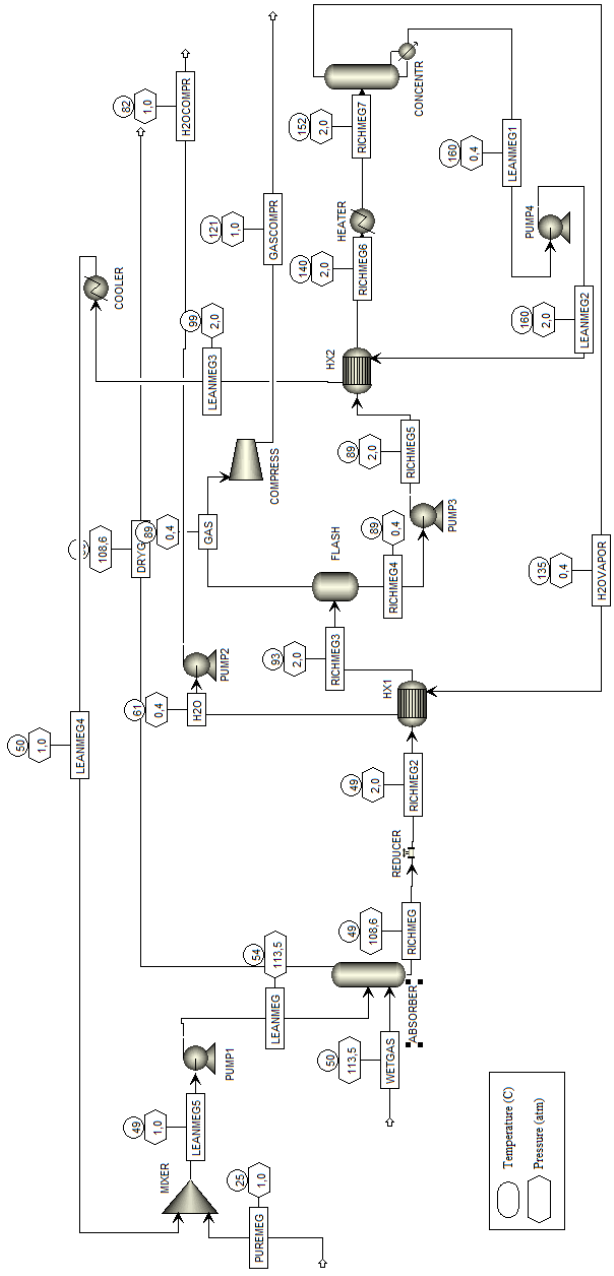

Figure C.1: Diagram of gas dehydration with vacuum regeneration showing pressure and temperature results.

C.1.2 Gas dehydration with vacuum regeneration and stripping gas

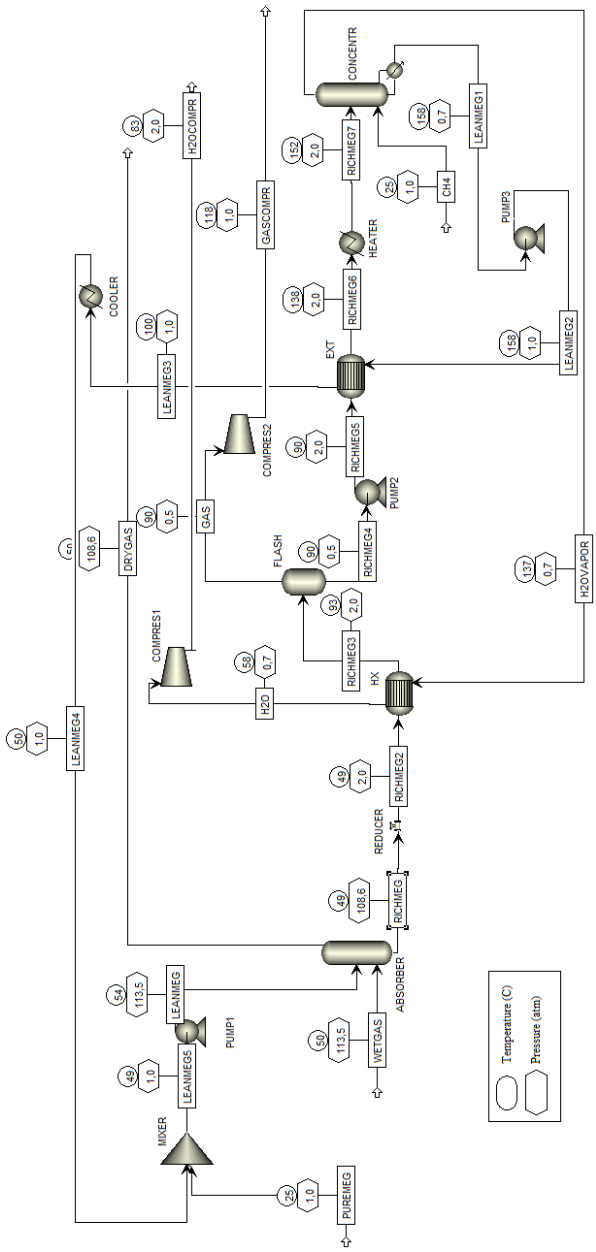

Figure C.2: Diagram of gas dehydration with vacuum and stripping gas regeneration showing pressure and temperature results.

C.1.3 Gas dehydration with DRIZO regeneration

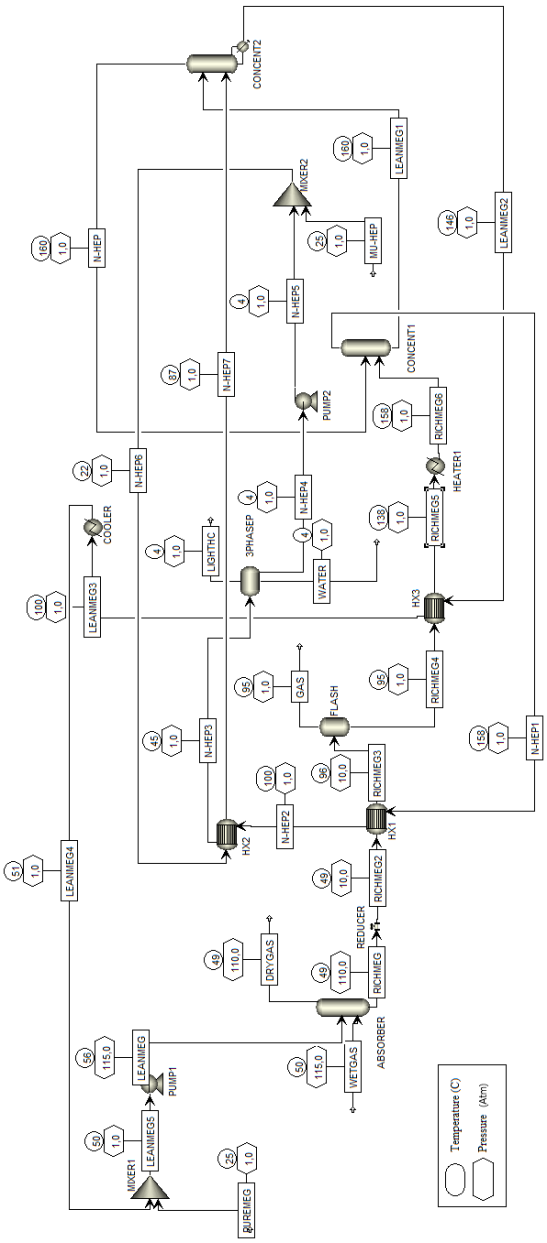

Figure C.3: Diagram of gas dehydration with DRIZO regeneration showing pressure and temperature results.

C.1.4 Gas dehydration with vacuum regeneration and MEG recovery

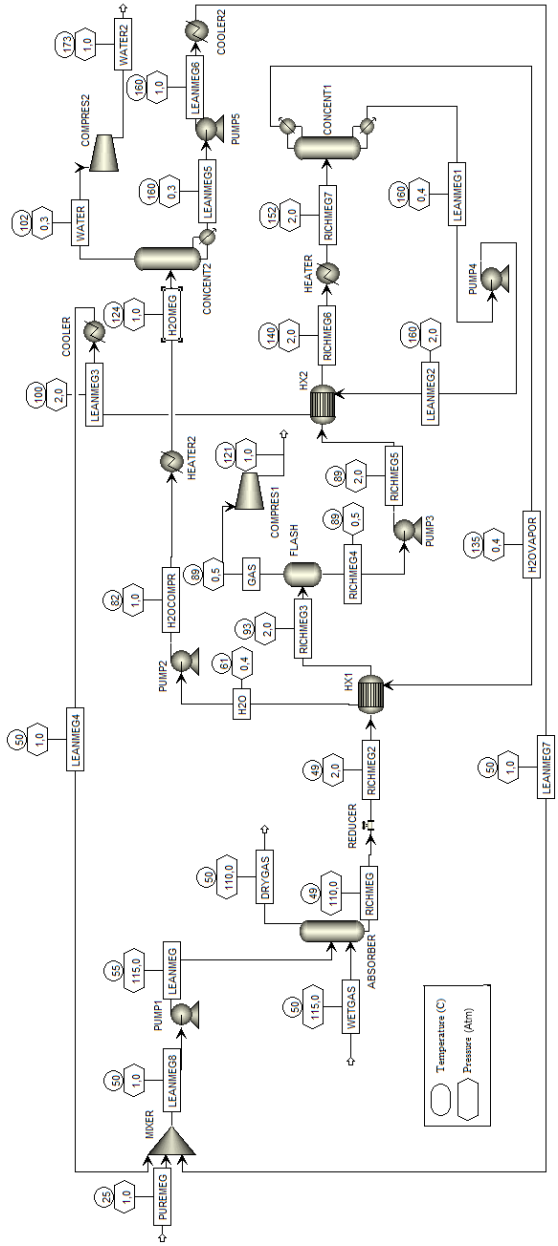

Figure C.4: Diagram of gas dehydration with vacuum regeneration and MEG recovery showing pressure and temperature results.

C.1.5 Gas dehydration with DRIZO regeneration and MEG recovery

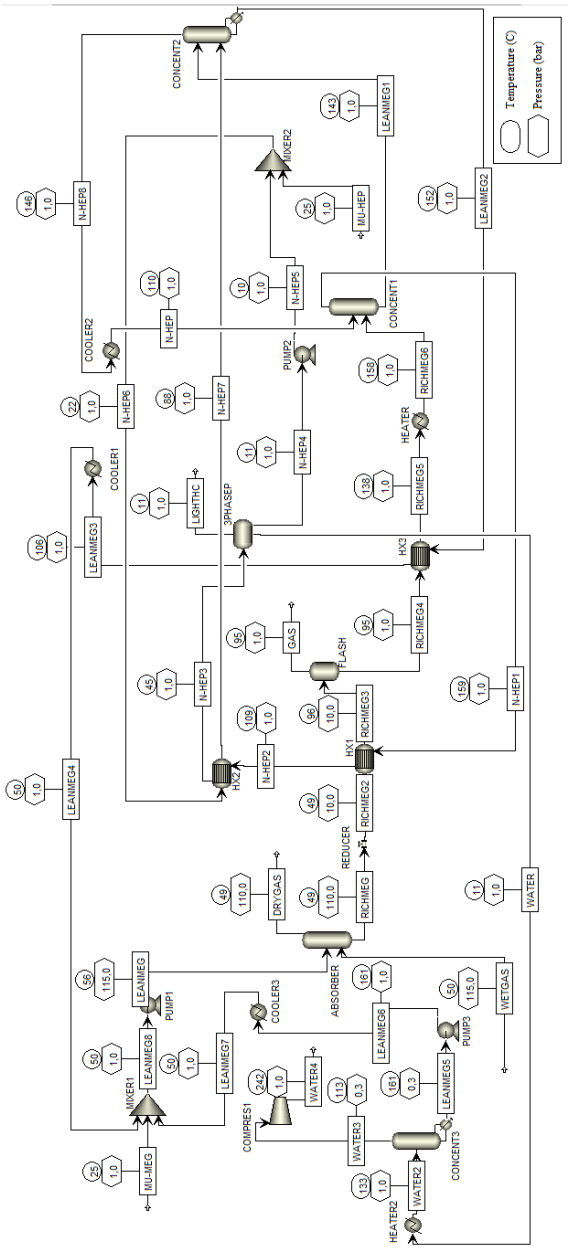

Figure C.5: Diagram of gas dehydration with DRIZO regeneration and MEG recovery showing pressure and temperature results.

Blanca Yuritzi Cervantes Gameros

NTNU
Kunnskap for en bedre verden